AN X-RAY STUDY OF THE BEHAVIOR OF TITANIUM FILMS ON SILICON SUBSTRATES

by

Frank E. Dietrich

Thesis submitted to the Graduate Faculty of the

Virginia Polytechnic Institute and State University

in partial fulfillment of the requirements for the degree of

MASTER OF SCIENCE

in

Metallurgical Engineering

APPROVED:

C. R. Houska, Chairman

W. R. Hibbard

T. P. Floridis

J. L. Lytton

June, 1977

Blacksburg, Virginia

LD
5655
V855
1977
D54
c.2

ACKNOWLEDGMENTS

The author expresses his thanks to Dr. C. R. Houska who provided the challenge and assistance required to complete this work. Thanks also go to Drs. T. P. Floridis and J. L. Lytton for their interesting and useful discussions.

Thanks are also due to Mr. Harry C. Dudley and Mr. Lawrence McDonald, both technicians for the Department of Materials Engineering. Appreciation is extended to Mrs. Teresa K. Belcher for the typing of the manuscript and Mrs. Jeanne Warner for her assistance. Thanks also go to Lawrence P. Johnson for his help in computer graphics.

The author wishes to express his thanks to his family and especially to Mr. James E. Kramer for his untiring encouragement and financial assistance to both his daughter and son-in-law. Long overdue thanks is offered to his wife, Robin, for her loving care and encouragement.

The author is grateful to the National Science Foundation for providing the funds that made this research possible.

TABLE OF CONTENTS

		Page
	ACKNOWLEDGMENTS	ii
	LIST OF FIGURES	iv
	LIST OF TABLES	viii
I.	INTRODUCTION	1
II.	REVIEW OF LITERATURE	3
III.	THEORY	9
IV.	EXPERIMENTAL PROCEDURES	24
V.	ANALYTICAL PROCEDURES	38
VI.	RESULTS AND DISCUSSION	43
	REFERENCES	168
	APPENDIX I	171
	APPENDIX II	187
	VITA	193
	ABSTRACT	

LIST OF FIGURES

Figure		Page
1.	Equilibrium phase diagram of the titanium-silicon system	6
2.	Plot of linear expansion vs. temperature for the components of a reacted thin film	10
3.	Illustration of axis designation for a texture diffractometer	12
4.	X-ray diffraction geometry	14
5.	High resolution K_{α_1} diffractometer with line source	33
6.	Schematic drawing of elimination of K_{α_2} component	34
7.	Plot of heat treatment temperature (^{o}C) vs. (time)$^{\frac{1}{2}}$ to fracture of cyclic anneals on thin films	48
8.	Scanning electron micrograph of titanium thick film surface (2.2 μm) after cyclic anneal at 650°C, total time of 2 hours	49
9.	Scanning electron micrograph of titanium thick film surface (2.2 μm) after cyclic anneal at 650°C, total time of 5 hours	50
10.	Scanning electron micrograph of titanium thick film surface (2.3 μm) after total annealing time of 1 hour at 625°C	51
11.	Scanning electron micrograph of titanium thick film surface (2.5 μm) after cyclic anneal at 600°C, total time of 7½ hours	52
12.	Experimental intensity simulation for as-received 2.2 μm titanium-silicon thin film, 2θ region from 35° to 45°	60
13.	Experimental intensity simulation for as-received 2.2 micron titanium thin film, 2θ region from 70° to 80°	61
14.	Experimental intensity simulation for step anneal for 2 hours at 350°C, 2θ region from 35° to 45°	62

Figure | Page

15. Experimental intensity simulation for step anneal for two hours at 350°C, 2θ region 72° to 78° 63

16. Experimental intensity simulation from step anneal for 2 hours at 450°C, 2θ region from 35° to 45° 64

17. Experimental intensity simulation for step anneal for 2 hours at 450°C, 2θ region 72° to 79° 65

18. Experimental intensity simulation for step anneal for 2 hours at 500°C, 2θ region from 35° to 45° 66

19. Experimental intensity simulation for step anneal for 2 hours at 500°C, 2θ region from 72° to 79° 67

20. Experimental intensity simulation for step anneal for 2 hours at 550°C, 2θ region from 35° to 46° 68

21. Experimental intensity simulation for step anneal for 2 hours at 550°C, 2θ region from 72° to 79° 69

22. Experimental intensity simulation for step anneal for 2 hours at 575°C, 2θ region from 35° to 45° 70

23. Experimental intensity simulation for step anneal for 2 hours at 575°C, 2θ region from 72° to 79° 71

24. Experimental intensity simulation for step anneal for 2 hours at 600°C, 2θ region from 35° to 46° 72

25. Experimental intensity simulation for step anneal for 2 hours at 600°C, 2θ region from 58° to 65° 73

26. Experimental intensity simulation for step anneal for 2 hours at 600°C, 2θ region from 71° to 79° 74

27. Experimental intensity simulation for step anneal for 2 hours at 625°C, 2θ region from 35° to 46° 75

28. Experimental intensity simulation for step anneal for 2 hours at 625°C, 2θ region from 59° to 63° 76

29. Experimental intensity simulation for step anneal for 2 hours at 625°C, 2θ region from 70° to 83° 77

30. Experimental intensity simulation for step anneal for 2 hours at 650°C, 2θ region from 32° to 45° 78

Figure | Page

31. Experimental intensity simulation for step anneal for 2 hours at 650°C, 2θ region from 60° to 63° 79

32. Experimental intensity simulation for step anneal for 2 hours at 650°C, 2θ region from 72° to 79° 80

33. Experimental intensity simulation for step anneal for 2 hours at 650°C, 2θ region from 82° to 87° 81

34A. Optical interference techniques measured the elastic bending of the silicon substrate taken at right angles . . 82

34B. Optical interference techniques measured the elastic bending of the silicon substrate taken at right angles . . 83

35. Optical interference techniques measured the elastic bending of the silicon substrate cut to within 3.5° of the 111 planes 84

36. Experimental intensity simulation for as-received, 2.3 μm titanium thin film, 2θ region from 34° to 42° . . . 85

37. Experimental intensity simulation for as-received, 2.3 μm titanium thin film, 2θ region from 52° to 54° . . . 86

38. Experimental intensity simulation for as-received, 2.3 μm titanium thin film, 2θ region from 62° to 64° . . . 87

39. Experimental intensity simulation for as-received, 2.3 μm titanium thin film, 2θ region from 70° to 84° . . . 88

40. Experimental intensity simulation for 15 minute anneal at 625°C, 2θ region 34° to 42° 89

41. Experimental intensity simulation for 15 minute anneal at 625°C, 2θ region 75° to 79° 90

42. Experimental intensity simulation for 15 minute anneal at 625°C, 2θ region from 80° to 84° 91

43. Experimental intensity simulation for 30 minute anneal at 625°C, 2θ region from 34° to 42° 92

44. Experimental intensity simulation for 30 minute anneal at 625°C, 2θ region from 59° to 62° 93

Figure | Page

45. Experimental intensity simulation for 30 minute anneal at 625°C, 2θ region from 70° to 83° 94

46. Illustration of cross-section of thin film structure for as-received and 350°C step anneals for 2 hours 95

47. Illustration of cross-section of thin film structure for 450°C step anneal for 2 hours. 96

48. Illustration of cross-section of thin film structure for 500°C anneal for 2 hours 97

49. Illustration of cross-section of thin film structure for 550°C step anneal for 2 hours. 98

50. Illustration of cross-section of thin film structure for 575°C step anneal for 2 hours. 99

51. Illustration of cross-section of thin film structure for 600°C step anneal for 2 hours. 100

52. Illustration of cross-section of thin film structure for 625°C step anneal for 2 hours. 101

53. Illustration of cross-section of thin film structure for 650°C step anneal for 2 hours. 102

54. Plot of "G" factor vs. disilicide thickness in final step anneal treatment at 650°C for 2 hours 103

55. Plot of strain vs. temperature increment above deposition temperature perpendicular to the crystallographic planes in step annealed thin films 104

56. Experimental intensity simulation for step anneal at 350°C for 2 hours, to illustrate the location of monosilicide in this film. 105

57. Terminal selection panel on the PDP 8/e rack 173

58. PDP 8/e computer 174

LIST OF TABLES

Table		Page
I.	Completed Reflections of $TiSi_2$ (C54)	106
II.	Atomic Scattering Factors	110
III.	Reflections for TiSi	112
IV.	Intensities for 2θ Region, As Received 2.2 μm Titanium Thin Film	120
V.	Intensities for 2θ Region, Step Anneal for 2 Hours at 350°C	122
VI.	Intensities for 2θ Region, Step Anneal for 2 Hours at 450°C	124
VII.	Intensities for 2θ Region, Step Anneal for 2 Hours at 500°C	127
VIII.	Intensities for 2θ Region, Step Anneal for 2 Hours at 550°C	130
IX.	Intensities for 2θ Region, Step Anneal for 2 Hours at 575°C	133
X.	Intensities for 2θ Region, Step Anneal for 2 Hours at 600°C	136
XI.	Intensities for 2θ Region, Step Anneal for 2 Hours at 625°C	140
XII.	Intensities for 2θ Region, Step Anneal for 2 Hours at 650°C	144
XIII.	Intensities for 2θ Region, as Received 2.3 μm Ti Thin Film	149
XIV.	Intensity for 2θ Region, 15 Minute Anneal at 625°C	152
XV.	Intensities for 2θ Region, 30 Minute Anneal at 625°C	154
XVI.	2θ Positions for Experimental Intensity Simulations	157

Table | Page

XVII. 2θ Positions for Experimental Intensity Simulations . . . 163

XVIII. Thin Film Specimen 2.5 Micron of Titanium Cut Within 3.5° of the 111 Planes Annealed at Various Temperatures for 2 Hours, Measured at Room Temperature 166

I. INTRODUCTION

Preliminary investigations of titanium-silicon thick films are incapable of presenting quantitative models describing their behavior at intermediate temperatures. The silicides associated with diffused thin film structures have received limited attention thus necessitating conclusive determinations of structure and lattice parameters. The confusion in the literature on the reaction between titanium films and silicon possibly stems from the acceptance of previous incomplete and inaccurate studies of the bulk silicides. The characterization of this transition metal system is the purpose of this study.

The nature of X-ray diffraction makes it a particularly attractive tool for analyzing diffusion on the order of several microns in specimens. Refinements in the analysis of diffraction data have made it possible to investigate uniform and non-uniform strains, grain size, stacking faults and other defects as well as texture and crystal structure. Grain boundary diffusion and volume diffusion in films can be studied quantitatively in detail with an X-ray technique. The titanium-silicon thin film system has been mainly examined with MeV He backscattering along with some supporting X-ray diffraction.

A detailed study on thick film specimens which are free of oxides at the interface was carried out. Titanium films of approximately two microns thick, a factor of ten thicker than in previous studies, were deposited on 111 oriented silicon single crystals. An additional complication evolved from the highly deformed nature of the deposited

metal films. The diffraction line broadening found with these films is probably considerably greater than that of cold worked titanium filings at room temperature. A computer simulation data analysis technique was developed to evaluate the diffused structure of the films.

The build-up of strain about the various interfaces and its affect on the long term mechanical stability of the reacted film is a major concern. Examination of both uniform and non-uniform strains resulting from various heat treatments and substrate orientations supplied some insight as to the origin and subsequent reduction of the mechanical instability.

Lattice parameters and structure factor determinations of both titanium monosilicide and disilicide eliminated a major problem for identification of these phases with X-ray diffraction. A range of compositions along with the identification of Ti_5Si_4 as a high temperature phase will modify the most recent phase diagram[15] (see Figure 1). Results of the bulk titanium silicides represent significant differences from those integrated intensities and lattice parameters previously reported.

Finally, it should be noted that the determinations presented in the following sections have not completely characterized the titanium-silicon system. A continuing effort in the examination of diffused films and bulk standards will eventually complete the study.

II. REVIEW OF LITERATURE

In the past ten years, a renewed interest in the silicides of titanium evolved from their importance in integrated circuits and energy conversion devices. These applications impose an acceptable period of operation at a given temperature and consequently encourage the development of new techniques to measure composition and structural changes on a fine scale. The thin film reaction between silicon and titanium may differ from the ordinary diffusion process in bulk samples at elevated temperatures. Baluffi and Blakely[1] have attempted to identify and describe a number of special characteristics for diffusion in thin films. Although preliminary work has been done on this system, it is not as clearly understood as many conventional engineering materials.

A technique using the energy spectrum of MeV backscattered He ions provides sensitive measurements of relative atomic composition as a function of depth. This method along with glancing X-ray diffraction furnish specific pictures of the transformations in thin films after thermal treatment. Although there is some disagreement as to whether ion backscattering is nondestructive[2,3] (since it may create some defects which could influence the diffusion data) it is at worst categorized as "nearly nondestructive"[4]. The subsequent information, which has been collected for the thick film reaction between silicon and titanium (less than one micron) has made use of this technique.

Silicide formation is most commonly obtained through direct reaction of a vapor deposited film on an oriented silicon substrate. Typically one, and in a few cases two, silicide phase(s) are formed in thin film structures after thermal treatment[3]. The minimum reaction temperature and the silicide phase(s) present in reacted thin film structures are dependent upon the extent to which the native silicon oxide film is present[2,3]. "The thickness of native oxide layer is markedly different for different substrate orientations."[3] Film cracking and peeling after thermal treatment, which is often enhanced for thicknesses greater than a few thousand Angstroms, has also been correlated with these silicon oxide layers[3].

Mayer and Bower[2] have reported that titanium disilicide forms at approximately one-half its absolute melting point (600°C) in thin film structures where the substrates are oxide free. Prior to the formation of $TiSi_2$, Tu[5] has suggested that the lower free energy monosilicide of titanium will form. In both the zirconium and hafnium-silicon systems, these transition monosilicides have formed during thermal treatment[3], but no direct evidence was found for the analogous titanium-silicon system. A relationship of $(\text{time})^{\frac{1}{2}}$ was found for the growth of titanium disilicide[3], which is characteristic of a diffusion dominated process. Silicon was identified as the diffusing species in the titanium-silicon system[6] by the use of implanted nobel gas markers.

It has been postulated[6] that since silicon is the diffusing species, it will leave vacancies near the silicon-silicide interface.

If these vacancies coalesce to form voids, the silicide could fracture easily under an applied stress. Balluffi and Blakely[1] have reviewed several explanations as to the origin of relatively large biaxial stresses often present in thin films[7,8]. Commonly found stresses of the magnitude 10^9-10^{10} dynes cm^{-2}[7,8,9] are likely to affect the thin film diffusion process and the stability of the cohesive interface forces. Dearnaley and Hartley[10] emphasized that several intermediate phases formed in the diffusion zone are brittle and easily susceptible to fracture. These effects are recognized in oxide films but little attention has been given to thin metal film processes.

Direct information on crystal structure, grain size, internal strains, and the texture in thin film structures has not been obtained with ion backscattering. It should be pointed out that there is disagreement among authors[11,12] as to the structure of $TiSi_2$. Titanium disilicide, identified by Mayer and Bower[2], was reported to be of the orthorhombic C49 type. Preliminary work by Kato and Nakamura[13] using X-ray diffraction has reported both the C49 and C54 orthorhombic structures in the same thin film of titanium and silicon. Cotter, Kohn and Potter have claimed that $TiSi_2$ is dimorphous[11]. Another author[14] has inferred that the C49 orthorhombic disilicide is a ternary phase containing aluminum.

An examination of the phase diagram[15] for the titanium-silicon system (Figure 1) indicates that a number of intermediate compounds are observed under equilibrium. At the reported reaction temperature for thin films, approximately one-half the absolute melting point,

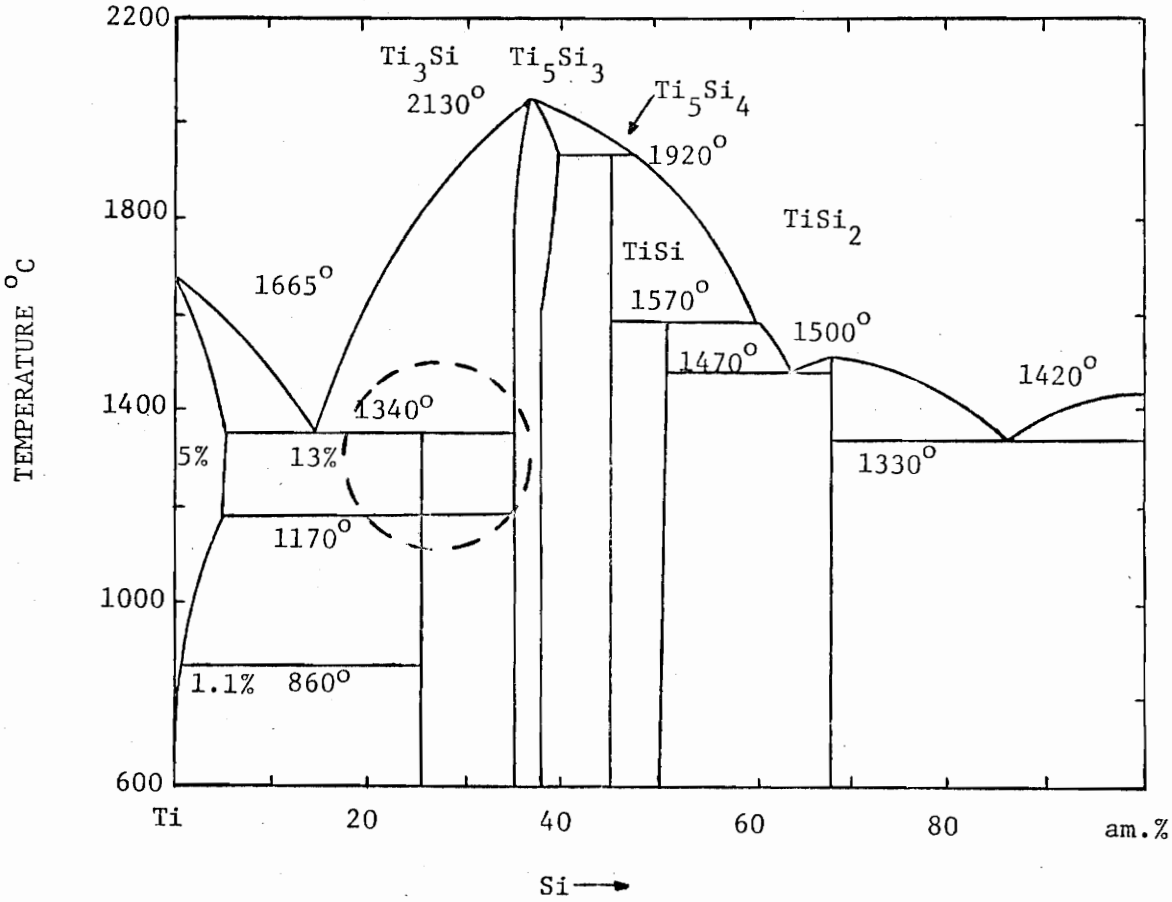

Figure 1. Equilibrium phase diagram of the titanium-silicon system[15]. *Area in dotted circle is incorrect.*

the solubility of silicon in titanium is less than one percent. The solubility of titanium in silicon is negligible. The crystal structures for the Ti-Si system are: orthorhombic $TiSi_2$ with a C54 structure[12], a = 8.236, b = 4.773 and c = 8.523A; a C49 structure[11] also orthorhombic, a = 3.62 $\pm$ 0.01, b = 13.76 $\pm$ 0.01 and c = 3.60 $\pm$ 0.01; TiSi is also orthorhombic[16] a = 6.544, b = 3.638, and c = 4.997; Ti_5Si_3 is hexagonal of the $D8_8$ type with a = 7.429 and c = 5.1392A.[17]

Reacted transition metal films yield silicides which range from nearly random to textured or epitaxial[18], and consequently some preferred orientation or texture may be anticipated in any sample. The subsequent study is an effort to exemplify the use of X-ray diffraction as a technique which can better characterize both texture and strain effects in thick films. Emphasis is placed upon the strains which are present in the plane of the film and their effect upon the stability of the reacted structure.

Summary

1. Existing studies have been of a preliminary nature using nearly nondestructive techniques, mainly MeV backscattering with some supporting X-ray diffraction.
2. There have been no studies which have measured the effects of either stress or texture on the diffusion process in thin films.
3. Grain boundary diffusion and grain size have not been properly addressed in silicide formation.

4. The effects of epitaxial growth on the stability of the diffused film have not been addressed but have been shown to be important in the Pd-Si system by Hutchins and Shepla[19].
5. A detailed kinetics study on thin film specimens which are free of oxides at the interface is still to be carried out.
6. Conclusive determinations of structure and lattice parameter of both TiSi and $TiSi_2$ in bulk samples are absent.

III. THEORY

An X-Ray Diffraction Approach to a Kinetic Model

Introduction

X-ray diffraction provides non-destructive measurements of both volume diffusion and grain boundary diffusion[20,21,22] in films. High diffusivity paths, such as grain boundaries and dislocations, are known to be important at lower and intermediate temperatures and are of significance in determining the behavior of material systems.

Random to textured or epitaxial[18] silicides form in reacted transition metal films. The problem of texture must be considered if accurate measurements of the thickness of growing phases are to be made. The diffraction equations should be sufficiently general to treat phases with various degrees of preferred orientation.

Thick metal films are capable of withstanding a surprising amount of mechanical deformation during cooling from elevated temperatures. The deformation results from large differences in thermal expansions of the individual materials (see Figure 2). Strain data can be measured in three ways: (a) X-ray line shifts (uniform strain), (b) line broadening (non-uniform strain), and (c) the elastic bending of the substrate.

An X-ray diffraction approach is described along with experimental results to illustrate methods which enable the determination of a kinetic model. Only after understanding the texture and strain

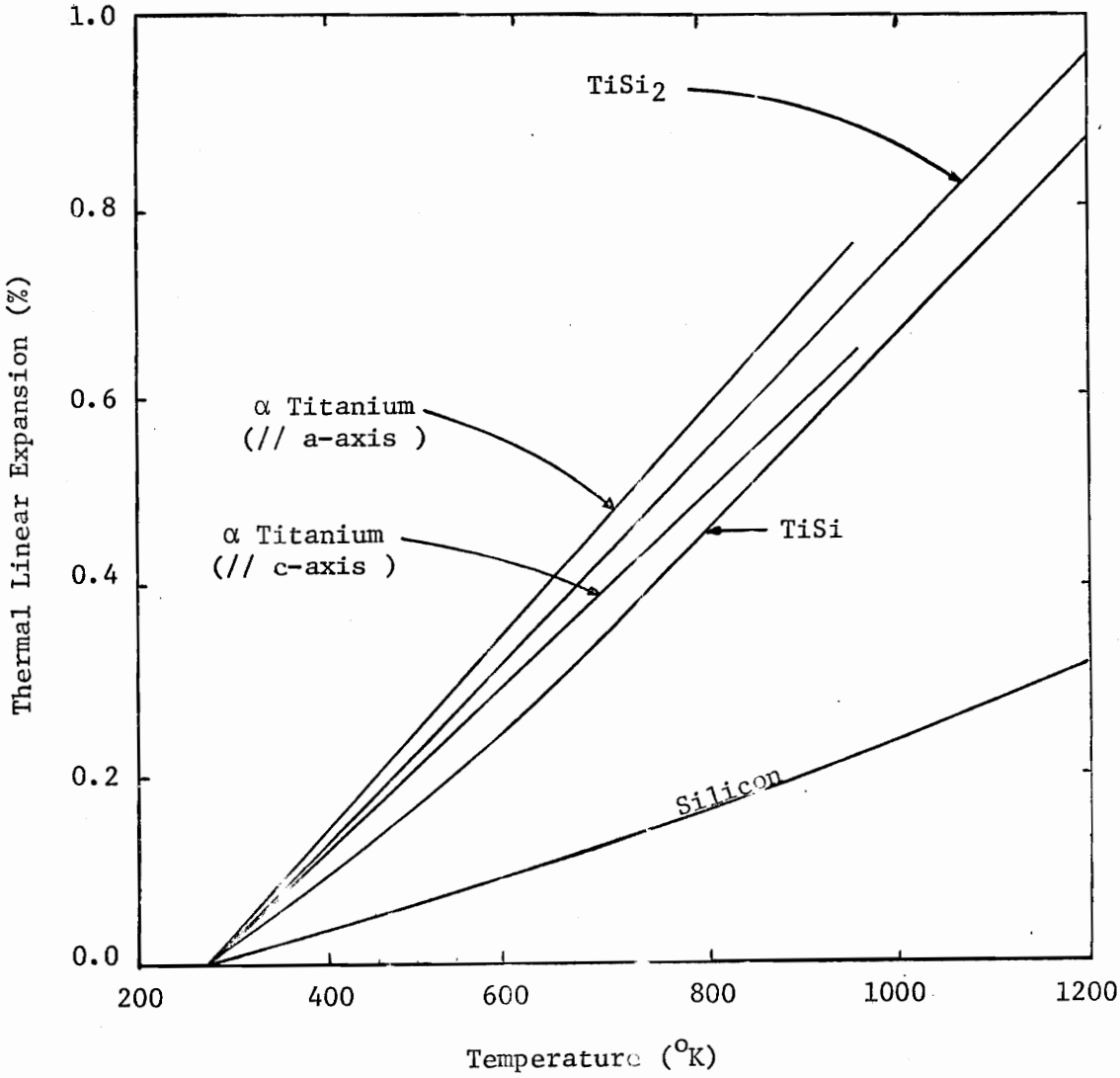

Figure 2. Plot of linear expansion vs. temperature[28] for the components of a reacted thin film.

developed in thick films, along with the identity of reactant products either deposited at the grain boundaries or at the interface, will this system be characterized.

X-Ray Diffraction Theory

The diffraction equations below are for a polycrystalline film deposited on a silicon single crystal substrate. Polycrystalline materials require texture information to obtain quantitative results. The use of parafocusing geometry results in simultaneous measurements of an orientation function and the reactant phase thickness. At later stages of this development the diffraction equations will reflect the experimental limitations observed in this study.

Two mutually perpendicular angles, χ and Φ (Figure 3), allow various sample orientations. Phi is perpendicular to the specimen surface. The plane containing the incident and diffracted beam also parallel to the specimen surface contains the χ axis. Specimen size limitations restrict examination to 60° in χ and a full rotation in Φ. Chi should be taken as 0° when the specimen surface is perpendicular to the plane defined by the incident and diffracted beams.

The area of the specimen sampled by the X-ray beam is given by

$$A_e = A_o/\sin\theta \cos\chi \qquad (1)$$

where A_o = cross sectional area of the incident beam, and θ = angle of incidence. Sampling depths range from the specimen surface to a depth at which the absorption from the material above will reduce the diffracted beam intensity to that of statistical background.

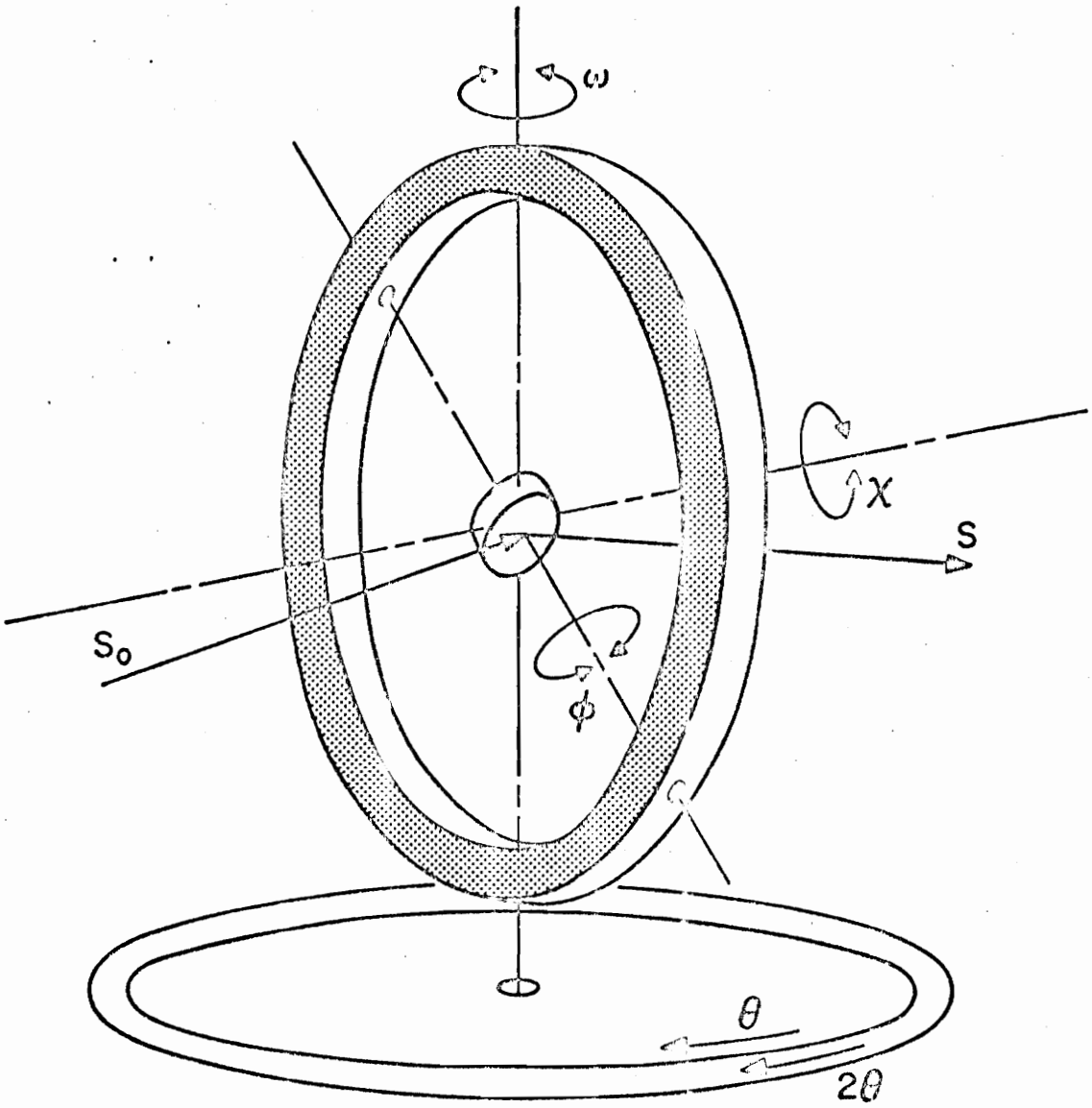

Figure 3. Illustration of axis designation for a texture diffractometer.

The maximum path length of the X-ray beam (Figure 4) 1-2-5 depends on the linear absorption coefficient as well as on θ. As the sampling plane with cross section A_e is lowered parallel to the surface and the interface, regions of composition "m" are examined. The fraction of irradiated area with composition "m" intersected by the sampling plane, at a depth "Y" is defined by the function $H_m(Y)$. For one dimensional volume diffusion, the sampling plane will pass through regions of uniform composition, $H_m = 1$ in the depth Y_m to $Y_m + \Delta Y_m$, and $H_m = 0$ elsewhere. Irregular composition surfaces associated with high diffusivity paths may also intersect the sampling plane. In either case the function $H_m(Y)$ will be useful in subsequent calculations, since X-ray intensity is proportional to the volume of diffracting material of composition "m".

The total volume of material of composition "m" is given by

$$V_m = A_e \int_o^w H_m(Y)dY \qquad (2)$$

where w is the sample thickness. The form of equation (2) neglects absorption of the incident and diffracted beams, i.e. the term

$$\exp\ [-K_m \overline{\mu(Y)} Y] \qquad (3)$$

where $K_m = 2/\sin\ \theta_m \cos\ \chi$

must be included. The angle θ_m is the Bragg angle for an element of composition "m" and $\overline{\mu(Y)}$ is the average linear absorption coefficient for all material from the surface to a depth Y. Equations (2) and (3) combine into a single expression defined as the effective volume

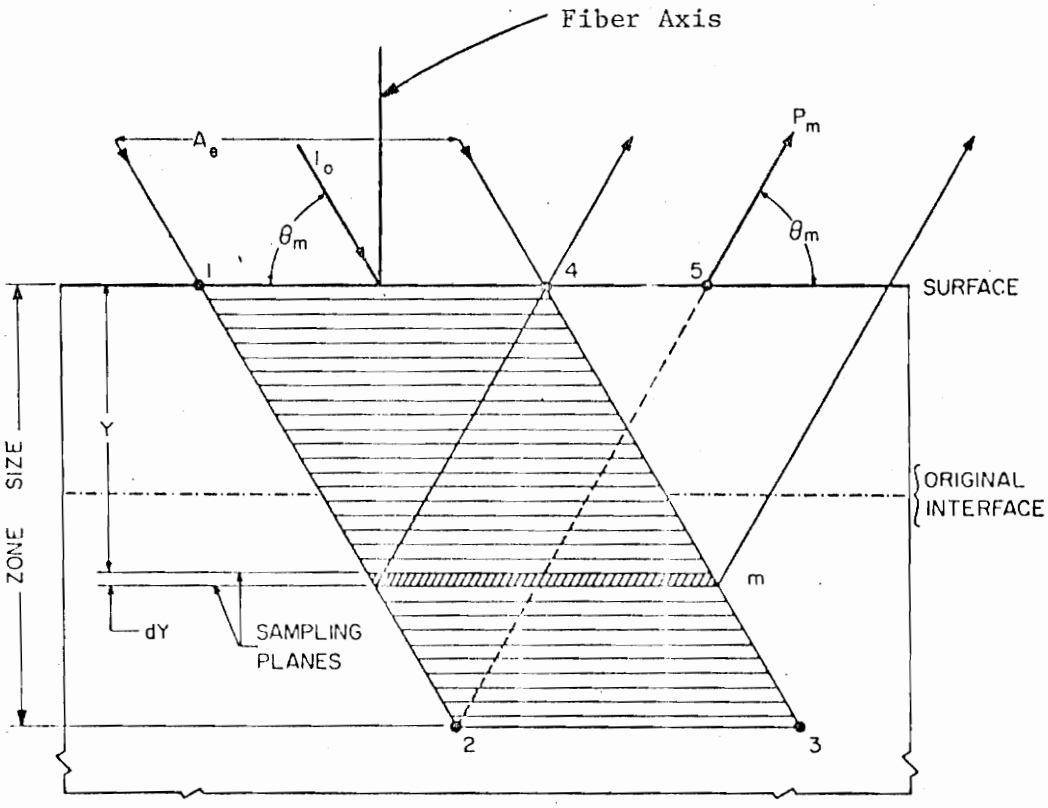

Figure 4. X-ray diffraction geometry.

$$\langle V_{me} \rangle = \langle O_m(\chi) A_e \int_0^{\infty} H_m(Y) \exp[-K_m \overline{\mu(Y)} Y] dY \rangle \tag{4}$$

The integral has been extended to ∞ since the integrand vanishes for thick substrates. The orientation factor, $O_m(\chi)$, represents the ratio of the actual pole density for a specific composition "m" to that of the ideally random case. Rotational symmetry may be assumed for the present application of diffused planar films deposited onto oriented single crystals.

The diffracted intensity is proportional to the effective volume, $\langle V_{me} \rangle$, and is given by the following equation

$$P_m = I_o Q_m \langle V_{me} \rangle \tag{5}$$

where Q_m, the reflectivity per unit length,[23,24]

$$Q_m = \frac{r_e^2 \lambda^3}{V_m^2} \quad \frac{1 + \cos^2 2\theta_m \cos^2 2\alpha}{\sin 2\theta_m (1 + \cos^2 2\alpha)} \quad pF_m^2 \exp[-2M_m] \tag{6}$$

The constant terms are:

I_o = intensity of incident beam,

r_e = classic radius of the electron (= e^2/mc^2)

λ = X-ray wavelength.

Terms dependent upon the composition, m, of the diffracting element:

V_m = volume of unit cell,

$$F_m = \text{structure factor} = \sum_1^N f_n \exp[2\pi(hu_n + kv_n + \ell w_n] \tag{6a}$$

f_n = atomic scattering factor,

u_n, v_n, w_n = coordinates of the atoms in the unit cell

N = number of atoms per unit cell

$\exp[-2M_m]$ = Debye-Waller factor,

θ_m = Bragg angle for diffracting composition

α = angle for the monochromator.

Equation (4) may be written in terms of an average over a hemisphere for a specific θ_m

$$\langle V_{me} \rangle = \frac{A_o}{\sin \theta_m} \int_o^{\pi/2} O_m(\chi) \tan \chi \int_o^{\infty} H_m(Y) \exp[-K_m \overline{\mu(Y)} Y] dY d\chi \qquad (7)$$

with the $\int_o^{\pi/2} O_m(\chi) \sin \chi \, d\chi = 1$ (7')

The integral can be carried out if the transformation products are planar and of uniform composition to a depth Y. The general case has several planar phases between the surface and the diffracting phase. The intensity for an intermediate phase of composition "m" is

$$P_m = I_o Q_m [\frac{A_o}{2\mu_m} \int_o^{\pi/2} O_m(\chi) \sin \chi \, [1 - \exp(-K_m \mu_m Y_m)] \times$$

$$\exp(-K_m \overline{\mu(Y)} Y)] d\chi \qquad (8)$$

where Y = distance to the surface,

Y_m = thickness of planar composition "m", and the average linear absorption coefficient is given by:

$$\overline{\mu(Y)} = \frac{1}{Y} \int_{o}^{Y} \mu(Y)dY \tag{9}$$

The integrated intensity of a single uniform phase with a texture represents the limiting case of equation (8):

$$P_m = I_o Q_m \frac{A_o}{2\mu_m} \int_{o}^{\pi/2} O_m(\chi) \sin \chi)d\chi \tag{10}$$

letting $Y \rightarrow 0$ and $Y_m \rightarrow \infty$. The last integral is unity by (7') and the effective volume expression reduces to

$$\langle V_{me} \rangle = \frac{A_o}{2\mu_m} \tag{11}$$

which is the effective volume for a uniform phase.

Existing literature on silicide formation in thin films indicates that the planar model is adequate. Equations (4), (7'), and (8) (or simplifications) can be used to determine phase thickness, Y_m, and the distribution function, $O_m(\chi)$. In the case of epitaxial phases, methods are available to give similar information[20,21,22]. In this case, X-ray rocking curves and integrated intensities supply the distribution of subgrains and phase thickness respectively.

Experimental Limitations

The long term mechanical stability of the reacted thick film is limited by the build-up of strain about the various interfaces. X-ray data obtained by systematic isothermal anneals provide diffraction lines which overlap and are considerably broader than

those obtained from cold worked metal filings. Chi rotation, carried out with an Eulerian cradle, would result in a complex analysis of the X-ray data. A simplification of the development presented above is given in the following section.

The effective volume, equation (4), reduces to the following when conventional reflection geometry is assumed

$$\langle V_{me} \rangle = A_e g \int_o^\infty H_m(Y) \exp[-K_m \overline{\mu(Y)} Y] dY \tag{12}$$

where $g = O_m(\chi)$ and chi is restricted to $\pm 3.4^o$. The intensity for an intermediate phase of composition "m" is given by

$$P_m = I_o Q_m A_e g[1 - \exp(-K\mu_m Y_m)] \exp[-K_m \overline{\mu(Y)} Y] \tag{13}$$

where Y = distance to the surface

Y_m = thickness of planar composition "m" and the average linear absorption coefficient is given by equation (9). The orientation factor, g (eqn (12)), designates the volume fraction of grains that have {hkℓ} plane normals lying parallel to the fiber axis (see Figure 4).

Bulk standards allow the X-ray data to be reduced to the effective volume term of the various silicides (and pure materials) given by equation (11). From an ideal powder standard of α, the intensity is

$$P_\alpha = I_o Q_\alpha \frac{A_o}{2\mu_\alpha} \tag{14}$$

where "g" = 1, a randomly oriented material. For a given hkℓ reflection the ratio of a standard powder to that of the general case of a thick film structure yields the following intensity relationship:

$$\frac{\langle P_{\alpha'}\rangle}{P_\alpha} = \frac{Q_{\alpha'}}{Q_\alpha}\,\frac{\mu_\alpha}{\langle\mu_\alpha\rangle}\,\chi_\alpha g[1 - \exp(-K_m\langle\mu_\alpha\rangle Y_\alpha]\exp[-K_m\overline{\mu(Y)}Y] \qquad (15)$$

Harris[25] has shown that the values of $g_{hk\ell}$, averaged over all orientations, is equal to unity:

$$\frac{\Sigma\, g_{hk\ell}}{N} = 1 \qquad (16)$$

where N is the total number of reflections. If only a few reflections are available, equation (16) may no longer be valid.

Equation (15) or a modification of it can be used to consider a homogeneous dispersion of "α" in a thick film or a columnar reaction product at the grain boundaries. In this case the grain size is assumed to be much smaller than $1/\mu_\alpha$. Through the use of the preceding equations, a kinetic model for silicide formation in the titanium-silicon system will be developed.

Simulation of X-ray Patterns

The complexity of X-ray diffraction patterns obtained from highly deformed materials necessitate the use of computer simulation in their analysis. Symmetrical diffraction peaks are often represented by simple mathematical functions. Gaussian or Cauchy distributions

are often inadequate in representing the X-ray intensity distribution near the peak position and at its extremities. A Pearson Type VII distribution[26] can be varied from the Gaussian to a Cauchy by appropriate selection of a parameter in the function. A modified Lorentzian and other forms of this function can be used to effectively approximate many X-ray diffraction peaks[27].

The Pearson distribution has the following form:

$$Y(X) = Y_o[1 + (X - \bar{X})^2/(ma^2)]^{-m}, \tag{17}$$

and the maximum value, Y_o, at $\bar{X}$. The integration of Pearson distribution yields

$$I = \int_{-\infty}^{\infty} Y_o[1 + (X - \bar{X})^2/(ma^2)]^{-m} dX = \sqrt{\pi m}\ a \frac{\Gamma(m - \frac{1}{2})}{\Gamma(m)} Y_o \tag{18}$$

where I is equal to the total integrated intensity. This integration contains the distribution maximum and solving

$$Y_o = \frac{I}{\sqrt{\pi m}\ a} \frac{\Gamma(m)}{\Gamma(m - \frac{1}{2})} \tag{19}$$

where "a" is related to the full width at the $1/p^{th}$ maximum.

$$W(Y_o/P) = 2a\sqrt{m(P^{1/m} - 1)} \tag{20}$$

The limiting forms of the Pearson distribution are

$$\text{Cauchy, } m = 1, \quad Y(X) = Y_o[1 + (X - \bar{X})^2/a^2]^{-1} \tag{21}$$

$$Y_o = I/(a\pi)$$

and Gaussian, $m = \infty$, $Y(X) = Y_o \exp[-(X - \bar{X})^2/a^2]$ (22)

$$Y_o = I/(a\sqrt{\pi}).$$

The form of the Gaussian is derived by expanding the function as a binomial and considering the limiting form of the general term of the series. This study will make use of intermediate forms of the Pearson Type VII distribution in simulating X-ray diffraction patterns.

Diffuse Intensity

The contributions to diffuse intensity from thermal vibrations, Compton modified, and X-ray fluorescence is part of the measured integrated intensity which is not included in equation (6). Thermal vibrations reduce the intensity of crystalline reflections (Debye-Waller factor, exp[-2M]) and also produce a diffuse intensity (TDS). The incident radiation will fluoresce the absorbing element, given the required absorption edge and produce an additional contribution to the diffuse intensity. Compton modified scattering is present in any diffraction pattern. Significant information on the reacted specimen is available from these intensities.

The diffuse intensity from Compton modified and TDS can be approximated by the form

$$I^D_{Comp.,TDS} = K_1(1 - \exp[-K_2 \frac{\sin^2\theta}{\lambda^2}]) \quad (23)$$

which gradually increases with 2θ. This is a convenient form for

fitting the experimental data, and both constants can be related to theory at a later time if needed.

The X-ray fluorescence from titanium by the incident CuK_{α_1} radiation takes the form

$$I(CuK_{\alpha_1}) = K_1'(1 - \exp[-K_2'/\sin\theta]) \tag{24}$$

where $K_2' = [\mu_{Ti}(Cu) + \mu_{Ti}(Ti)]T$

$\mu_{Ti}(Cu)$ = linear absorption coefficient of titanium with Cu radiation

$\mu_{TiSi_x}(Cu)$ = linear absorption coefficient of silicide with Cu radiation

$\mu_{Ti}(Ti)$ = linear absorption coefficient of titanium with Ti radiation

$\mu_{TiSi_x}(Ti)$ = linear absorption coefficient of silicide with Ti radiation

where $\mu_{Ti} = \frac{X}{T} \langle\mu_{Ti}\rangle + \frac{T-X}{T} \langle\mu_{TiSi_x}\rangle$

T = thickness of titanium-silicide films

X = Thickness of titanium

and $K_1' = I_o\ C\ A_o/\{\mu_{Ti}(Cu) + \mu_{Ti}(Ti)\}$ (24a)

I_o = intensity of incident beam

A_o = cross sectional area of the incident beam

C = intensity of TiK_α/intensity of CuK_α = efficiency constant which increases with decreasing 2θ.

The effective volume of titanium after each diffusion treatment can be cross-checked by the use of this fluorescence, which is independent of orientation. The application of these two forms of diffuse intensity will be described in detail in the Analytical Procedures (Section IV).

IV. EXPERIMENTAL PROCEDURES

An examination of both thick films and bulk powder standards were necessary to complete this study. The existing ASTM powder diffraction card files for TiSi and $TiSi_2$ were discovered to be incomplete or inaccurate, and standards had to be prepared. These silicide standards along with a Ti powder sample supplied the fundamental information essential to pursue the development of a kinetic model of silicide formation in titanium-silicon thick films.

This chapter describes the procedures employed in the preparation and reaction of both thick films and bulk powder standards. Certain preliminary results from the preparatory stage of the powder standards are also presented. A detailed description of the experimental equipment is given for completeness.

A. Thick Film Preparation

This is an important stage of the research because one of the purposes of this study is to obtain a thin film structure free of the native silicon oxide layer. In order to clean this interface, the silicon substrates were first placed in acetone in an ultrasonic cleaner for twenty minutes. The samples were then sputter etched in the same chamber where the metal films were later deposited. This procedure did not allow the Si to be exposed to oxygen prior to Ti deposition. The etching was done at 0.8 kV, 60 watts for 30 minutes. The samples were subsequently heated to 340 and 360°C*, and the

*Samples (b) were heated to 275°C in order to examine the effects this different substrate temperature would have on the fracture process.

titanium was then deposited at 2.1 kV and 300 watts. The sputtering pressure of argon was 5 microns. The purity of the Ti target was 99.9%. Auger spectroscopy was used to determine the amount of sputter etching required to remove the native oxide film on the silicon substrate. Specimens were prepared at the Oak Ridge National Laboratory by the Isotope Research Materials Laboratory.

Three different sets of thin film samples were received from the Oak Ridge National Laboratory at different stages of the study:

1. Ti-Si specimens with a uniform deposit of 2.3 microns of Ti within 0.95 to 1.00 of the theoretical density. The substrates were cut to within 2.5^{o} of the 111 planes and measured 0.5 x 0.5 x 0.01".
2. Ti-Si specimens with a uniform deposit of 2.5 microns of Ti within 0.95 to 1.00 of the theoretical density. The substrates were cut to within 3.5^{o} of the 111 planes and measured 0.7 x 0.7 x 0.02".
3. Ti-Si specimens with a uniform deposit of 2.2 microns of Ti within 0.95 to 1.00 of the theoretical density. The substrates were cut to within 0.5^{o} of the 111 planes and measured to 0.875" in diameter, thickness of 0.013". These substrates were purchased from Pensilco in Bradford, Pennsylvania with a dislocation density of less than 500 cm^{2} resistivity, 1 ohm-cm, and polished on both sides.

Samples for cyclic annealing studies measuring 0.1 x 0.1" were cut from the as-received sampled using an ultrasonic milling machine.

The specimens were sandwiched between two glass slides using pyseal cement. A 345 mesh boron carbide abrasive was used for cutting. All samples were cleaned in hot (50°C) chloroform which was found to be the solvent inert to both titanium and silicon, yet it readily removes pyseal cement.

B. Bulk Standards Preparation

High purity silicon and titanium hydride powders, supplied by Ventron Corporation's Alpha Products[30], were used in preparing the samples. Emission spectroscopy supplied by the manufacturer found the silicon powder to be highly pure (iron the greatest at 500 ppm). Wet chemical analysis of the hydride found 94.5 $\pm$ 0.1 weight percent titanium, and from hydrogen evolution, 4 $\pm$ (0.1-0.3) weight percent hydrogen. All powders were mixed in methanol and evacuated in a vacuum desicator (10^{-3} torr) and allowed to dry.

Titanium and silicon were mixed in the exact stoichiometric ratio of:

18.8206 grams TiH_2

21.1794 grams Silicon

to prepare a 40 gram sample. The mixed powder was placed in a 3-inch long, high alumina boat, and subsequently evacuated to 10^{-6} torr in an ion sorption vacuum system (see annealing furnaces, Section IV).

A total reaction time of 279 hours of annealing ensured complete reaction of the sample in five steps at 1000°C. The first anneal was 111 hours, of which 5 hours at 10^{-4} torr was due to hydrogen evolution. All subsequent anneals were at 10^{-6} torr during the

reaction. The weight loss could be attributed entirely to hydrogen evolution in the initial anneal.

After each anneal (111, 24, 48, 48, 48 hours) the samples were removed from the furnace and reduced to less than 37 μm (-400 mesh) particle size with a steel impact mortar. X-ray patterns were taken without the use of a binder, and throughout the anneals the diffraction lines remained sharp and no shifts were observed. Full reaction was found after the fourth anneal with no evidence of residual titanium or silicon. A fifth anneal was carried out to assure completeness of the reaction. All X-ray patterns were made using a graphite diffracted beam monochromator. This allowed very weak peaks to be observable.

Titanium and silicon were mixed in the stoichiometric ratio of:

25.5973 grams of TiH_2

14.4027 grams of Silicon

for preparation of a 40 gram sample. All preliminary preparation methods were identical to those employed with the disilicide.

A total reaction time of 528 hours at 1000°C in 11 steps assured complete reaction of the standard. All anneals were 48 hours in length of which 7 hours of the initial anneal was at 10^{-4} torr. Weight loss again could be attributed entirely to hydrogen evolution during the initial anneal. All sequential anneals were at 10^{-6} torr as in the disilicide treatment.

The X-ray diffraction patterns obtained with the same conditions as before contained peak position shifts. Examination of the final

sample found Ti_5Si_3 and TiSi in the completely reacted state. A 10 atomic percent deficiency in silicon was determined and a corresponding sample prepared.

All conditions remained the same as those of the previous samples except the reaction temperature was increased to 1050°C. Seven treatments of 48 hours in length produced a sample of only monosilicide. The X-ray diffraction lines remained sharp and shifted to lower 2θ positions during the treatment.

Each silicide powder of less than 400 mesh was filled into the cavity of an aluminum sample holder after the final anneal. Acetone and Duco cement (10 parts to 1) was used as a binder after the powder was settled with acetone. This produced a sample with limited surface roughness.

C. Annealing Procedure

Thin film and bulk sample heat treatments were carried out in oil free, high vacuum furnaces which incorporate sorption and ion (20 liter/sec) pumping. Using both control and specimen thermocouples, temperature measurements were within $\pm$ 2°C. Interlocks in both furnaces did not permit operation unless a vacuum of 10^{-4} torr or better was maintained. Both furnaces and a general procedure is described in the following section.

1. Bulk Standard Treatments

Powder samples were reacted at 1000 or 1050°C in a horizontal tube furnace positioned around a quartz furnace tube which contained

the powders under constant vacuum. A West furnace controller provided many different constant rise and fall rates, ranging from $20^{o}F/hr$ to $300^{o}F/min$ (0.001 to 1.0). Temperature was measured on a Brown Electronic recorder with a chromel-alumel thermocouple which was in contact with an alumina boat containing the powders. The furnace control thermocouple was platinum-10% rhodium. A three-inch constant temperature zone was measured at 1000° or $1050^{o}C$ which was the reaction temperature for all powder samples. Prior to heat treatments of all powders, each alumina boat was air-baked at $1000^{o}C$ for 8 hours in an alundum tube inserted in the furnace.

A fused quartz, 3/4 inch I.D., tube was thoroughly cleaned in acetone and methyl alcohol prior to any heat treatments. The alumina boat located in the end of the tube was sealed to the vacuum system by tightening two flanges against a copper gasket. The furnace was positioned around the glass tube so that the constant temperature zone enclosed the entire specimen.

If the following recommended start-up procedures are employed, the inefficient pumping of samples to reaction vacuums will be eliminated.

The ion pump is isolated from the remainder of the system during an exposure to atmosphere. Dry nitrogen is bled to eliminate the vacuum and a constant purge is continued during exposure to increase pumping efficiency. A roughing vacuum is produced by filling the sorption pump with liquid nitrogen. After approximately 15 minutes the valve between the ion pump and the remainder of the system may

be opened after valving off the sorption pump. The vacuum should stabilize at 5×10^{-5} torr and be allowed sufficient time to pump well below this level.

The initial anneal produces a large amount of hydrogen at the reaction temperature and is easily handled by the sorption pump. During this anneal it is necessary to supply liquid nitrogen to the sorption pump so that the roughing vacuum is not lost. This is necessary for 5 to 7 hours at which time the ion pump may be bled into the system. All subsequent anneals were done at 10^{-6} torr at the ion pump. The rise rate of the furnace was set at 200°F per hour. At the end of each anneal the samples were allowed to air cool by retracting the furnace.

2. Thick Film Treatments

Thick film specimens were enclosed in a one-inch I.D. fused quartz tube and evacuated to 5×10^{-5} torr. The vacuum was produced with the same procedure described in the previous section. The specimens were suspended in the tube on a horizontal high alumina platform which eliminated contact of the specimen with the quartz. A water cooled, open coil furnace was positioned around the sample tube to produce a 3/4 inch constant temperature zone at 650°C (the maximum heat treatment temperature).

Heat treatments of all thin films were carried out with the "Thermac" controller in the remote option. This option follows a predetermined time-temperature profile ruled on a totating drum. The limiter and gain controls were adjusted such that there was a

maximum of $2^{o}C$ deviation between the chromel-alumel specimen and command thermocouples. Limiter control enables the maximum voltage applied to the heating coil to be any desired fraction of the full line voltage. The width of the proportional band is dependent on the gain setting; increasing the gain will narrow the proportional band. For optimum control, the gain was 8 with the limiter set on 4.

Cycled specimens (see Section VI and Figures 9-12) were heat-treated with $50^{o}C$ per minute heating and cooling rates at temperature times of 5, 10, and 15 minutes. All stepped and isothermal anneals had heating and cooling rates of $100^{o}C$ per minute.

D. X-Ray Measurements

The two X-ray diffractometers used to collect all data on bulk and thin film specimens will be briefly described in this section. Distinct advantages obtained through the use of this equipment are emphasized.

1. Powder Diffractometer

A Siemens[32] diffractometer, allowing the specimen to be rotated about the Φ axis (see Figure 3) independently of the detector carriage, collected all data on the powder standards. The diffractometer was used with a one-half degree entrance, 0.2 mm receiver slit, and a Soller slit in the incident beam. The data was collected with a scintillation counter, a pulse height analyzer, and an E&S Industries diffracted beam graphite monochromator. All final runs were made at

$1/8^{o}$ per minute. A silicon powder* standard was used to provide a small correction to the bulk sample line positions. Integrated intensities were measured using a planimeter after subtracting background.

The peak to background ratio was considerably improved with the use of a diffracted beam graphite monochromator. This diffractometer set-up allowed relatively low intensity line measurements.

2. Single Crystal Diffractometer

The X-ray unit used to collect all data on the diffused thin films was basically a modified Siemens[32] diffractometer, equipped so that the $K_{\alpha 2}$ component is eliminated. The instrument halfwidths for a line source are 0.037^{o} and 0.081^{o} at $2\theta \approx 40^{o}$ and 95° respectively, which is only a factor of two larger than the natural half-width due to the spectral distribution of the $K_{\alpha 1}$ line using Cu radiation.

The $K_{\alpha 2}$ component of the radiation from the high voltage fine focus Cu tube was removed with an incident beam Jagodzinski singly bent quartz crystal monochromator (see Figures 5 and 6). The total elimination of the $K_{\alpha 2}$ component would result in an asymmetry of the instrumental function. A ratio of 1:200 between $K_{\alpha 1}$ and $K_{\alpha 2}$ intensities provided an insignificant contribution of $K_{\alpha 2}$ without causing excessive high angle asymmetries. The monochromator was adjusted at this position and remained there during the completion of the experiments.

The data was collected with a one-half degree entrance slit, 0.05 degree receiver slit, a scintillation counter and pulse height

*Supplied by National Bureau of Standards.

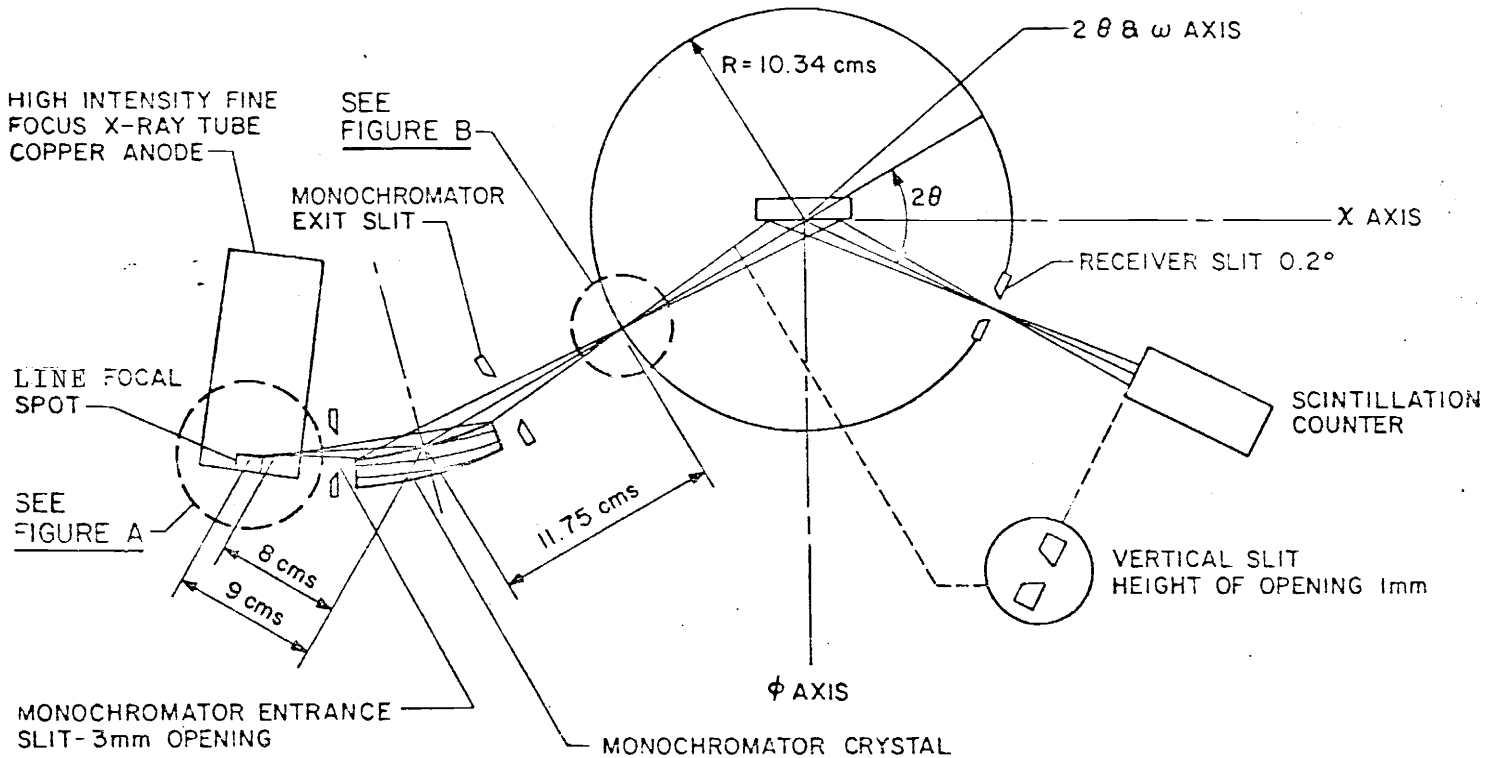

Figure 5. High resolution K_{α_1} diffractometer with line source.

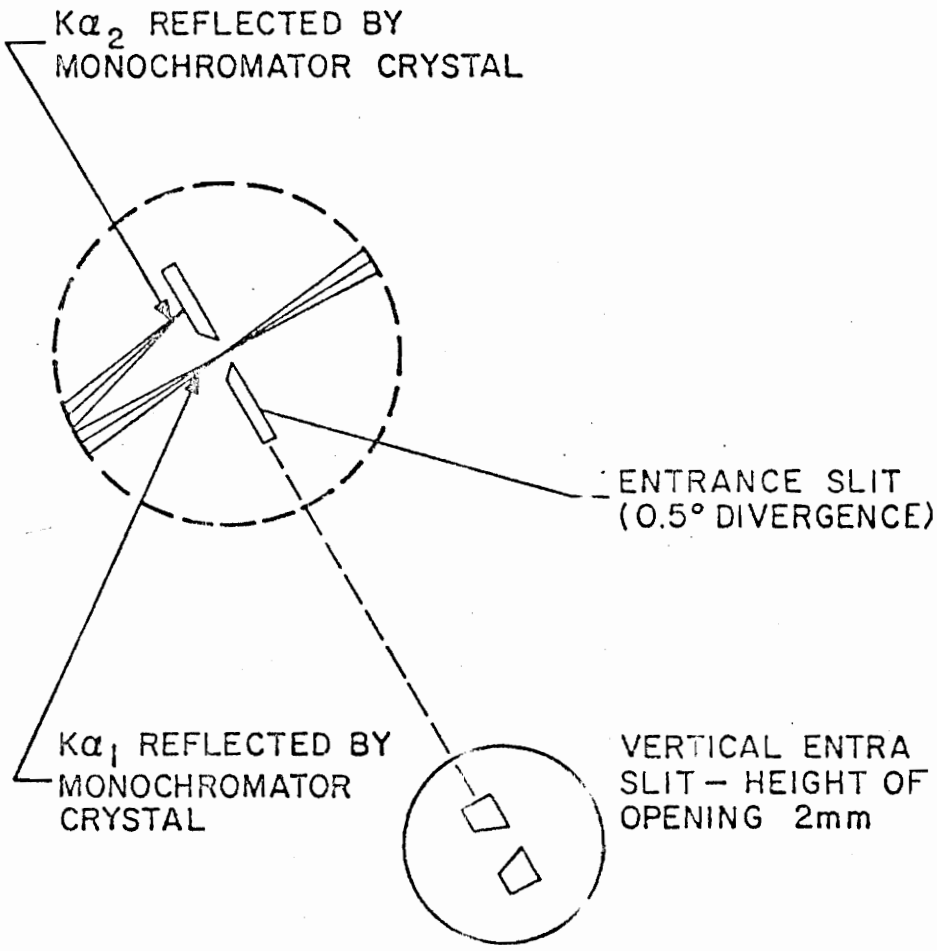

Figure 6. Schematic drawing of elimination of $K_{\alpha 2}$ component (Section B).

analyzer. The arrangement provided high resolution and refined line shape making it well suited for defect studies.

Use of the Diffractometer: The high voltage generator was warmed up at the operating voltage for several hours prior to data collection. The pure silicon 2θ positions were found to be in constant error over the 2θ region (30° to 150°) and corresponding corrections were made to the experimental line positions. The detector panel settings were:

Detector Voltage:	1200
Pulse Height Analyzer:	2.0 (base and window)
Linear Amplifier:	4 x 64

on both diffractometers

3. Thin Film Thickness Measurements

The weight gain measurement supplied by Oak Ridge Laboratory was varified using an X-ray diffraction method. Using the integrated intensity of one or more orders of the substrate reflections, the thickness can be calculated as follows:

$$t = \frac{\ell n(I/I_o)}{\mu_{Ti} K} \tag{25}$$

t = film thickness

I = intensity measured in the plated condition

I_o = intensity in the unplated condition

μ_{Ti} = absorption coefficient of film material

$K = \frac{2}{\sin \theta_{Si}}$

The silicon single crystal substrate first order reflection will be decreased by extinction. The use of the third order reflection will minimize this effect and yield reliable thickness measurements.

4. Locating the Specimen

The mounting of thick film specimens in vaseline eliminated additional contributions to the large amount of strain present in the titanium. Destruction of the sample was inevitable if conventional backings were used (i.e. mounting clay), resulting in a local fracture of the titanium from the substrate. The sample was positioned by the weight of a glass slide placed on the sample which caused the vaseline to creep. This located the sample surface parallel to the face of the X-ray specimen holder.

The thick films were cleaned of vaseline in ios-octane after each X-ray examination. Prior to heat treatment, all specimens were cleaned in acetone to remove all traces of the iso-octane and then rinsed in methanol.

E. Optical Interference Techniques

The elastic bending of thick film specimens has been measured using an optical interference (Newton rings) technique. Strains in the plane of the metallic film distort the substrate into a saucer-like shape, thus presenting difficulties in mounting the specimens (see previous section). Information on the deflection of the specimen resulting from stepped annealing upwards from the deposition temperature will compliment the strain measurements obtained with X-rays.

A monochromatic mercury (5461 Å) light along with an optical flat were used to produce a pattern of contours for the film surface. The factors that determine the nature of the interference are differences in optical path length and phase changes on reflection. Assuming normal incidence, the respective minimum and maximum intensities are

$$2d = m\lambda \tag{26a}$$

$$2d = (m+\tfrac{1}{2})\lambda \tag{26b}$$

where λ = wavelength

$m = 0,1,2,\ldots$

d = deflection from one ring to the next.

Perfect flatness will form a pattern of uniform brightness. Each fringe represents a change in height of 18 millionths of an inch.

The surface of the specimens were wiped clean and the optical flat placed in contact with the metallic side of the thin film. It is essential at all times to have the flat level with the surface. The monochromatic light, at normal incidence, illuminated the surface so that a reflection of it could be seen in the sample. The pattern was viewed from an angle of 30° to the specimen normal through a macroscope (5X). The photographs taken of each fringe pattern were enlarged to 8" x 10", and the distance between fringes was measured.

V. ANALYTICAL PROCEDURE

Calculations of the structure factors and relative intensities for various crystalline reflections of a material are dependent upon the atomic positions of the atoms in the unit cell. Substances of the orthorhombic crystal structure yield X-ray patterns containing a larger number of reflections than those of a cubic material and accordingly less non-zero structure factors. The diffracted intensity pattern for a structure composed of several phases will consist of the individual intensities from each set of crystalline planes parallel to the surface. The difficulty in determining the individual contributions from each phase to the total diffracted intensity is magnified if uniform and non-uniform strain along with composition variations are present in the material.

The computer analysis of both complex diffraction patterns and the general forms for the structure factors will be discussed in the following section. The simulation of the entire diffraction pattern determines the effective volume of each phase present in the reacted structure. This is possible only after having determined the experimental structure factors for the constituents.

Silicide Standards

The calculated relative integrated intensity for a powder can be expressed by a combination of equations 5, 6, and 11. The diffracted relative intensity, neglecting a thermal correction:

$$I_{rel} = \frac{1 + \cos^2 2\theta \cos^2 2\alpha}{\sin 2\theta(1 + \cos^2 2\alpha)} pF_e^{\,2}/I_{max}$$

$$\alpha = 13.3^{o}$$

can be calculated by the computer program listed in Appendix II.

Atomic scattering factors for titanium and silicon are presented in Table II.

In general, F_e is a complex number, and it expresses both the amplitude and phase of the resultant scattered wave. The structure can be expressed as:

$$F_e = \sum_{1}^{N} f_n[\cos 2\pi(hu_n + kv_n + \ell w_n) + i \sin 2\pi(hu_n + kv_n + \ell w_n)] \tag{28}$$

where f_n = the atomic scattering factor.

The diffracted intensity is proportional to $|F_e|^2$ which is obtained by multiplying the expression above by its complex conjugate.

If the space group and structure are known for a material, the u_n, v_n, w_n can be introduced into equation 28) and the structure factor can be calculated for each crystalline reflection. Experimental structure factors and those determined from equation 28 can confirm the positions of each atom in the lattice (u_n, v_n and w_n) by the following relationship:

$$R = \frac{\Sigma||F_o| - |F_e||}{\Sigma|F_o|} \tag{29}$$

where F_o = observed structure factors

F_e = calculated structure factors (see Eq. 6a)

when R is called the residual for a set of structure-factor magnitudes. In principle, $R < .50$ suggests a correct structure, although a considerably smaller R is necessary to lend credibility to the proposed structure.

Lattice parameters are determined from agreement of the high angle lines and a deviation of no more than 0.02° of those at low angles. The initial approximation of each parameter is obtained from $hk\ell$ planes of the form; two indices zero and the other having a large value, along with substantial line intensity. An iterative computer program has been written which gives four decimal place accuracy in each lattice parameter.

Thin Film Diffraction Pattern Simulation

An X-ray intensity simulation program was used to calculate the total diffracted intensity from a diffused thick film structure. Contributions from each reflection of a phase located as a dispersion or a film were summed to represent the total measured X-ray intensity. The diffuse intensity was considered as a combination of temperature diffuse, Compton modified and X-ray fluorescence scattering. A Pearson type VII distribution approximated the symmetrical diffraction peaks, since the asymmetry of instrumental function can be neglected due to the large line broadening found in all crystalline reflections.

Detail about a simulated diffraction peak is obtained by solving equation (17), which determines a 2θ position given an intensity:

$$2\theta = \overline{2\theta} + \left(\left[ma^2 \frac{Y(x)}{I_\alpha} \frac{\sqrt{\pi m}\, a\, \Gamma(m-\frac{1}{2})}{\Gamma(m)}\right]^{1/m} - 1\right) \qquad (17')$$

$\overline{2\theta}$ = the peak position

where $Y(x)$ is the measured intensity at any 2θ position. The intensity, I_α, is related to that of the powder standards by the following:

$$I_\alpha = I_{Std}\, g\, x_\alpha [1 - \exp(-K_m \langle\mu_\alpha\rangle Y_\alpha)] \exp[-K_m \langle\overline{\mu(Y)}\rangle Y] \qquad (15')$$

$K_m = 2/\sin\theta$

for the general case.

The full halfwidth, $B_{\frac{1}{2}}$, and full quarter width, $B_{\frac{1}{4}}$, can determine the "m" of the Pearson function for a peak having a shape intermediate between a Cauchy and Gaussian distribution by:

$$m = \frac{\ln 2}{\ln\left(\frac{B_{\frac{1}{4}}}{B_{\frac{1}{2}}} - 1\right)} \qquad (30)$$

and "a" is related by equation (20). Uniform strain is treated simply by the increasing or decreasing $\bar{X}$ in equation (17').

The form for Compton modified and TDS scattering (equation 23) is evaluated by fixed point iteration at two high angle points. Using equation (24), the fluorescence from titanium is fit to two low angle points and substituting the mass absorption coefficients[38] is expressed by:

$$I = K_1(1 - \exp[.1391T/\sin\theta]) \tag{31}$$

$$K_1 = \frac{I_o C A_o}{1391.06}$$

where T is the thickness of the titanium film in microns. The two diffuse intensity expressions are summed to represent the background present in the recorded diffraction pattern.

The criterion imposed upon the simulations are those of conservation of material and that "g" will sum to unity. Each diffraction region of interest is fit with the diffuse intensity from the predetermined functions to which is added the contributions of each diffracting phase. Reflections of the diffracting phase are considered initially random in orientation (g=1). Uniform and non-uniform strain along with a preferred orientation are introduced as the simulation progresses. As a planar reactant product grows, a linear variation of "g" from the substrate interface to the metallic film is introduced. The simulation of the entire diffraction pattern provides a model for the amount, distribution, and structural perfection of the reacted sample.

A comparison of the experimental data, introduced as points, and the simulated X-ray regions are viewed on a Tektronix graphics terminal during the refinement procedure. An area difference routine of the simulated and experimental intensities increase the ease at which an operator can converge upon a solution. The computer program along with details of operation will be presented in a College of Engineering technical report.

VI. RESULTS AND DISCUSSION

Results of isothermal, cyclic, and step annealed titanium-silicon thick films will be presented in this chapter. Silicide powder results represent the fundamental link in the analysis of the reacted thick film structure. Thick film results are related to the bulk standard kinetics observed and the appropriate analogies will be made. All computer simulated experimental data is included to emphasize its central role in the present analysis.

Silicide Powder Results

Titanium disilicide was confirmed to be face-centered, C54 orthorhombic, a space group of D_{2h}^{24} = Fddd[32]. The atomic positions are:

8 Ti in 8a: $(000, \frac{1}{2}\frac{1}{2}0, \frac{1}{2}0\frac{1}{2}, 0\frac{1}{2}\frac{1}{2}) + 000, \frac{1}{4}\frac{1}{4}\frac{1}{4}$

16 Si in 16e: $(000, \frac{1}{2}\frac{1}{2}0, \frac{1}{2}0\frac{1}{2}, 0\frac{1}{2}\frac{1}{2}) + x00, \bar{x}00, (\frac{1}{4}+x)\frac{1}{4}\frac{1}{4}, (\frac{1}{4}-x)\frac{1}{4}\frac{1}{4}$; x=1/3

The structure factors take the following forms for various hkℓ combinations:

$F^2 = 32(f_{Ti}-f_{Si})^2$; h = $3^n \pm 2$, k and ℓ are odd

$F^2 = 32(f_{Ti}+2F_{Si})^2$; h = 3^n, k and ℓ are odd

$F^2 = 64(f_{Ti}-f_{Si})^2$; h = 2^n, k and ℓ are even

$F^2 = 64(f_{Ti}+2f_{Si})^2$; h = n^3-n, k and ℓ are even

$F^2 = 0$; h, k and ℓ are mixed

where n = 1,2,3,...

The atomic scattering factors required in these forms were obtained from the "International Tables for X-Ray Crystallography"[34]. The

correctness of the structure was determined from equation (29) (see Section V). When titanium and silicon are considered in the neutral state, "R" was found to be 0.09. With silicon in the $^{+}4$ valance state and titanium in the neutral state, "R" is 0.07, and the corresponding integrated intensities are listed in Table I.

The peak to background ratio was considerably improved with the use of a diffracted beam graphite monochromater. This diffraction set-up allowed relatively low intensity line measurements. Results of the bulk titanium disilicide represent significant differences from those integrated intensities and lattice parameters previously reported[12,33]. Our study found a unit cell intermediate in size which may indicate that contaminates were present in previous samples because of the less perfect annealing conditions. The unit cell dimensions of $TiSi_2$ are:

	Laves & Wallbaum[12]	Duffin, Parthe & Norton[33]	Present Study
a_o (Å)	8.236	8.27_9	8.2668
b_o (Å)	4.773	4.81_9	4.7987
c_o (Å)	8.523	8.56_8	8.5503

The initial anneal produced a powder which consisted of monosilicide and silicon. This indicates that the lower free energy monosilicide of titanium forms prior to the formation of disilicide in bulk samples. X-ray patterns taken after each reaction displayed the absence of any significant solid solubility of either constituent

in the disilicide, since no line broadening or line shifts were observed.

Titanium monosilicide was previously[16] found to be D_{2H}^{16} space group, orthorhombic structure based on powder photographs. A study by Ageev and Samsonov[36] reported a C_{2V}^{1} space group. Photographic work, confirming the compound stoichiometric composition (36.95% by weight Si = 50 atomic %) and established that titanium and silicon are insoluble in this compound. The lattice parameters of the orthorhombic cell were:

	Brukel, Nowotny, Schob and Benesovsky[16]	Ageev and Samsonov[36]
a_o (Å)	6.54_3	3.61_1
b_o (Å)	3.63_8	4.96_0
c_o (Å)	4.99_7	6.47_9

The atomic positions for the D_{2H}^{16} space group were:

$\pm$ (X,¼,Z; (½-X),3/4,(1/2 + Z)

where Ti: X = 0.179, Z = 0.127_5

Si: X = 0.03_2, Z = 0.61_1

and for a C_{2V}^{1} space group:

Ti (000,½½½,00½,½½0)

Si (½0.412*, ½0.588, 0.350½, 0.350 3/4)

---

*The parameter Z is given, but a diagram makes it clear that it is incorrect.

The monosilicide sample of Burkle[16] was sintered at 1000°C in an inert atmosphere from titanium hydride and silicon powders. Ageev and Samsonov[36] used iodide derived titanium (99.7%) and silicon (99.7%) synthesized by sintering the powders in an electric arc furnace with a copper bottom and tungsten electrode with no protective atmosphere specified. The above information is presented to evaluate the validity of the proposed structure for titanium monosilicide by these authors.

Titanium and silicon reacted at 1000°C in their corresponding stoichiometric ratio produced a two phase equilibrium bulk sample. The presence of Ti_5Si_3 and TiSi in this sample identified Ti_5Si_4[37] as a high temperature compound and a modification of the equilibrium phase diagram (see Figure 1) is warrented. The low temperature existence of TiSi at its stoichiometric composition was found not to exist but instead, one ten atomic percent richer in silicon.

The lattice parameters for both compositions are:

	TiSi	$Ti_{40}Si_{60}$
a_o (Å)	6.5291	6.5358
b_o (Å)	3.3643	3.6363
c_o (Å)	4.9915	4.9969

and the respective integrated intensities are presented in Table III (a) and (b). Table III (c) displays a comparison of the Burkle[16] experimental intensities to those calculated for the reported D_{2H}^{16} space group. The residual, "R", is equal to 0.26.

Previous authors have not identified a range of solubilities for TiSi as in this study. A systematic shift of the crystalline reflections to lower 2θ positions in the X-ray patterns taken after each anneal identified this solubility. The volume of the orthorhombic cell for $Ti_{40}Si_{60}$ is considerably larger than the stoichiometric composition, thus indicating that silicon will occupy additional positions in the cell. An intensity calculation introducing titanium vacancies into the cell did not correspond to those measured experimentally. A structure identification of the monosilicide standard is unnecessary for the completion of the thick film study since experimental structure factors can be used.

Cyclic Heat Treatments

Large differences in thermal expansions (see Figure 2) between the silicon and titanium-silicides, and not a thermal fatigue process, were responsible for the mechanical instability of the thick films. Three separate times, 5, 10, and 15 minutes, at temperature were examined over a temperature range of 550 to 650°C (see Figure 7). Identical samples were cycled until fracture at a given temperature for different lengths of time at temperature. The results of these tests at 650, 625, and 600°C showed the fracture time to be independent of the total number of cycles in all samples (see Figure 7).

Samples cut to within a half-degree of the 111 planes exhibited a gradual fracture process (see Figures 8 and 9) initiating at the outer perimeter of the specimen. This fracture characteristic was also found in the larger samples diffused in step heat treatments described

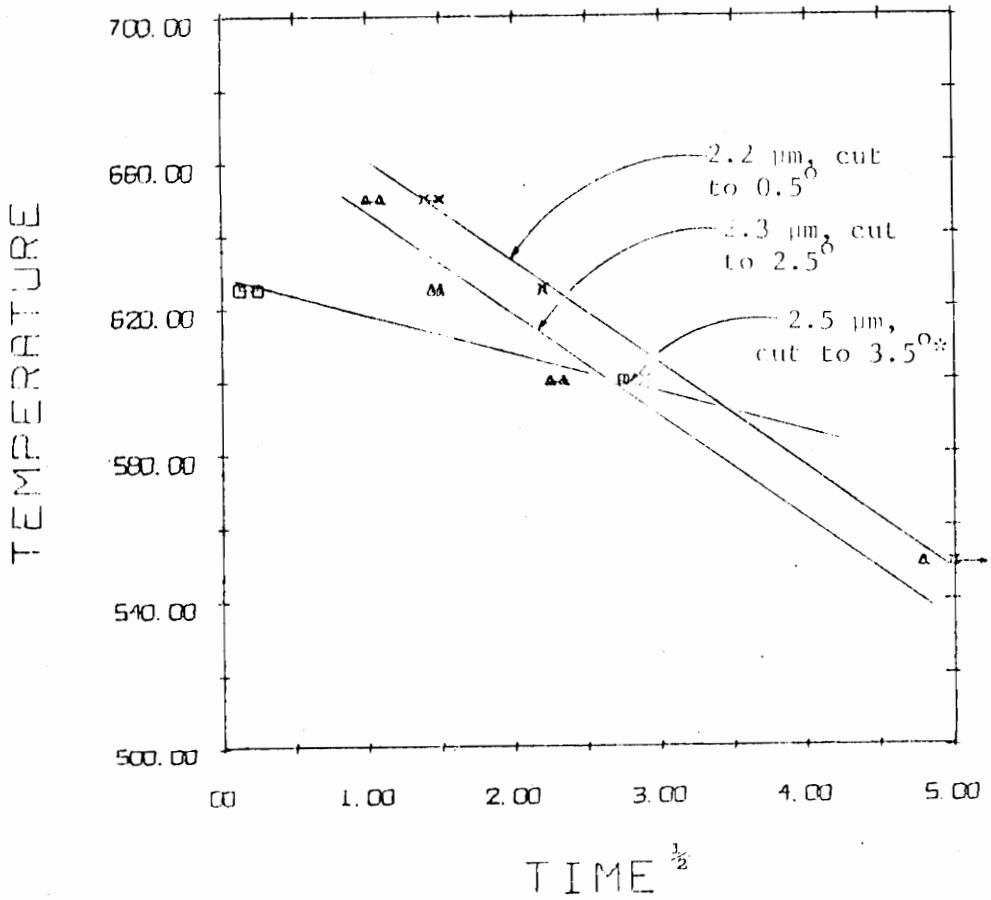

Figure 7. Plot of heat treatment temperature (°C) vs. $(\text{time})^{\frac{1}{2}}$ to fracture of cyclic anneals on thin films. The effect of substrate deposition temperature, film thickness, and cut of the silicon single crystal to the 111 planes on the mechanical stability of the reacted film are major concerns in these studies.

* Lower substrate deposition temperature.

Figure 8. Scanning electron micrograph of titanium thick film surface (2.2 μm) after cyclic anneal at 650°C, total time of 2 hours. Magnification 100X; Tilt = 20°.

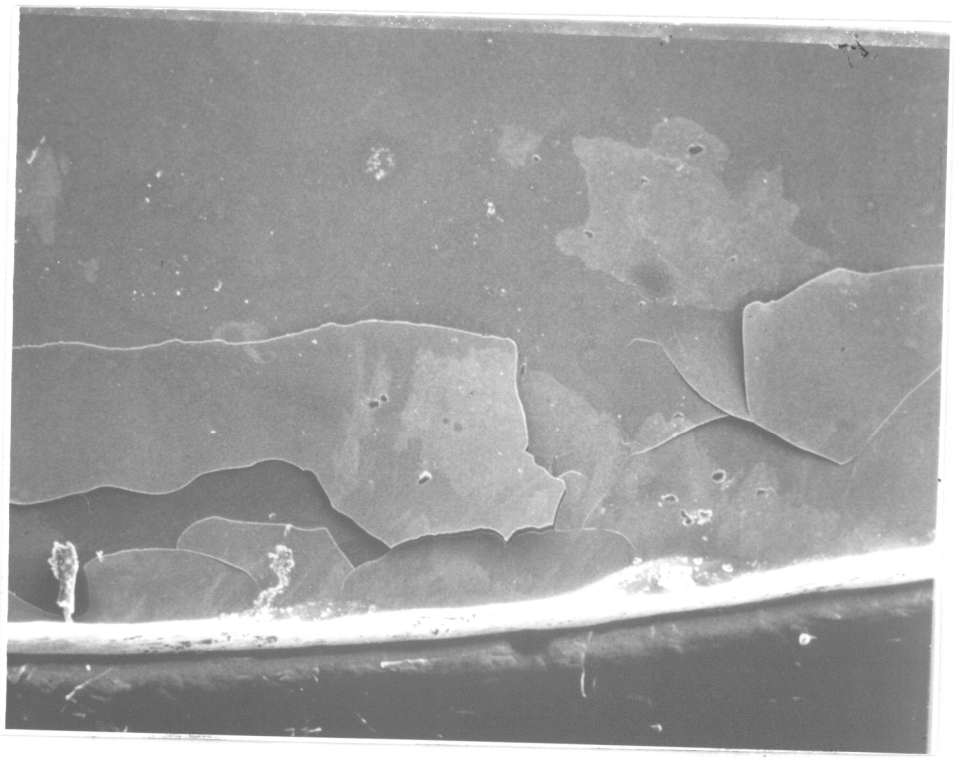

Figure 9. Scanning electron micrograph of titanium thick film surface (2.2 μm) after cyclic anneal at 650°C, total time of 5 hours. The entire film flaked off at this stage of annealing. Magnification 100X; Tilt = 20°.

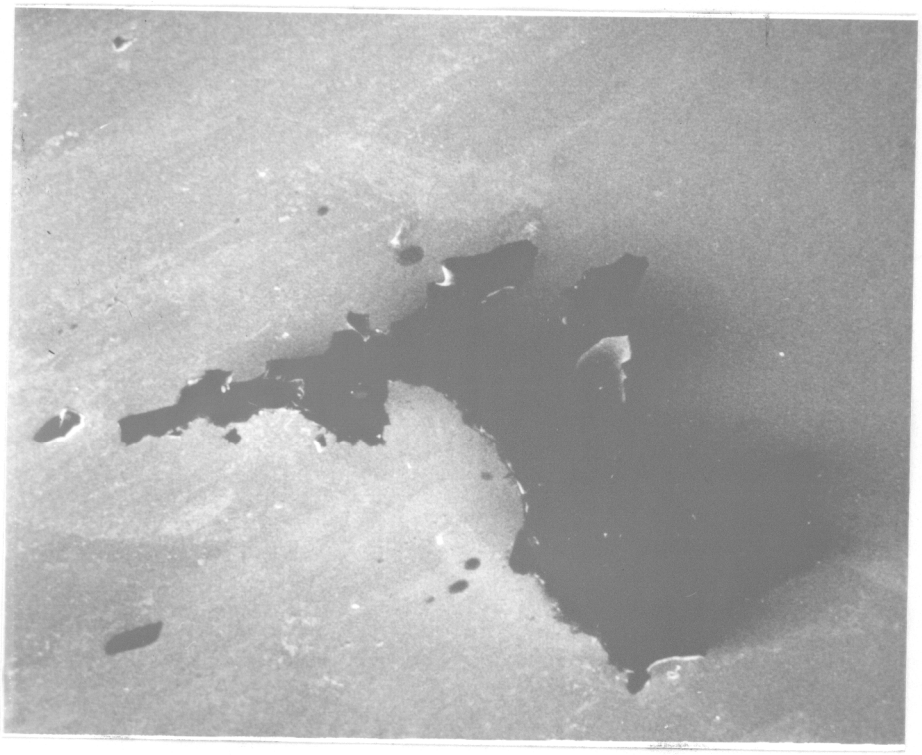

Figure 10. Scanning electron micrograph of titanium thick film surface (2.3 μm) after total annealing time of 1 hour at 625°C. Magnification 100X; Tilt = 20°.

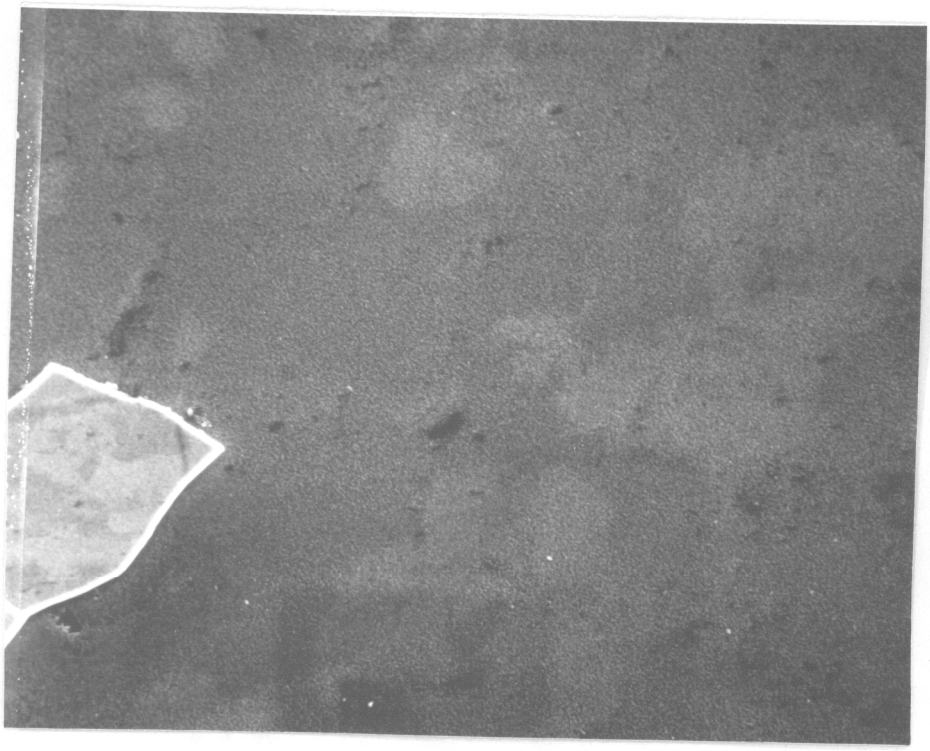

Figure 11. Scanning electron micrograph of titanium thick film surface (2.5 μm*) after cyclic anneal at 600°C, total time of 7½ hours. Magnification 500X; Tilt = 20°.

*Lower substrate deposition temperature.

in the latter part of this chapter. All other samples (described in Section IV) had a spontaneous fracture point (see Figures 10 and 11). The data collected on Figure 7 served in planning anneals for the larger X-ray samples.

Optimum deposition temperature appears to be at 350°C since greater interface instability exists in films deposited at 275°C. It appears, as in mechanical fatigue, that an endurance limit may exist allowing samples to be cycled indefinitely below this temperature. Complete information on the effect of substrate cut, film thickness, and surface roughness of the silicon substrate on the endurance limit is not available. An attempt to retain the reacted structures after one hour at temperature with a cooling rate of 3°C per minute resulted in the same characteristic fracture at approximately 300°C. In every case, fracture occurs on cooling after annealing within a well defined temperature range. Most often the fracture correlates with measurable silicide formation.

Step and Isothermal Anneals

A total of eight two-hour diffusion treatments at temperatures from 350 to 650°C were carried out on a 2.2 micron titanium thick film, cut to within one-half degree of the 111 planes. The first step anneal was chosen at 350°C to facilitate comparison with the as-received sample deposited under similar conditions. Subsequent temperature increments were determined from cyclic anneals and general observations of conditions allowing the metallic films to remain adherent. Since the mechanical instability results from differences

in thermal expansions of the individual materials, the temperature increment was systematically decreased as higher reaction temperatures were approached. Systematic step anneal upwards from the deposition temperature indicated that X-ray line shift, line broadening and elastic bending of substrate are influenced by silicide formation.

Tables IV through XII are a list of integrated intensities at different two-theta positions of all diffracted intensity above statistical background for each of the eight anneals. It should be emphasized that very little high angle diffracted intensity is present in these thick film samples. The computer simulations of these high angle regions are only semi-quantitative and all foundations for a diffuse model are based on the low angle regions. The half-widths of lines lying at 2θ positions greater than 50° are the only simulated parameters in which confidence can be placed. Figures 12 through 33 are the corresponding computer simulations where the points represent the experimental intensity. The individual simulated reflections along with the summed intensity is displayed in each figure for comparison of the fit. Table XVI lists the Pearson function parameters for each step anneal. A modified Lorentzian (m=2) best approximated the shape of the X-ray diffraction peaks throughout the anneals with the one exception being the titanium (011) at reaction temperatures of 600 through $650^{\circ}C$, where "m" equals five.

In order to measure the response of the elastically bent substrate to silicide formation, optical interference measurements of the deflection in the sample were made and the contours plotted on Figures

35a and b. The maximum deflection of the substrate decrease with increasing diffusion temperature or time corresponding to increased silicide formation. In contrast, Figure 36 displays the profile of a 2.5 micron thick film cut to within three and a half degrees of the 111 planes. The convex profile suggests that orientation of the silicon cut affects the amount of strain present in the film and thus the mechanical stability.

An isothermal anneal for times of 15 and 30 minutes at 625°C reflect the effect of substrate orientation on silicide formation. Samples cut to within two and a half degrees of the 111 planes exhibited a lack of appreciable strain in the plane of the metallic film. Tables XIII through XV are lists of integrated intensities at different two-theta positions for each anneal. The X-ray simulations needed to determine the preferred orientation and resolution of the silicides formed are presented in Figures 36 to 45. Once again, a modified Lorentzian distribution sufficiently approximated all diffraction peaks. Table XVII contains the parameters of the Pearson distribution for each individual reflection observed as a contribution to the total experimental intensity.

It is evident from each set of simulations for the step and isothermal annealed samples that two distinct orientations of the titanium are present although a strong basal plane orientation is common to both. The isothermal annealed specimen contained a tensile strain on the (010) prism planes and a compressive one along the basal plane (002) which decreased with increasing diffusion time. Titanium

monosilicide (0.1 μm) present at the interface was strongly preferred in the as-received sample. The silicide thickness increased to half a micron after treatment for 30 minutes and fractured on cooling from a subsequent anneal for an additional 30 minutes (see Figure 9). The fracture corresponded to the cyclic heat treatment analysis of these specimens (see Figure 7) and substantiated a previous conclusion for the fracture mechanism.

The titanium film remained adherent throughout all eight stepped anneals; however, cracks initiating at the perimeter of the sample were present after the final treatment. The existence of titanium monosilicide as a dispersed phase (see Figure 46) in the initial thin film structure exemplified the dominance of grain boundary diffusion and nucleation at 350°C. A step anneal at 350°C produced an approximate doubling of the volume fraction of monosilicide contained in the titanium, from two to five percent (see Figures 12-15). The monosilicide was random in orientation during all anneals and was a constant volume fraction of the remaining titanium film. If the monosilicide were a planar deposit at the interface, a 0.2 μm decrease of the plating would be required. The simulation was forced to fit at low angles, relaxing on the condition of "g" factors summing to one and conservation of material, yet the higher angle intensity region failed to yield a reasonable solution (see Figure 56).

Annealing upwards from the deposition temperature resulted in the formation of a planar titanium disilicide deposit (see Figures 47-49) at the original titanium-silicon interface. A linear decrease of "g"

from the silicon substrate with increasing silicide formation was observed (see Figure 54) in each subsequent anneal (see Figures 50-52). The final treatment at 650°C resulted in a maximum thickness of the disilicide (3.9 μm) and the formation of a planar deposit of monosilicide at the titanium-disilicide interface (see Figure 53).

Uniform tensile strains in the plane of the titanium film varied insignificantly for the crystallographic planes displayed in Figure 56 in this series of heat treatments. The prism planes (010), whose modulus of elasticity is ten smaller[39] when compared to the (002) and (011), showed the largest Poisson's contraction in the planes parallel to the surface. Correspondingly, the smallest non-uniform strain (line broadening) was associated with the (010) planes which are the slip planes in titanium[40]. The X-ray strain data does concur with the mechanical constants presented in that a low modulus of elasticity for a given plane will display a large Poisson contraction and less non-uniform strain. Line brodening increased with silicide formation for all reflections of titanium.

The disilicide reflection remained sharp after all stepped anneals, thus agreeing with the bulk sample which found titanium and silicon insoluble in $TiSi_2$. In the completely diffused sample, the monosilicide present as a film displayed additional line broadening, probably due to the range of compositions found for this silicide in the powder study. A weak preferred orientation of the TiSi in contrast to the orientation of the initial $TiSi_2$ layer, reflected the influence of distance from the single crystal silicon substrate.

Table XVIII is a list of X-ray data obtained for a step annealed sample, 2.5 microns thick and cut to within three and a half degrees of the 111 planes. The absence of any appreciable silicide formation indicated the lack of adhesion of the titanium film due to the lower substrate deposition temperature of 275°C.

Conclusions:

1. $TiSi_2$ was confirmed a C54 orthorhombic structure having corresponding structure factor forms and lattice parameters determined by this study. The compound is stoichiometric in composition exhibiting no solubility of titanium or silicon in it.
2. TiSi is not stoichiometric at low temperatures; rather a range of compositions and lattice parameters exist. Ti_5Si_4 is a high temperature compound, absent in equilibrium below 1050°C.
3. The thick film reaction between titanium and silicon differed from that of bulk samples, forming a large planar film of disilicide at the original interface. The disilicide film decreased the transport of silicon and a second reaction product of monosilicide formed at the titanium/disilicide interface.
4. The dominance of grain boundary diffusion and nucleation in a film diffused at a temperature of 350°C was observed, forming a dispersion of the lower free energy monosilicide. Temperatures of silicide formation[2] were higher in previous studies because of the presence of silicon oxide at the interface. The absence of degassing in the thick films verified that the method of preparation did eliminate the oxide layer on the substrate.

5. Mechanical instability of the film results from large thermal expansion differences of the components and silicide formation. The highly deformed nature, dependent on cut of the silicon crystal, warrented the use of computer simulation analysis of the X-ray diffraction patterns from the diffused structure.

Suggestions for Future Work

1. More detailed studies of the low temperature phase diagram for the titanium-silicon system is essential in characterizing the kinetics of silicide formation in thick film structures.
2. The effect of substrate orientations on silicide formation temperatures and phases characteristic to each should be explored holding the substrate deposition temperature at 350°C.
3. X-ray data obtained at temperature should provide sharper diffraction lines because of the absence of that mechanical deformation which is produced about each interface on cooling to room temperature. The intercomparison between at temperature data and room temperature data should provide considerable information on the deformation mechanisms which are active on cooling.

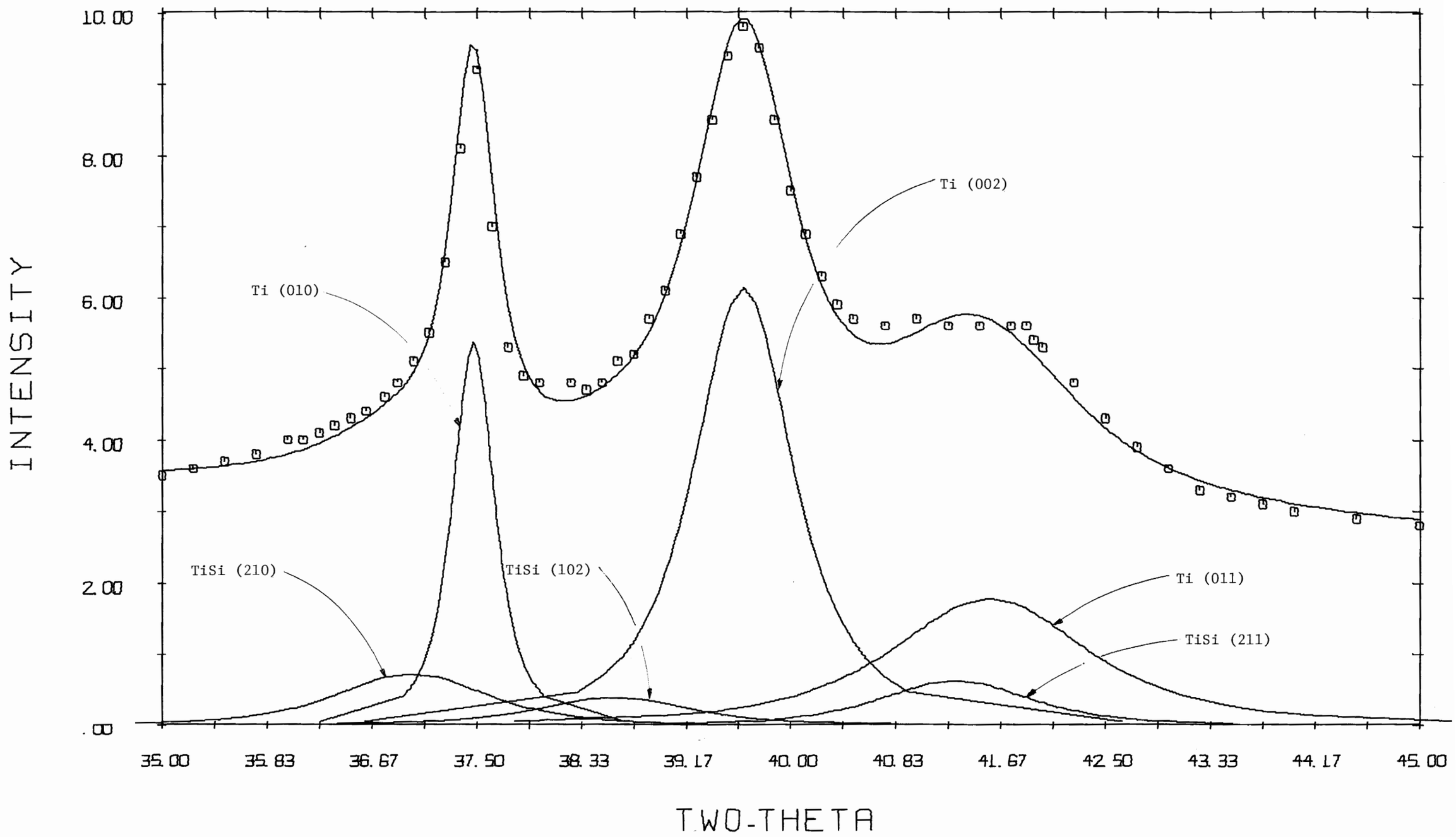

Figure 12. Experimental intensity simulation for as-received 2.2 μm titanium-silicon thin film, 2θ region from 35° to 45°.

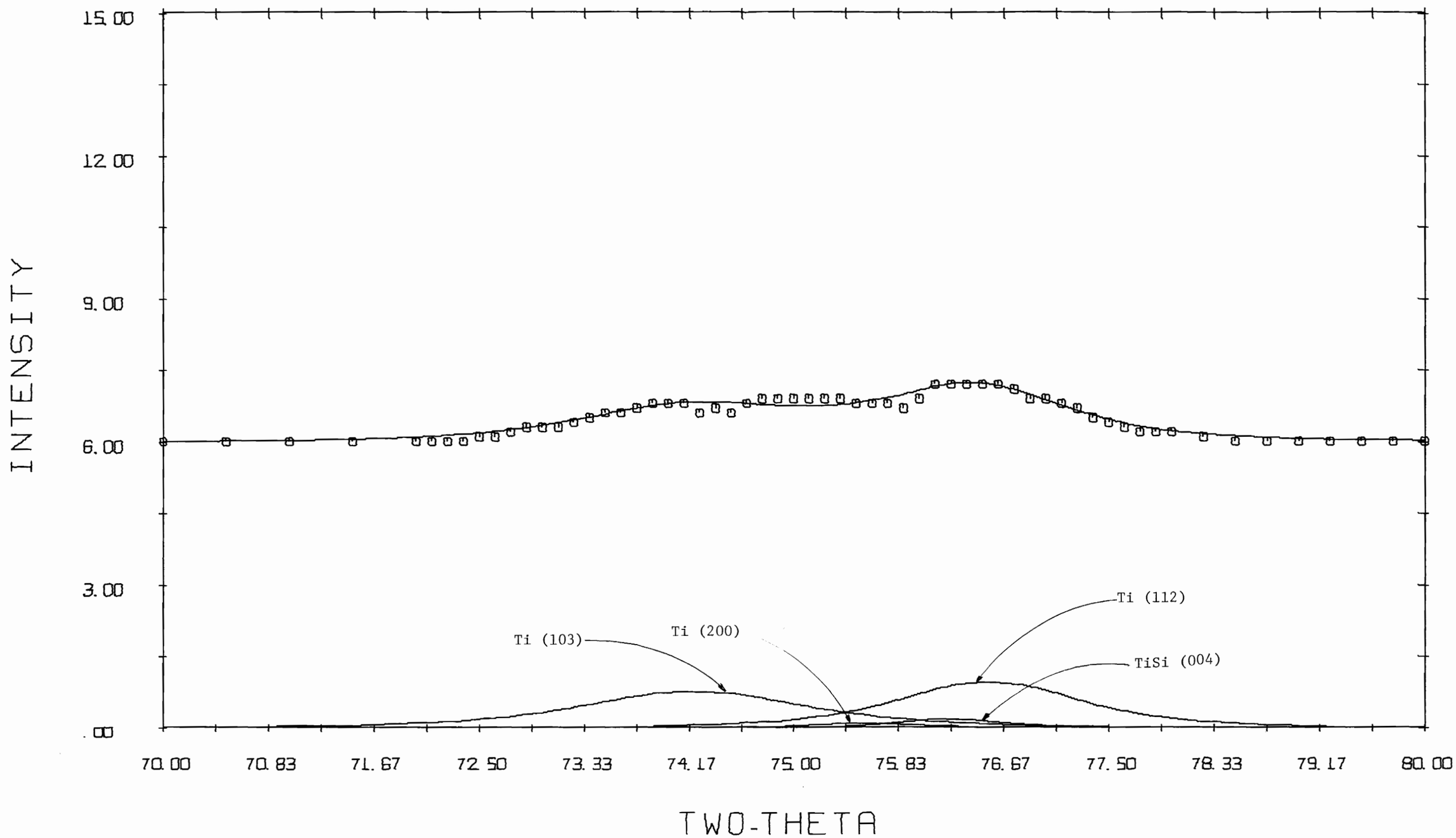

Figure 13. Experimental intensity simulation for as-received 2.2 micron titanium thin film, 2θ region from 70° to 80°.

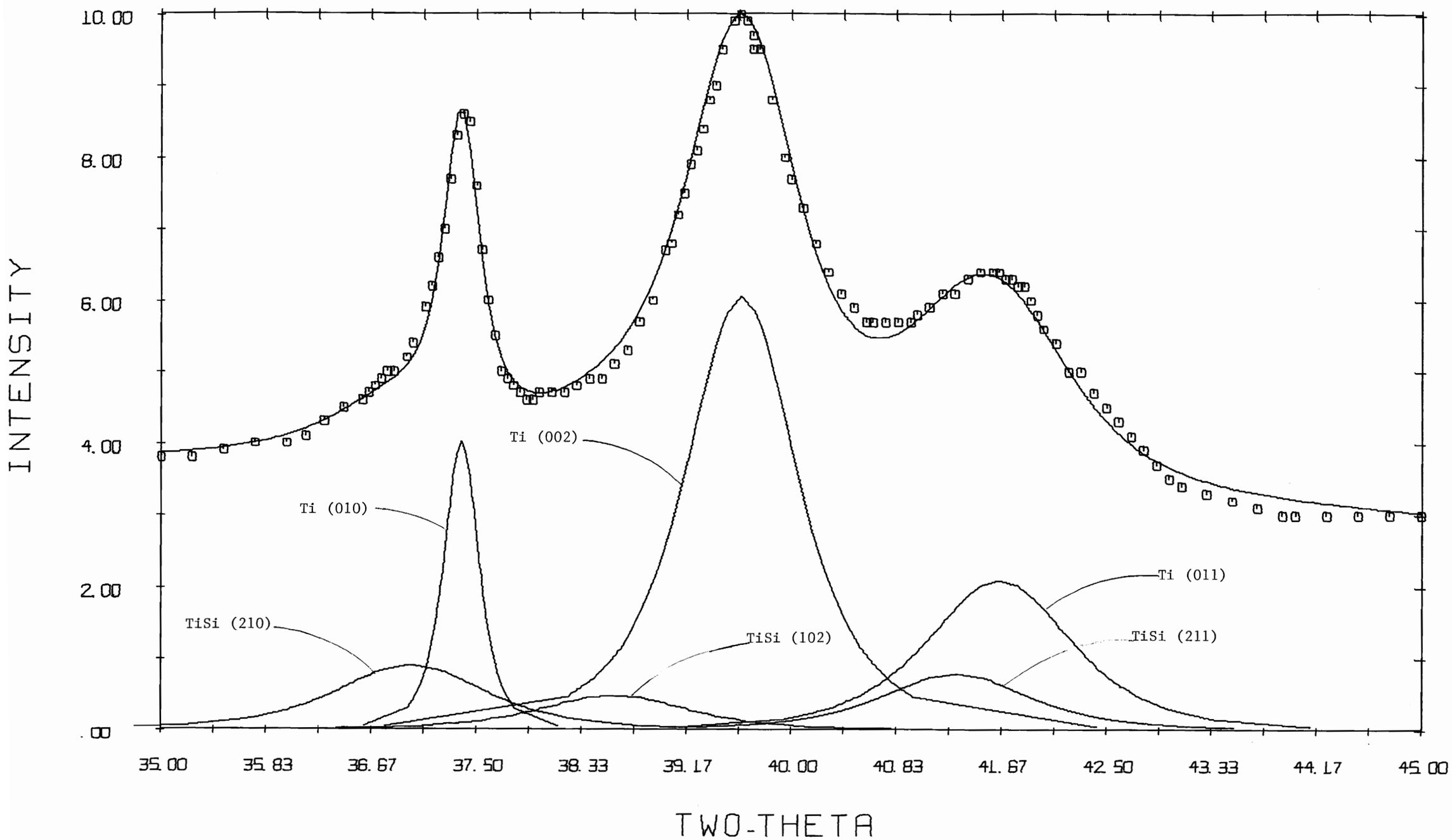

Figure 14. Experimental intensity simulation for step anneal for 2 hours at 350°C, 2θ region from 35° to 45°.

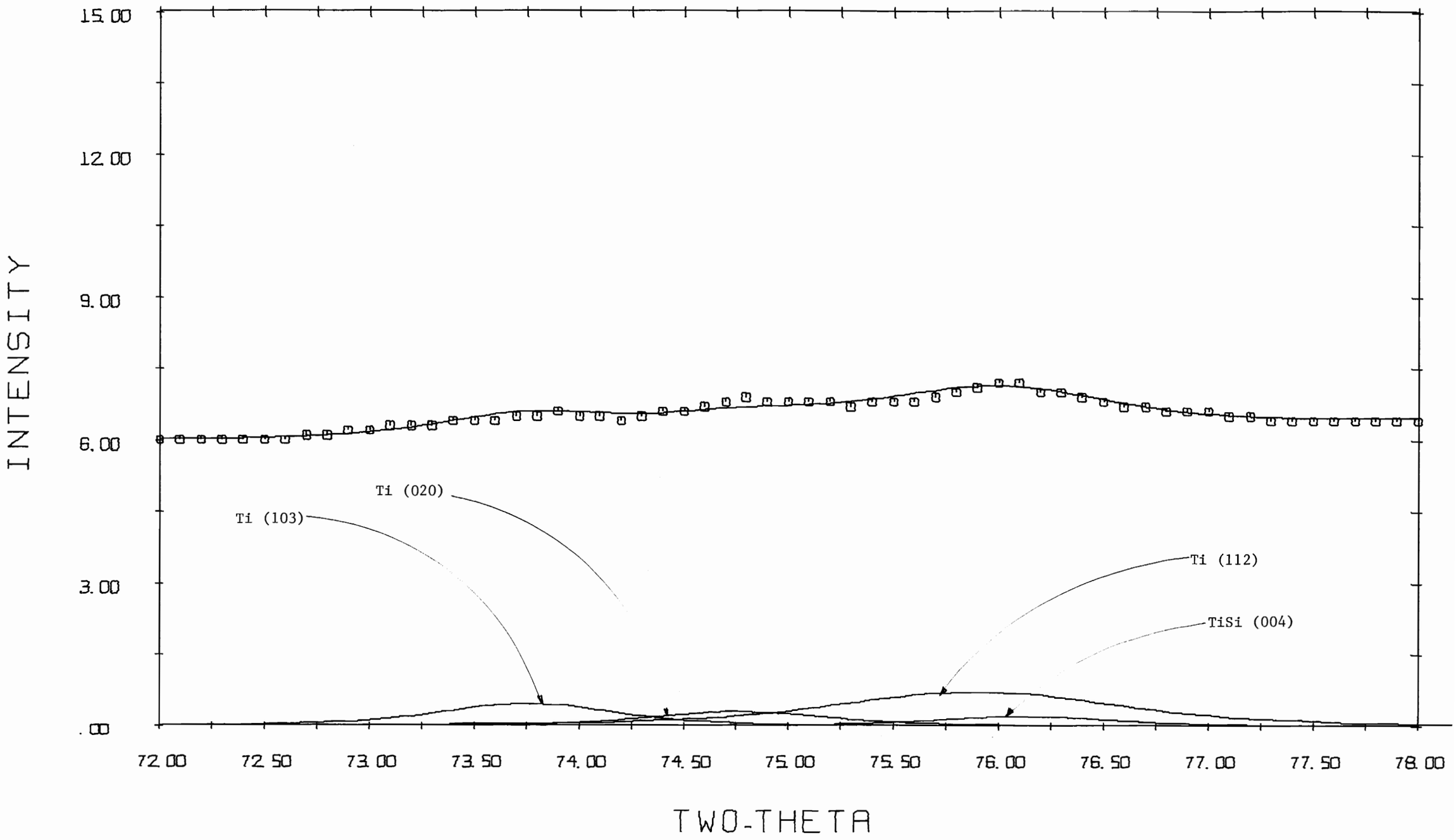

Figure 15. Experimental intensity simulation for step anneal for 2 hours at 350°C, 2θ region from 72° to 78°.

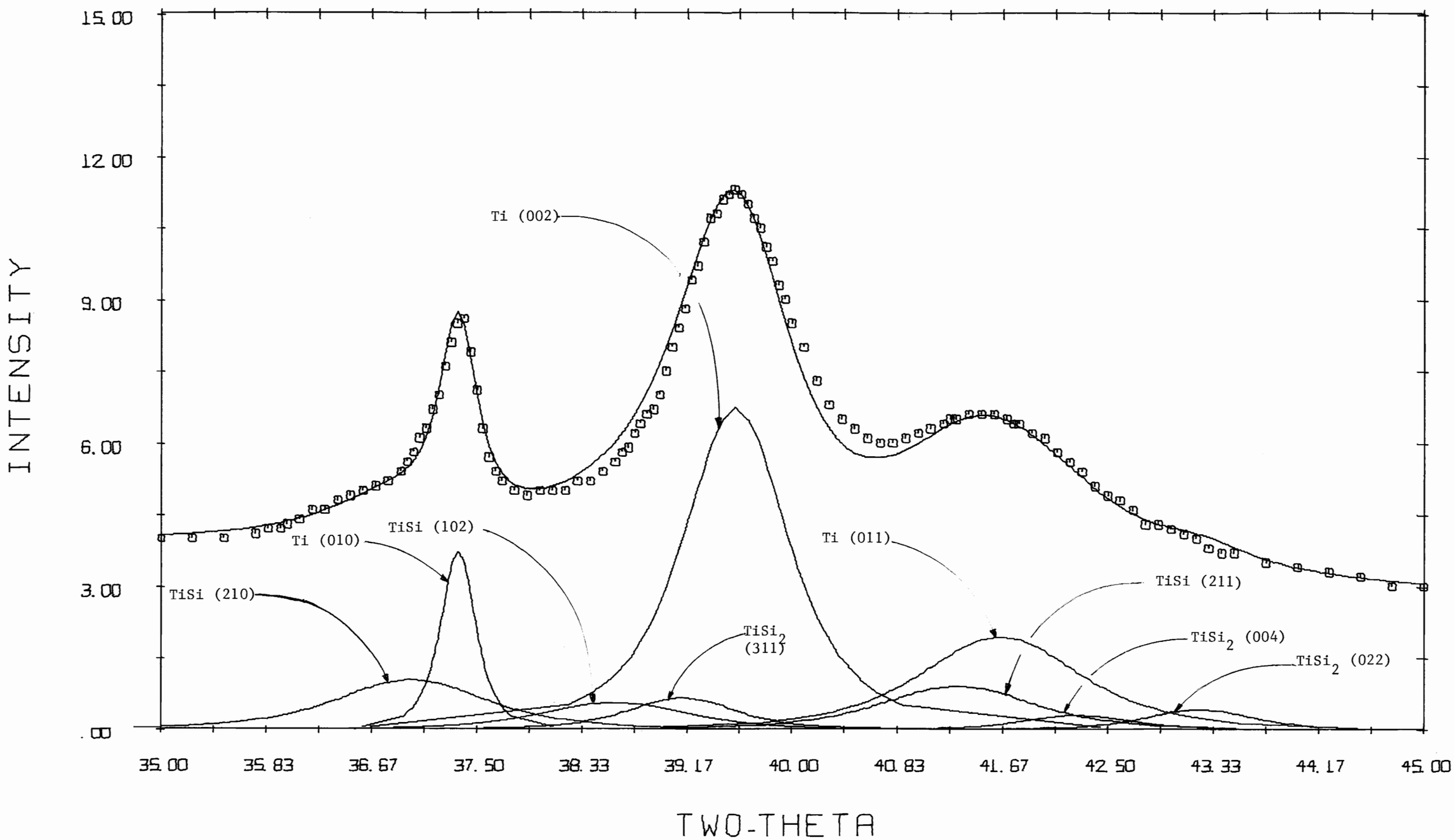

Figure 16. Experimental intensity simulation for step anneal for 2 hours at 450°C, 2θ region from 35° to 45°.

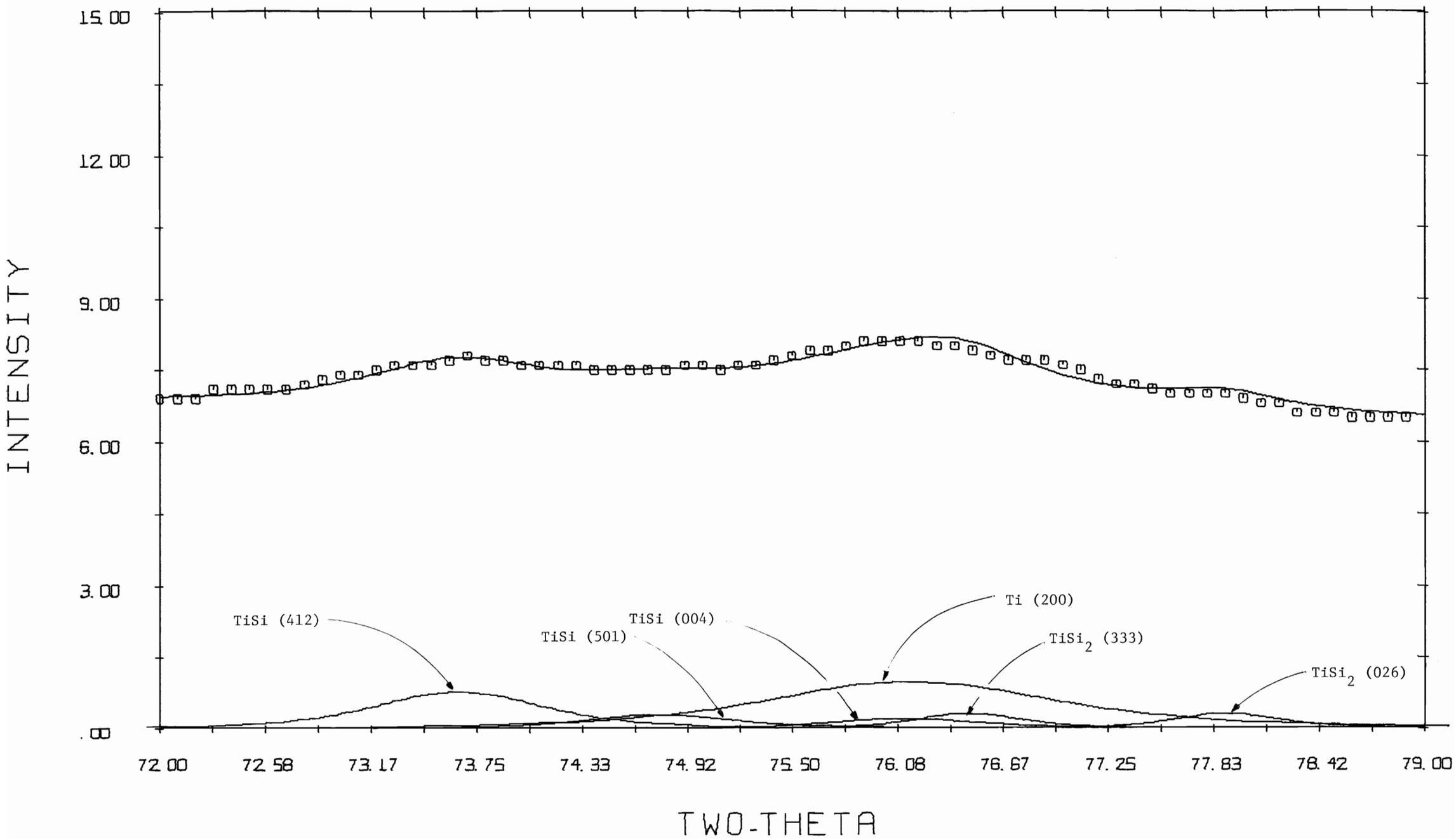

Figure 17. Experimental intensity simulation for step anneal for 2 hours at 450°C, 2θ region from 72° to 79°.

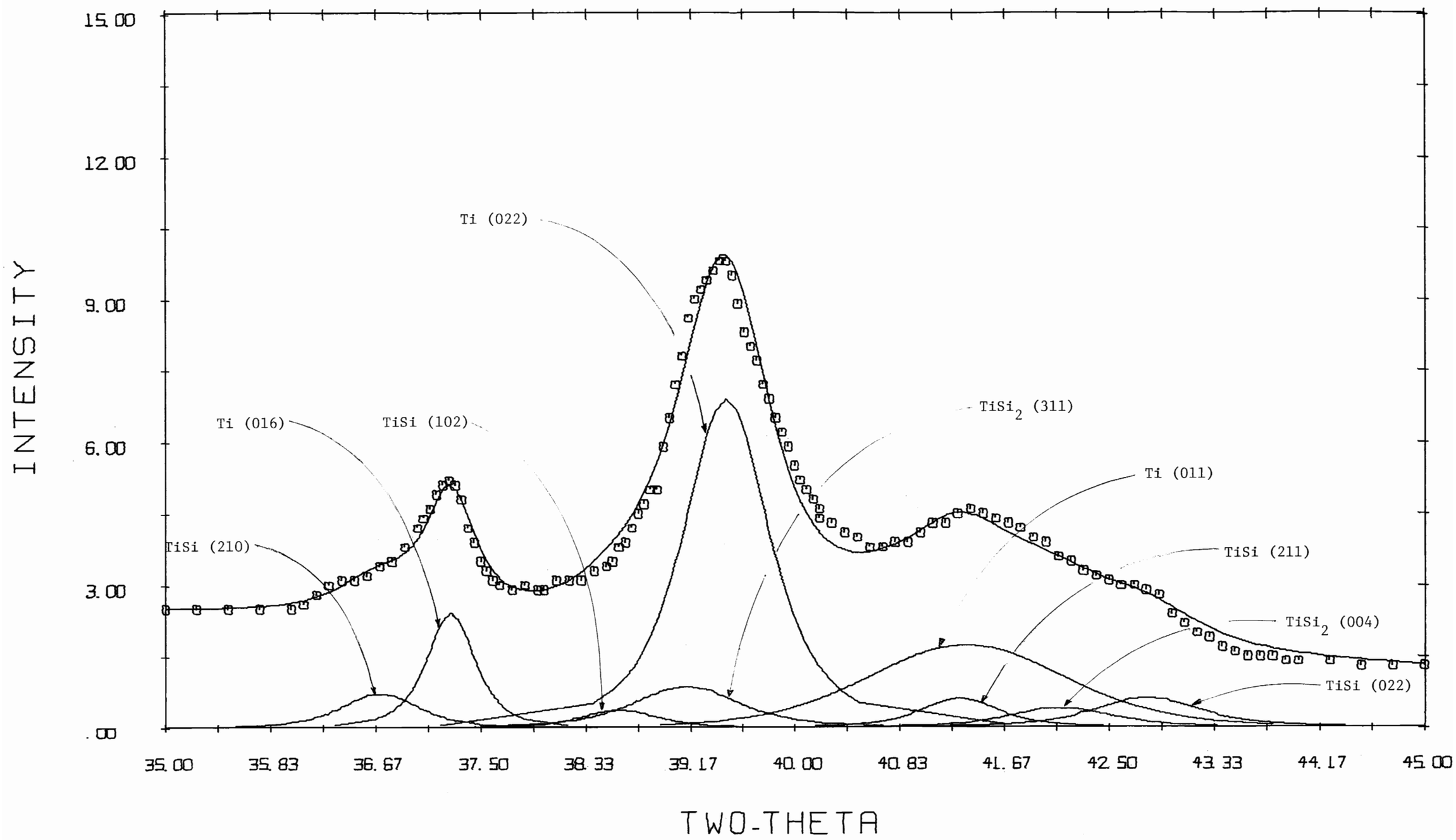

Figure 18. Experimental intensity simulation for step anneal for 2 hours at 500°C, 2θ region from 35° to 45°.

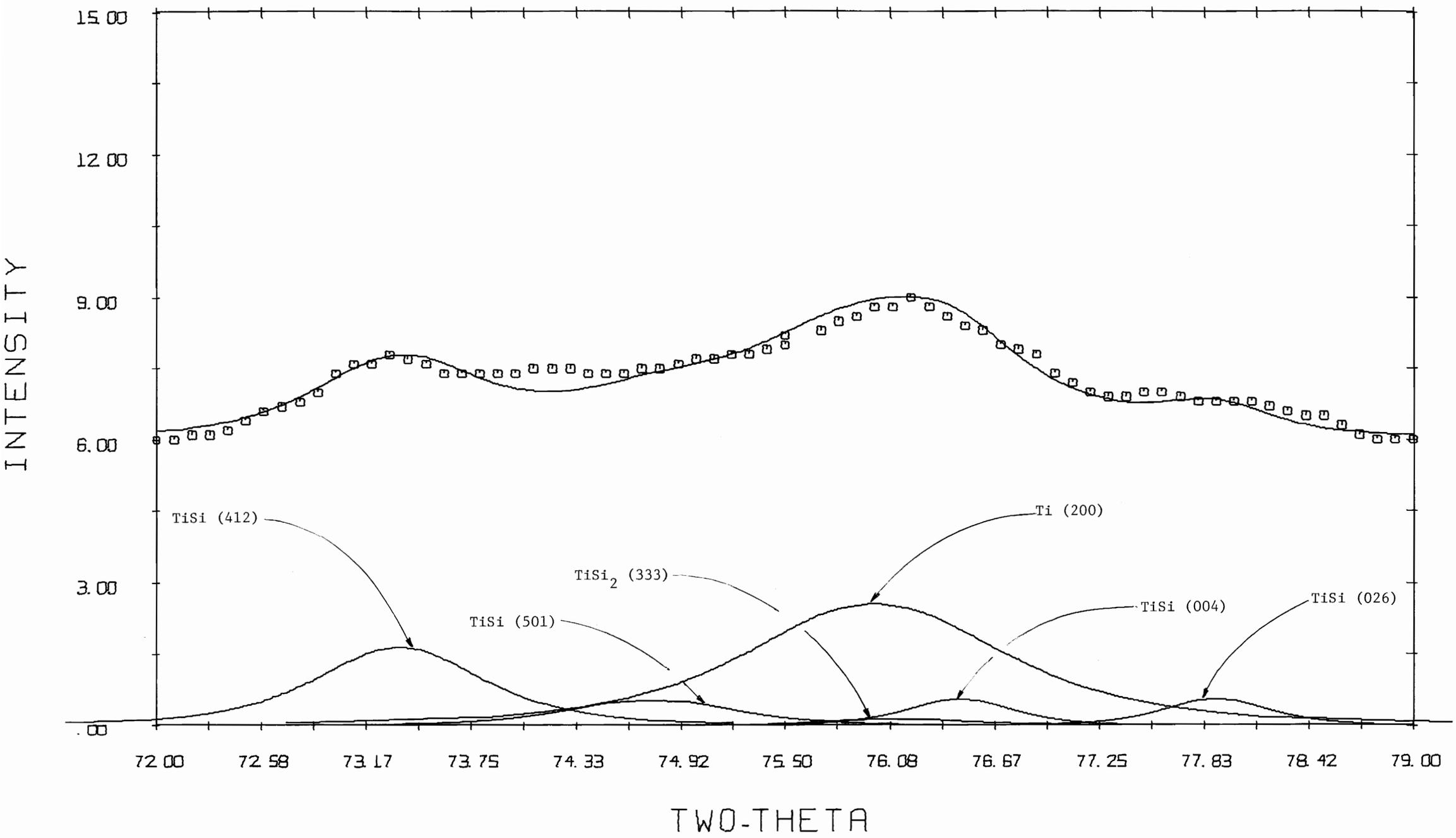

Figure 19. Experimental intensity simulation for step anneal for 2 hours at 500°C, 2θ region from 72° to 79°.

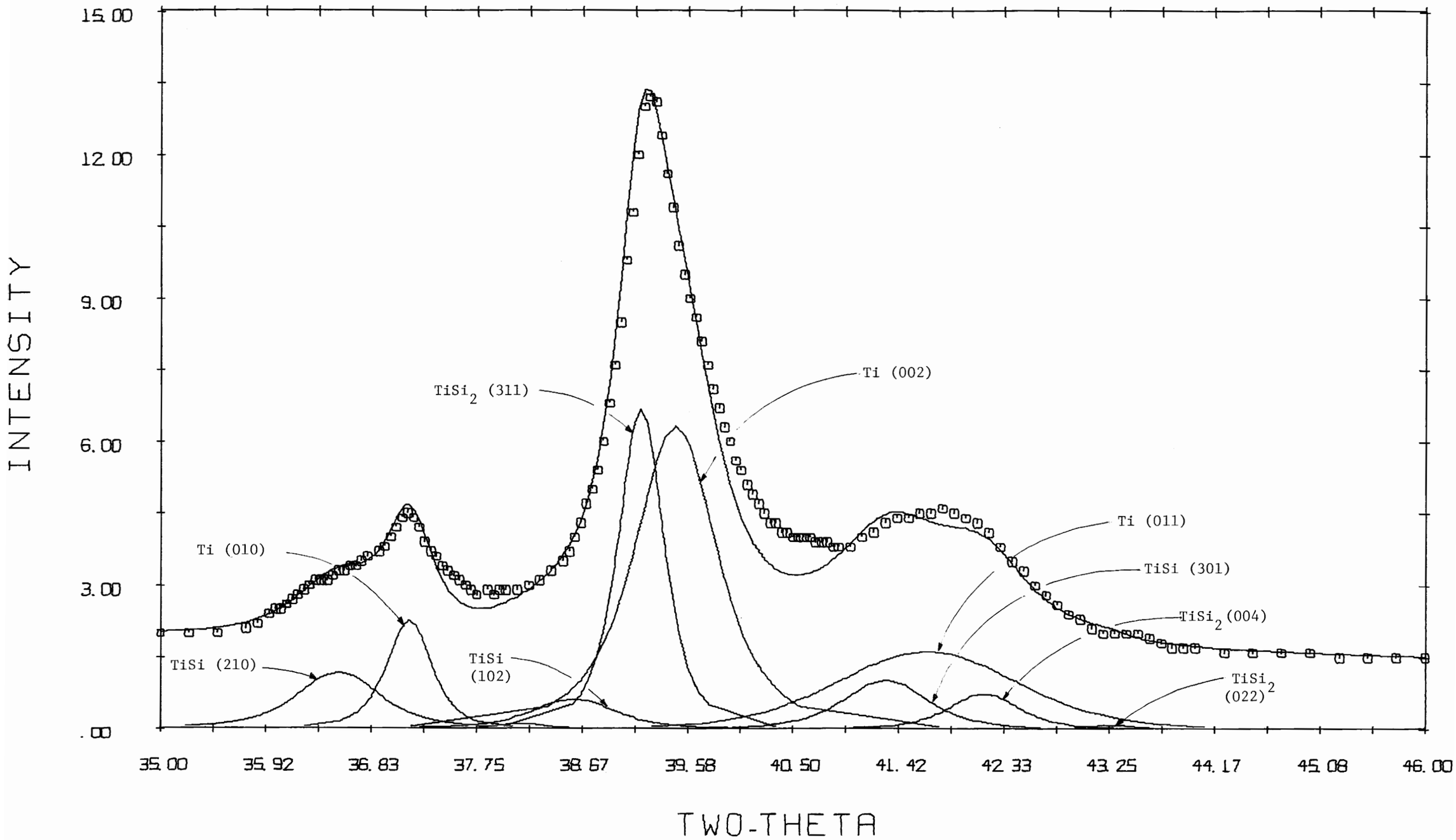

Figure 20. Experimental intensity simulation for step anneal for 2 hours at 550°C, 2θ region from 35° to 46°.

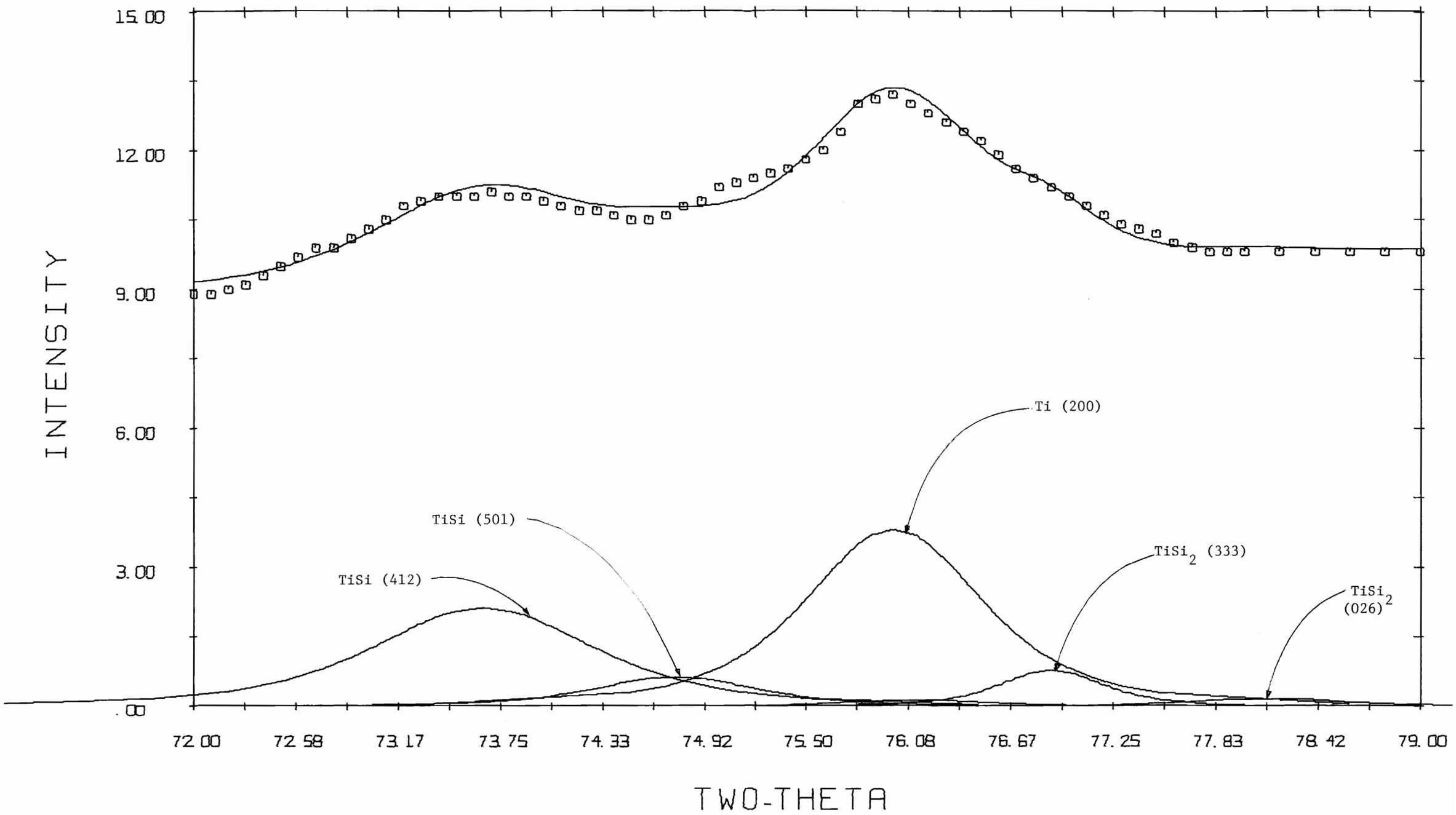

Figure 21. Experimental intensity simulation for step anneal for 2 hours at 550°C, 2θ region from 72° to 79°.

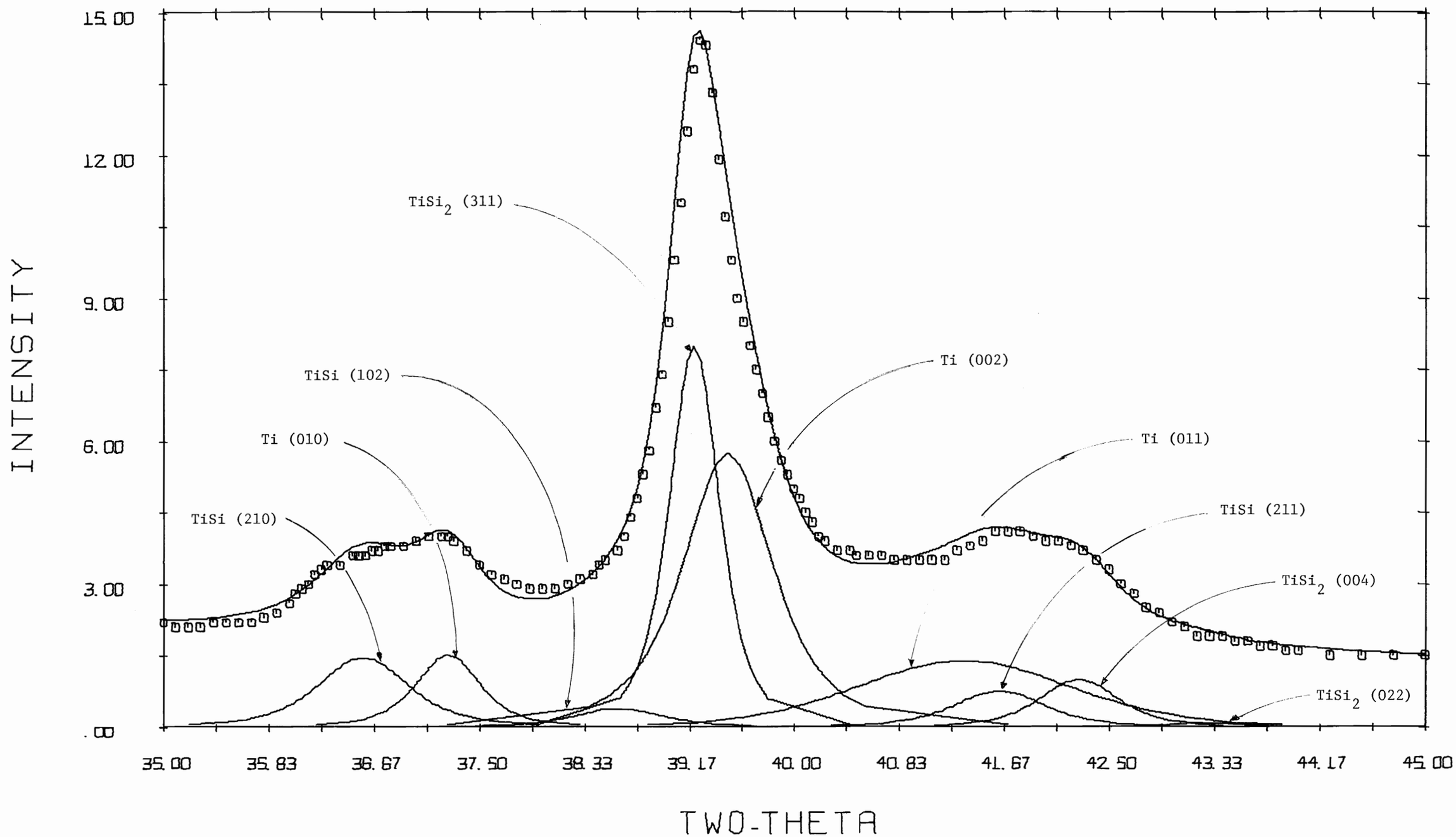

Figure 22. Experimental intensity simulation for step anneal for 2 hours at 575°C, 2θ region from 35° to 45°.

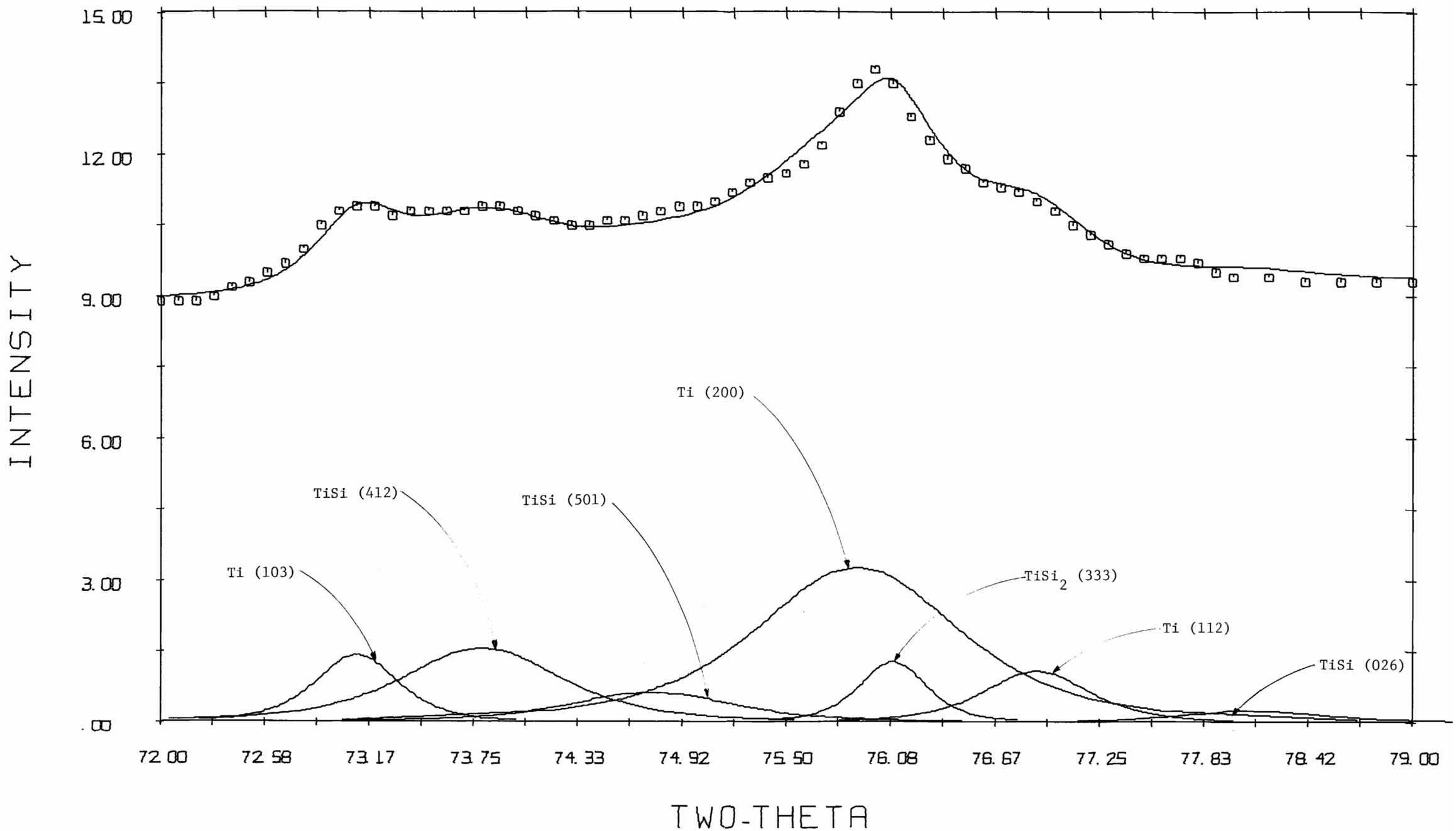

Figure 23. Experimental intensity simulation for step anneal for 2 hours at 575°C, 2θ region from 72° to 79°.

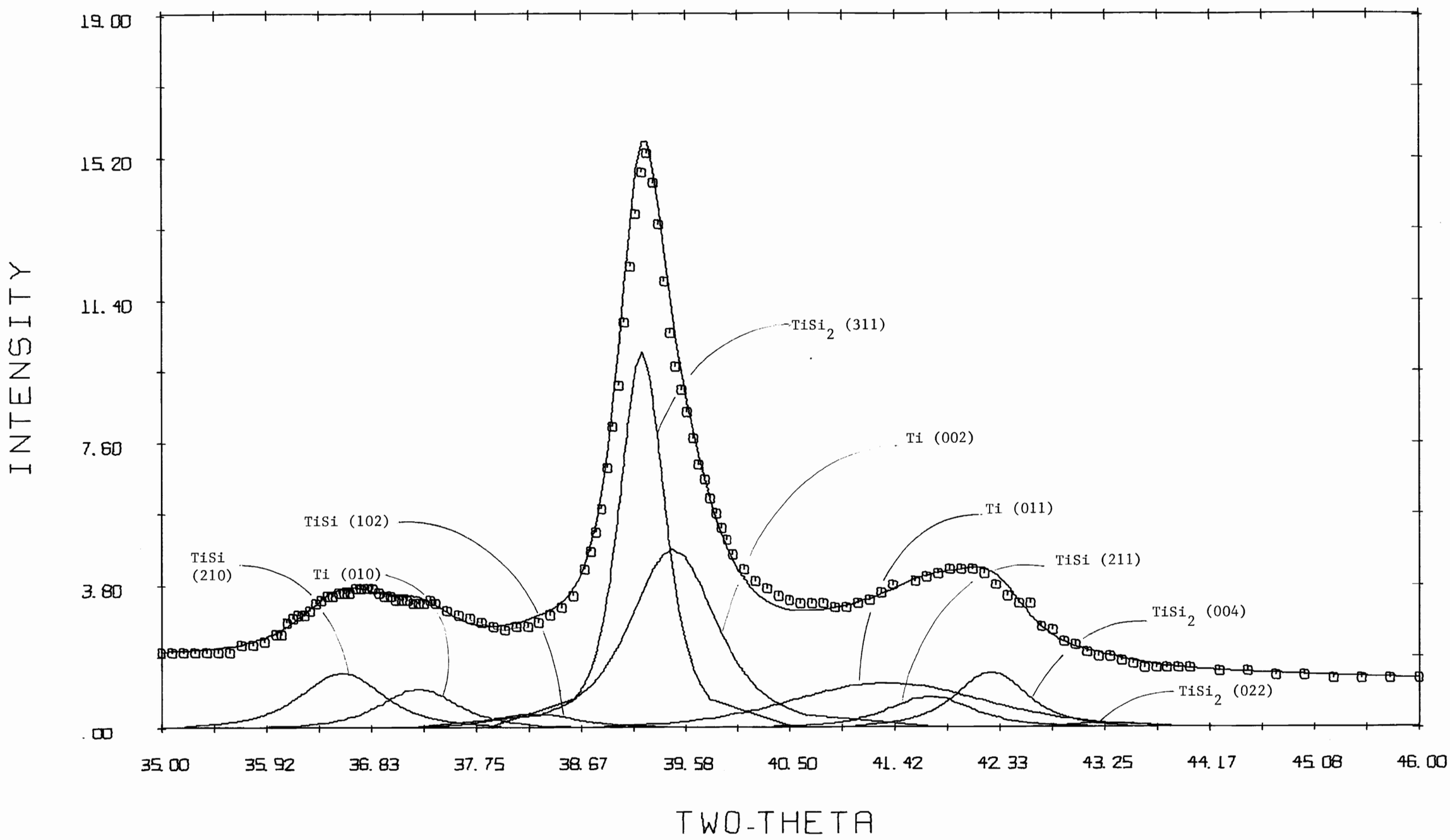

Figure 24. Experimental intensity simulation for step anneal for 2 hours at 600°C, 2θ region from 35° to 46°.

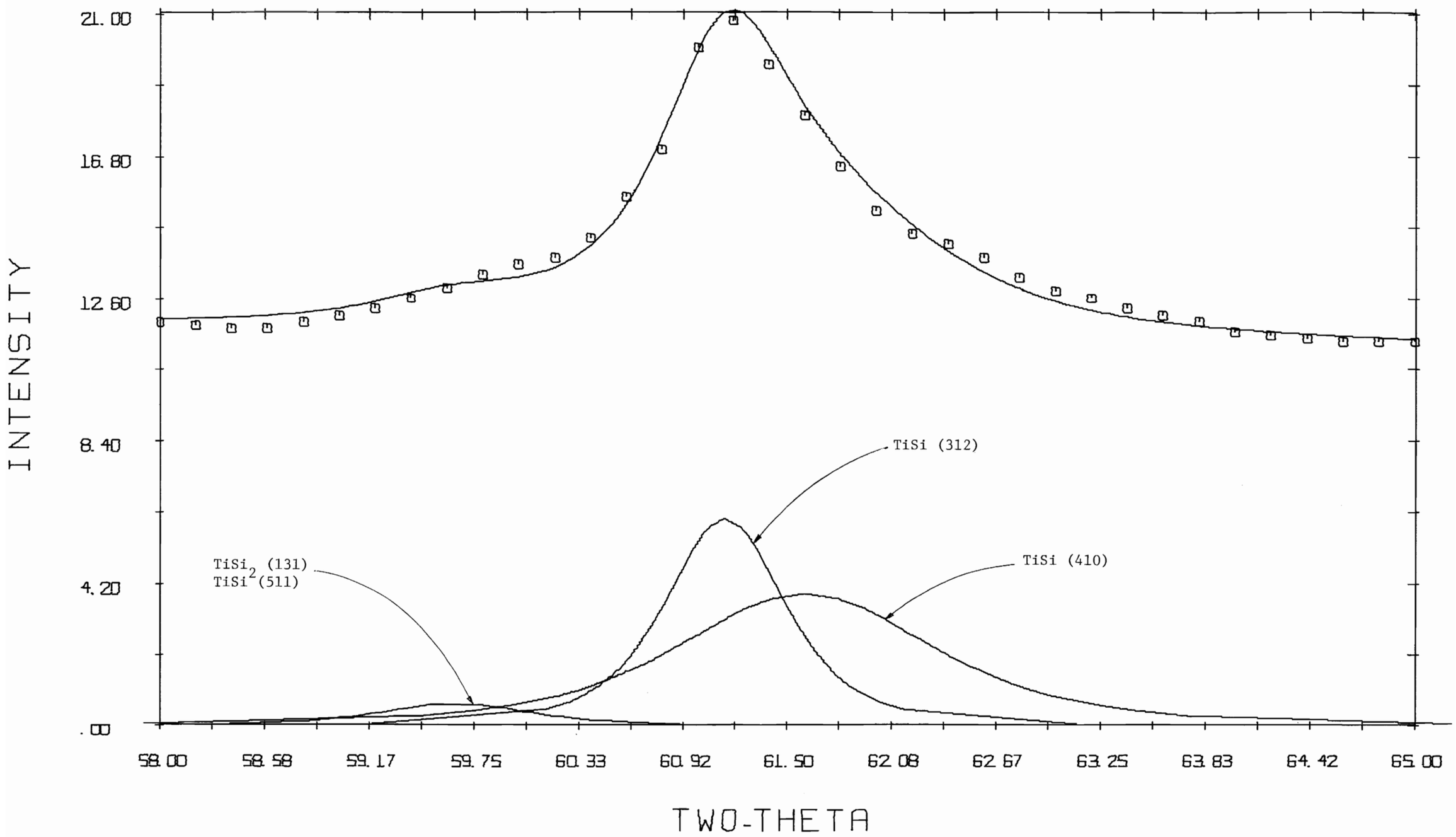

Figure 25. Experimental intensity simulation for step anneal for 2 hours at 600°C, 2θ region from 58° to 65°.

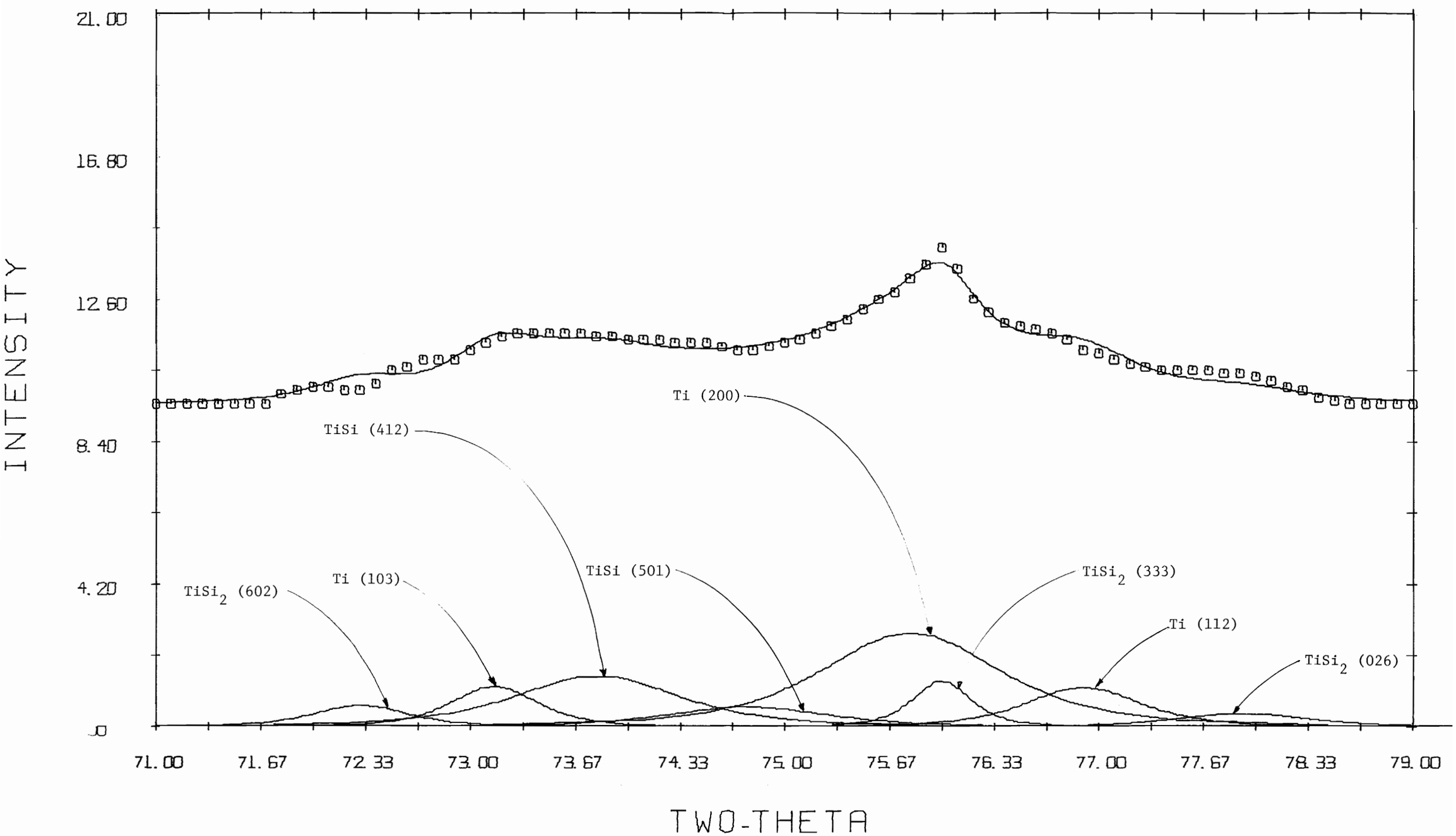

Figure 26. Experimental intensity simulation for step anneal for 2 hours at 600°C, 2θ region from 71° to 79°.

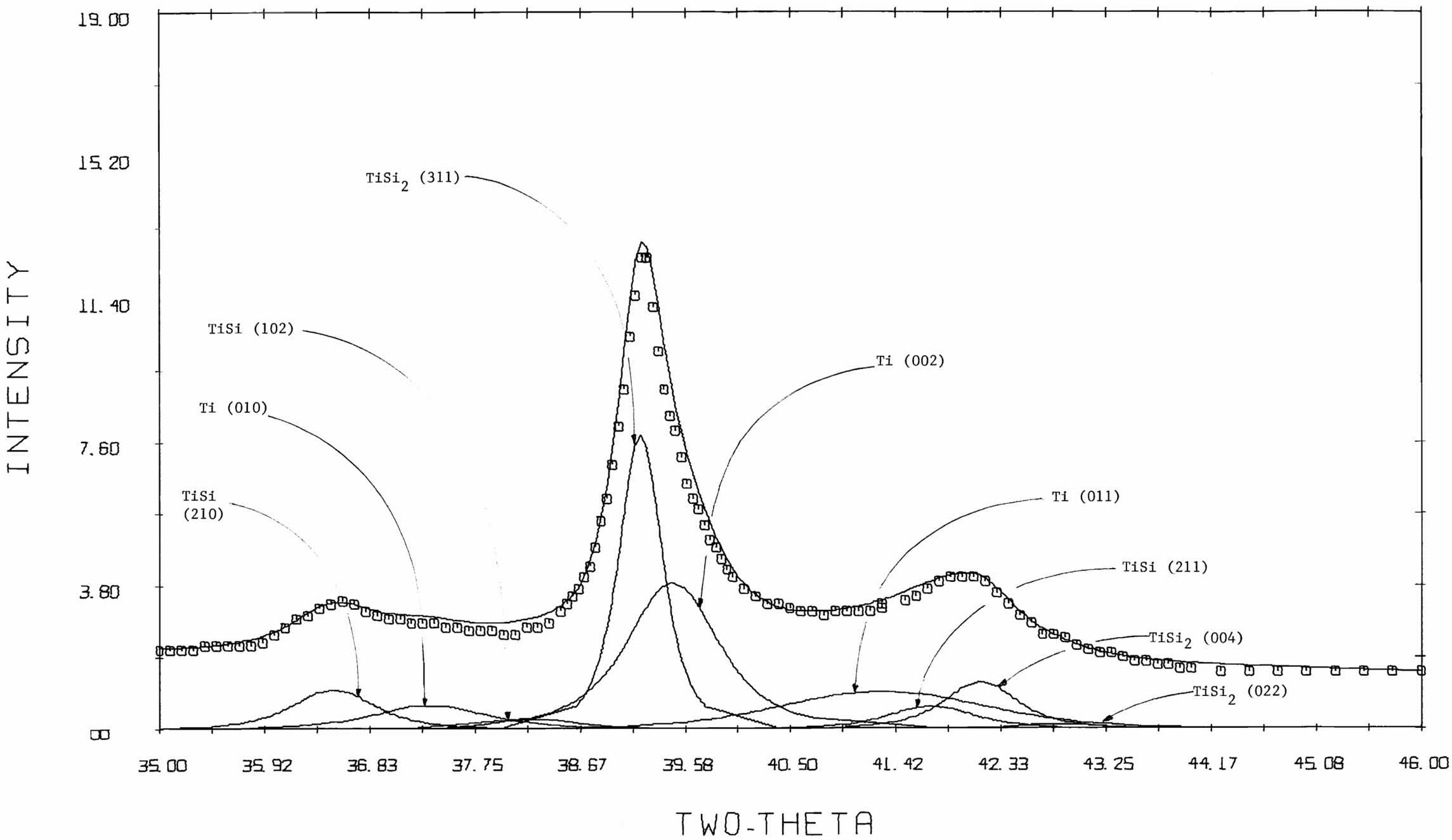

Figure 27. Experimental intensity simulation for step anneal for 2 hours at 625°C, 2θ region from 35° to 46°.

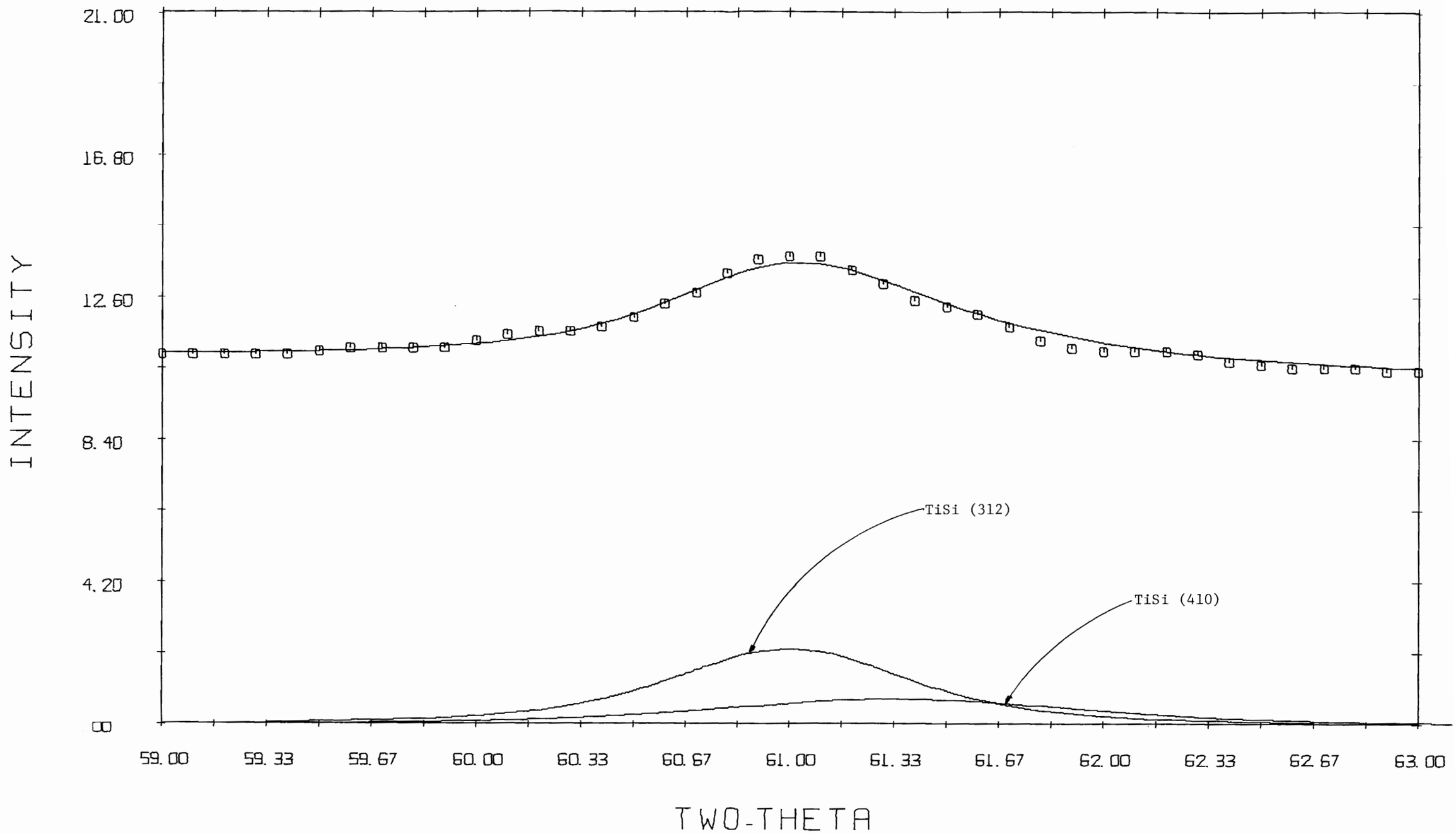

Figure 28. Experimental intensity simulation for step anneal for 2 hours at 625°C, 2θ region from 59° to 63°.

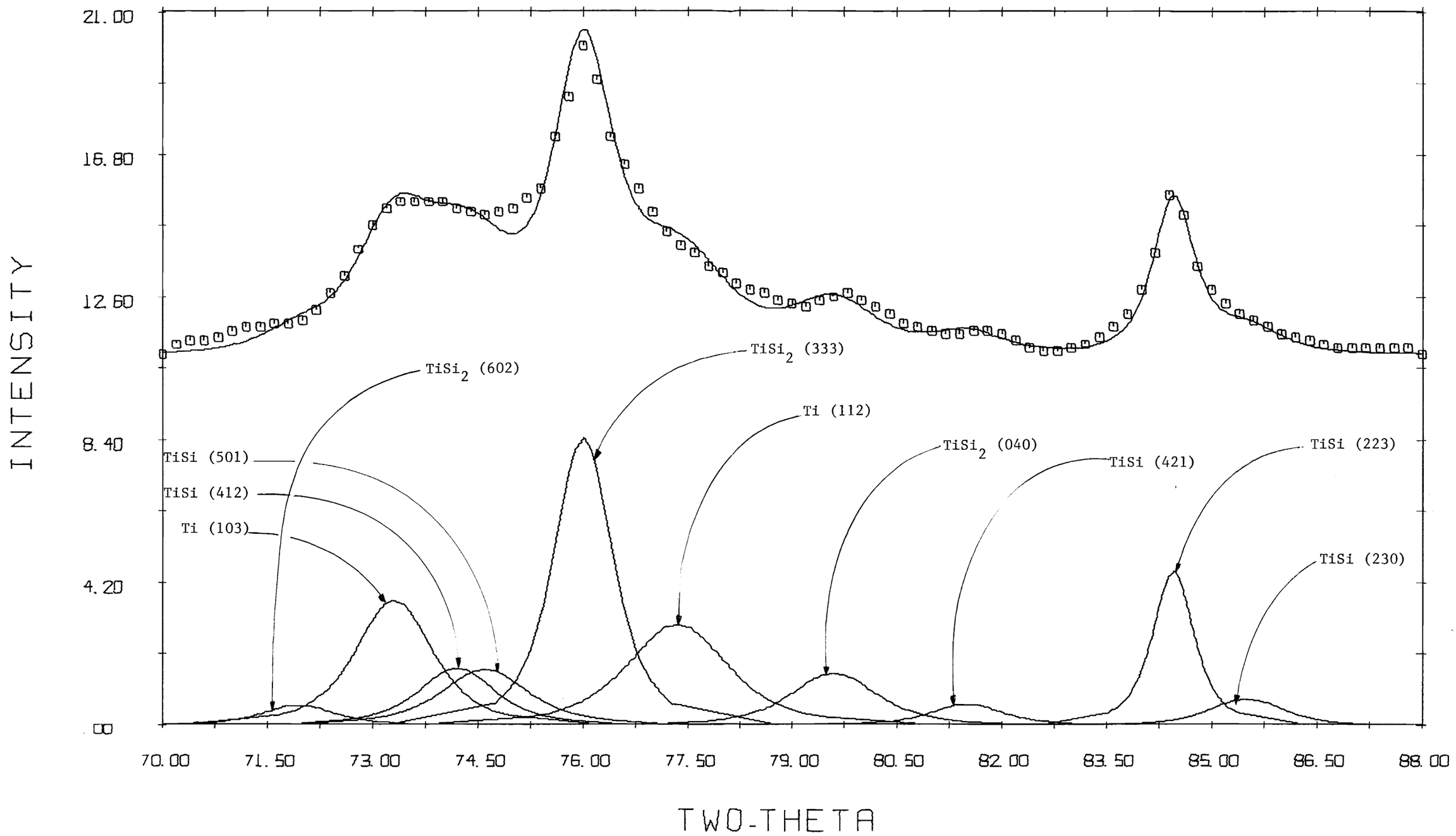

Figure 29. Experimental intensity simulation for step anneal for 2 hours at 625°C, 2θ region from 70° to 88°.

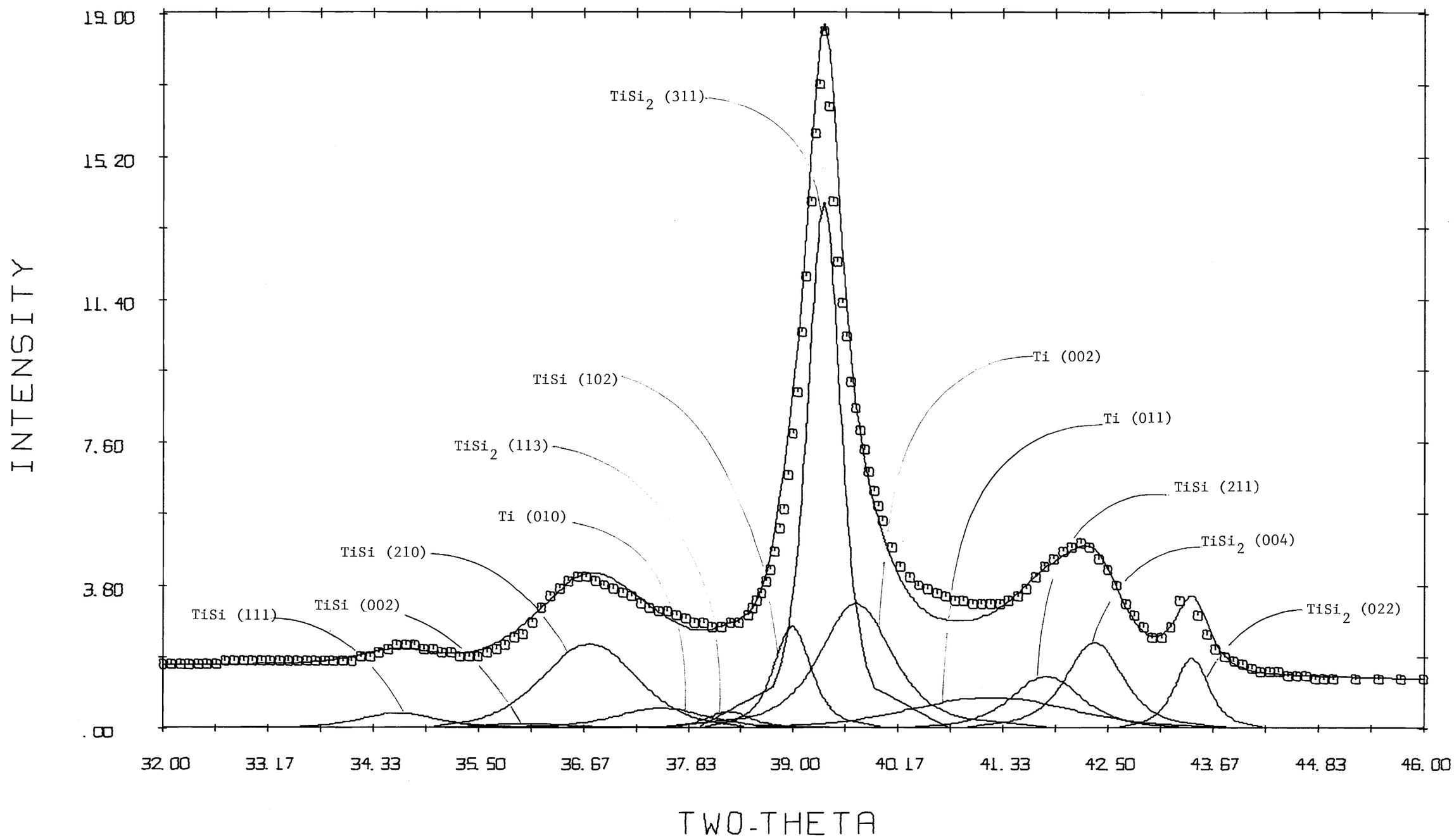

Figure 30. Experimental intensity simulation for step anneal for 2 hours at 650°C, 2θ region from 32° to 46°.

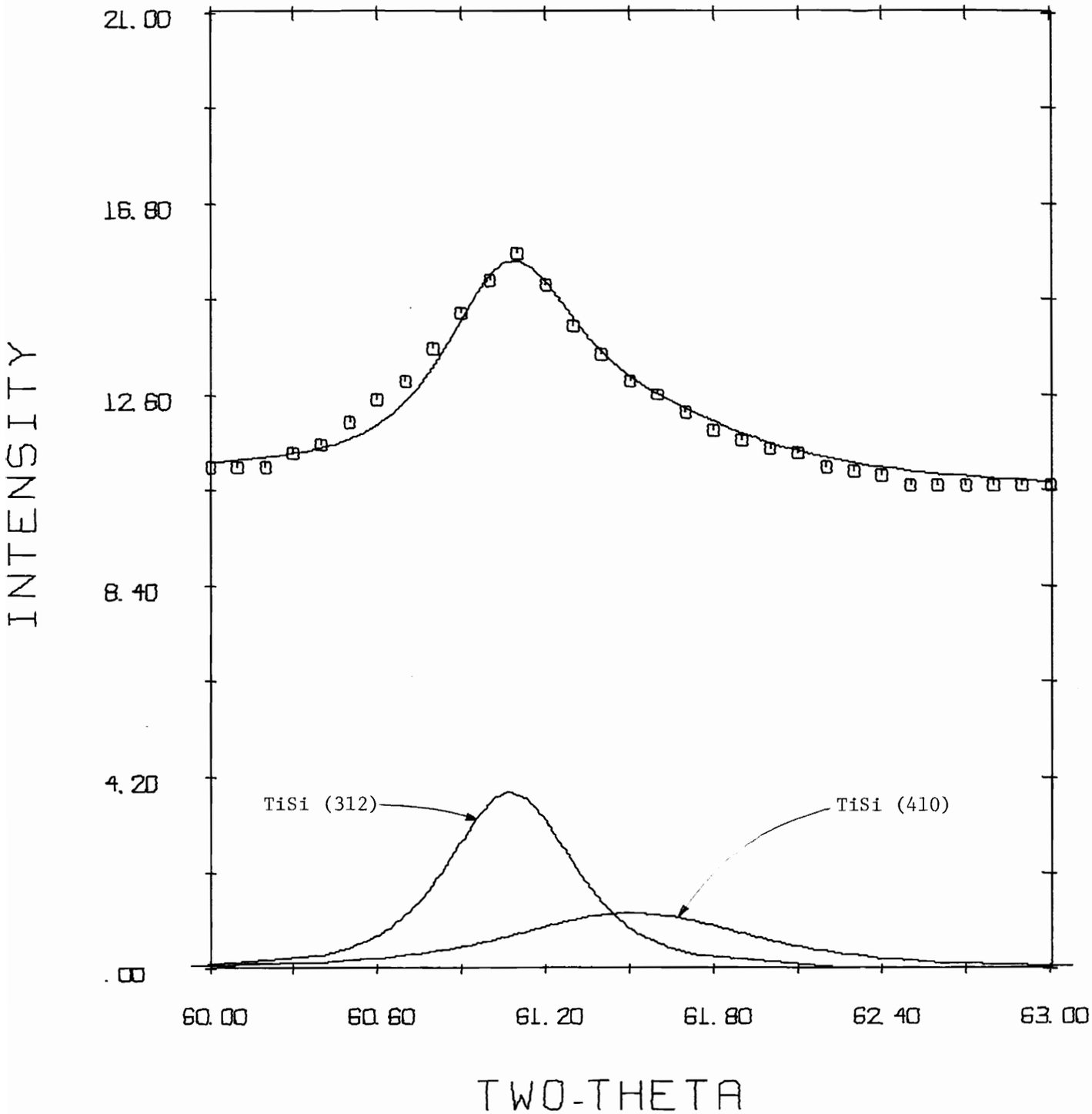

Figure 31. Experimental intensity simulation for step anneal for 2 hours at 650°C, 2θ region from 60° to 63°.

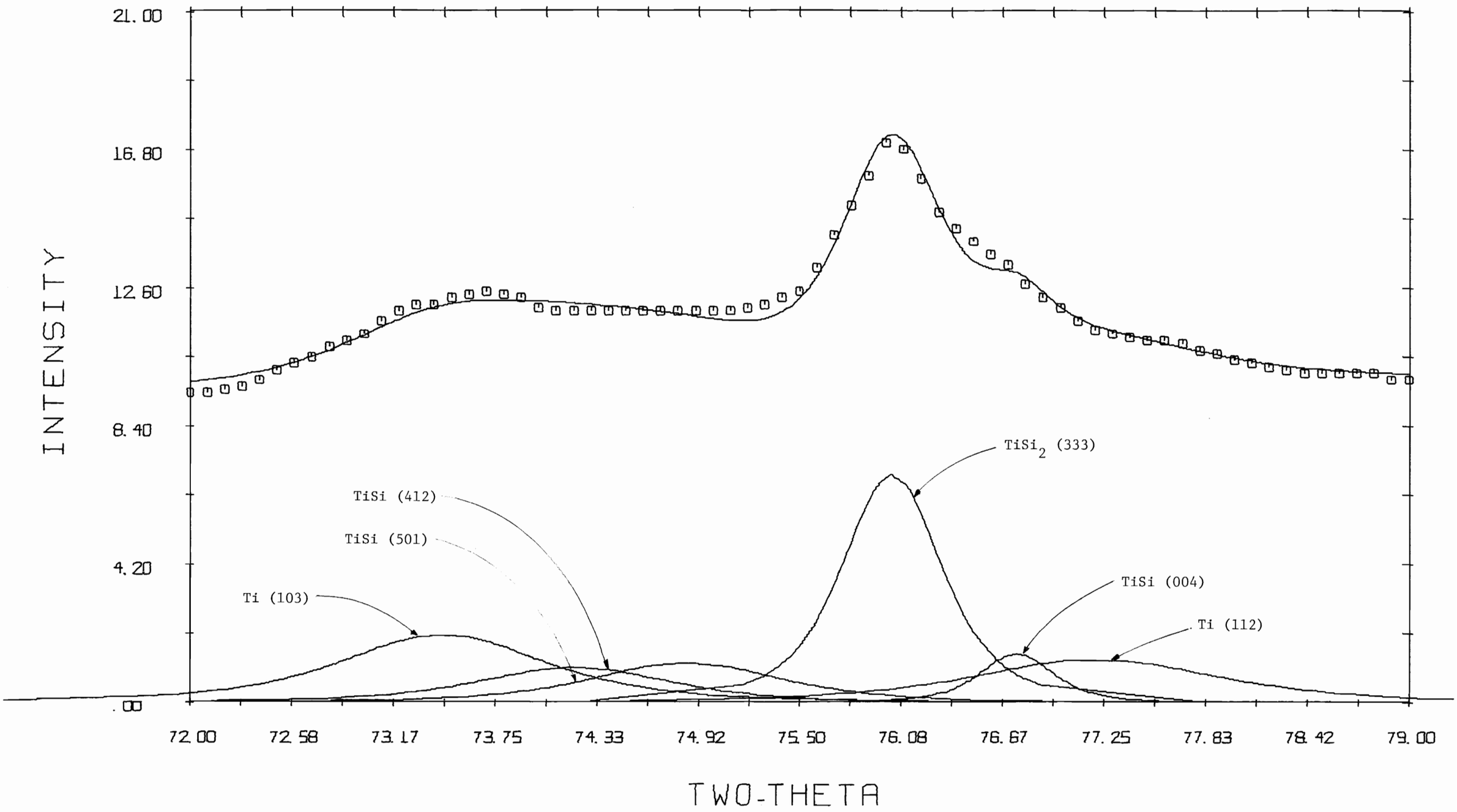

Figure 32. Experimental intensity simulation for step anneal for 2 hours at 650°C, 2θ region from 72° to 79°.

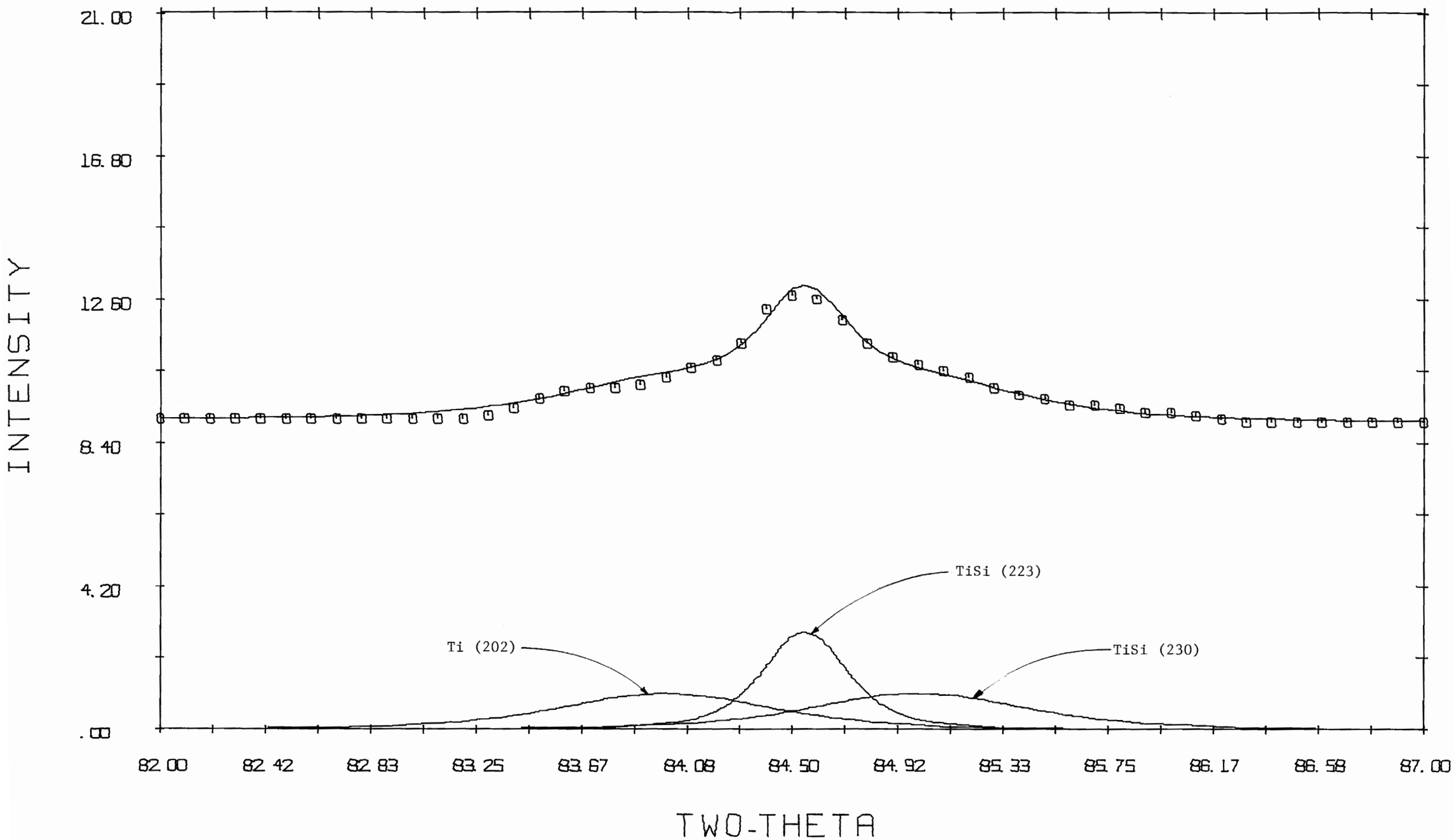

Figure 33. Experimental intensity simulation for step anneal for 2 hours at 650°C, 2θ region from 82° to 87°.

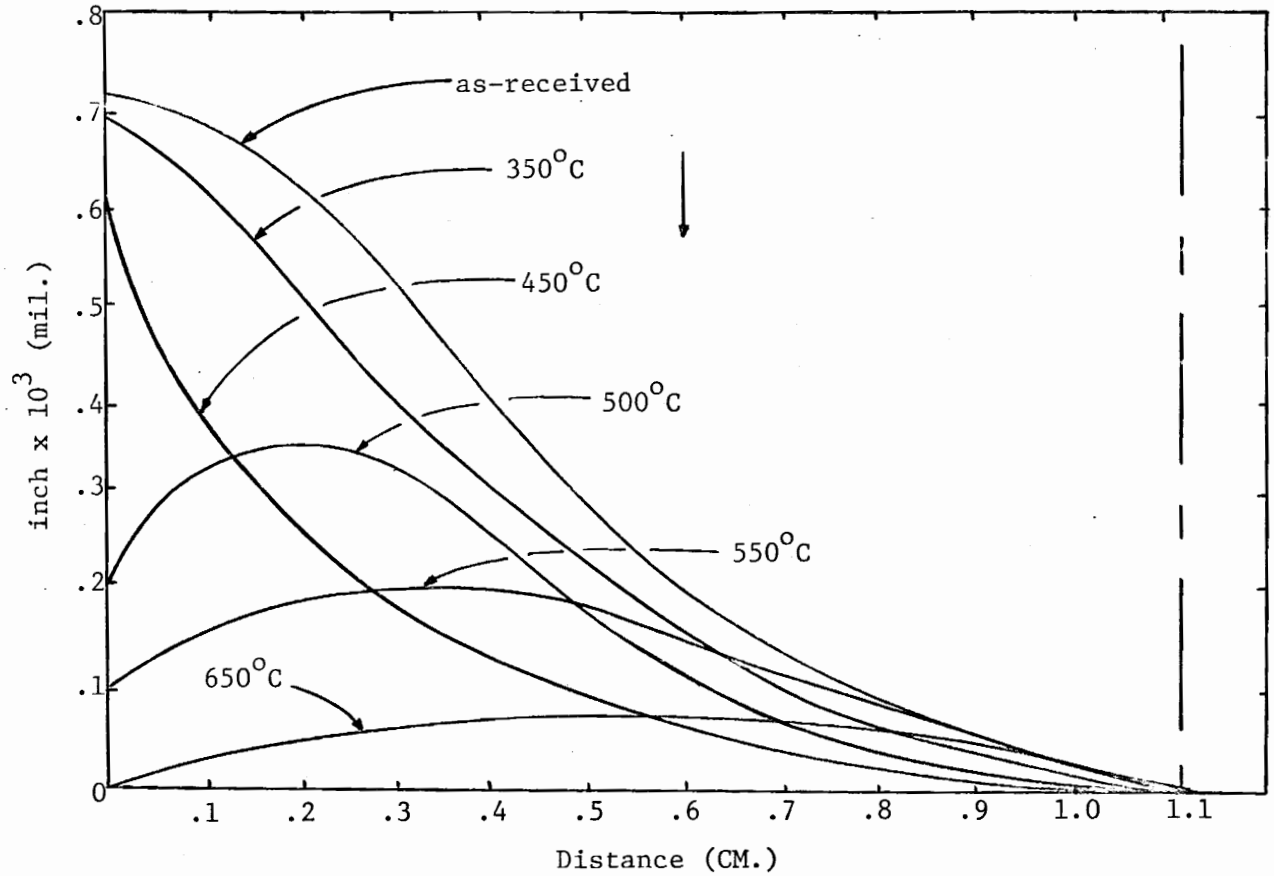

Figure 34A. Optical interference techniques measured the elastic bending of the silicon substrate taken at right angles. Vertical arrow indicates the surface on which the titanium film was deposited.

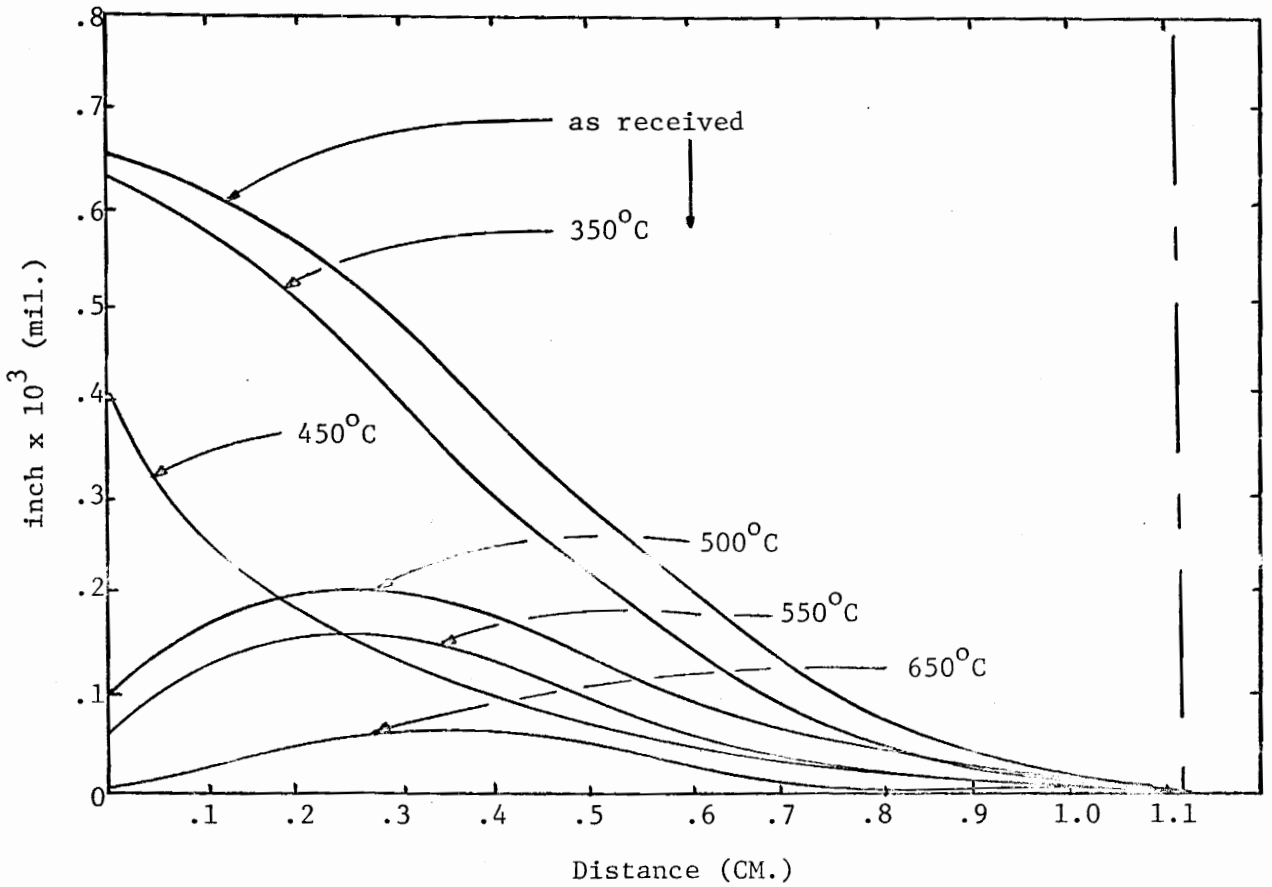

Figure 34B. Optical interference techniques measured the elastic bending of the silicon substrate taken at right angles. Vertical arrow indicates the surface on which the titanium film was deposited.

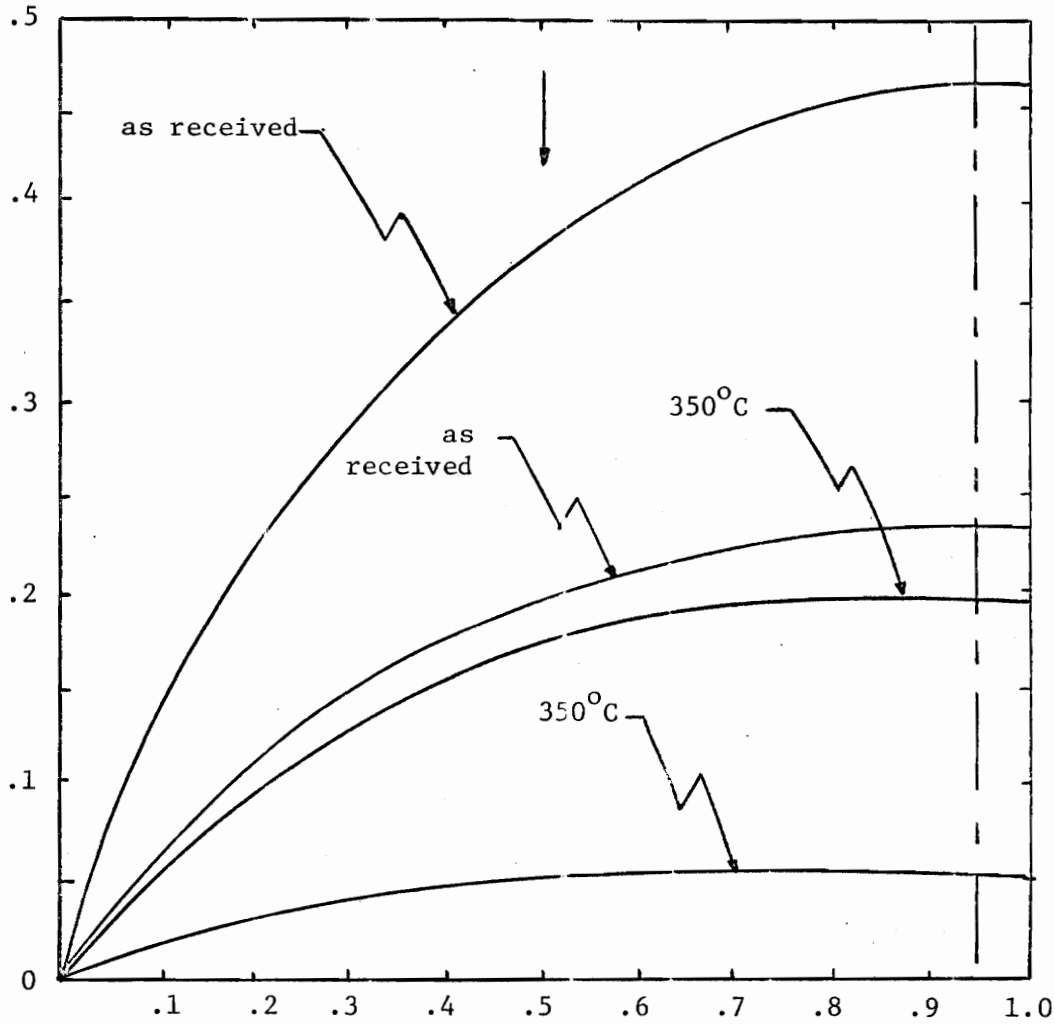

Figure 35. Optical interference techniques measured the elastic bending of a silicon substrate cut to within 3.5° of the 111 planes. This graph contains measurements taken at right angles to one another for two step anneals. Vertical arrow indicates the surface on which the titanium film was deposited.

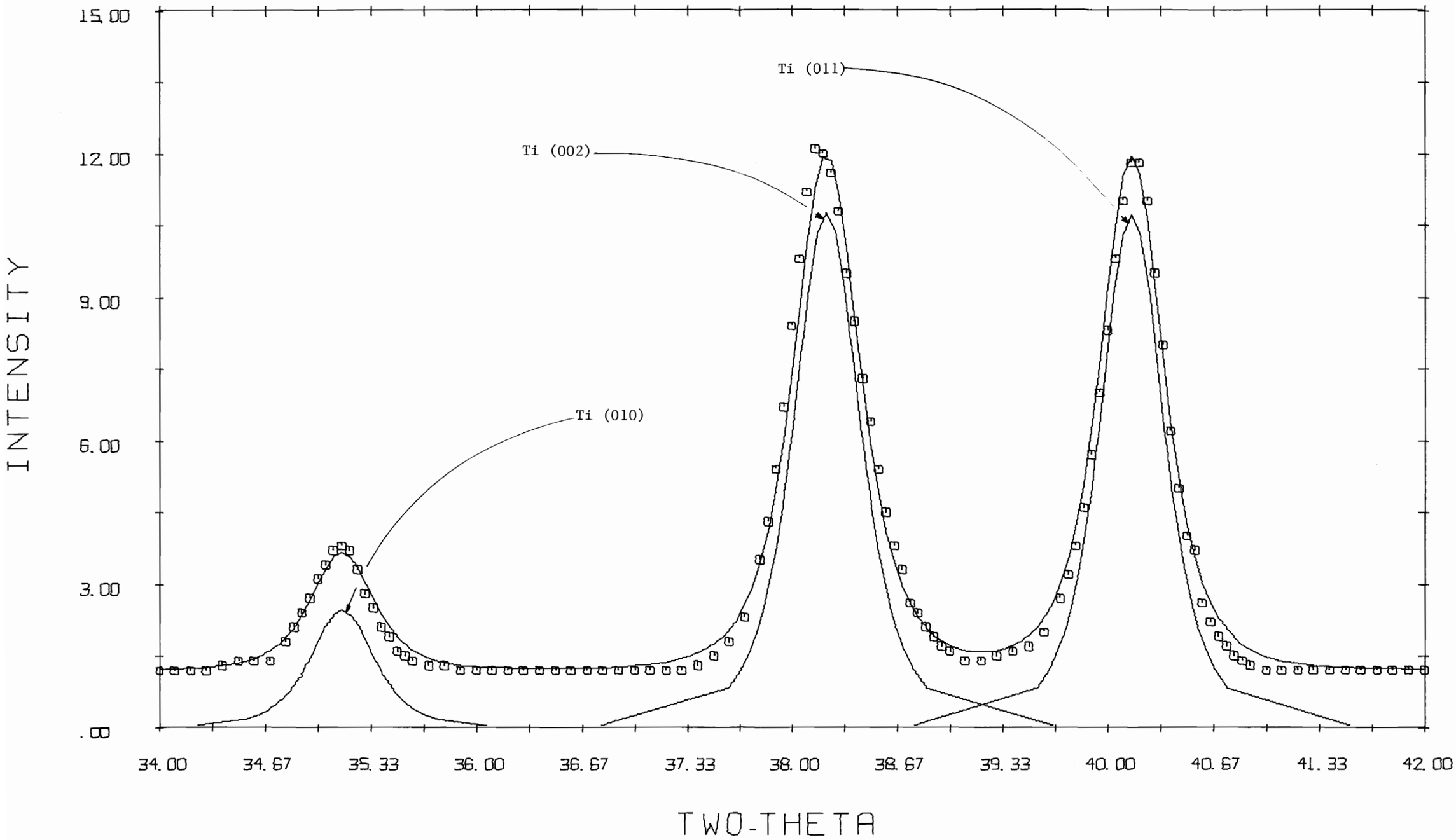

Figure 36. Experimental intensity simulation for as-received, 2.3 μm titanium thin film, 2θ region from 34° to 42°.

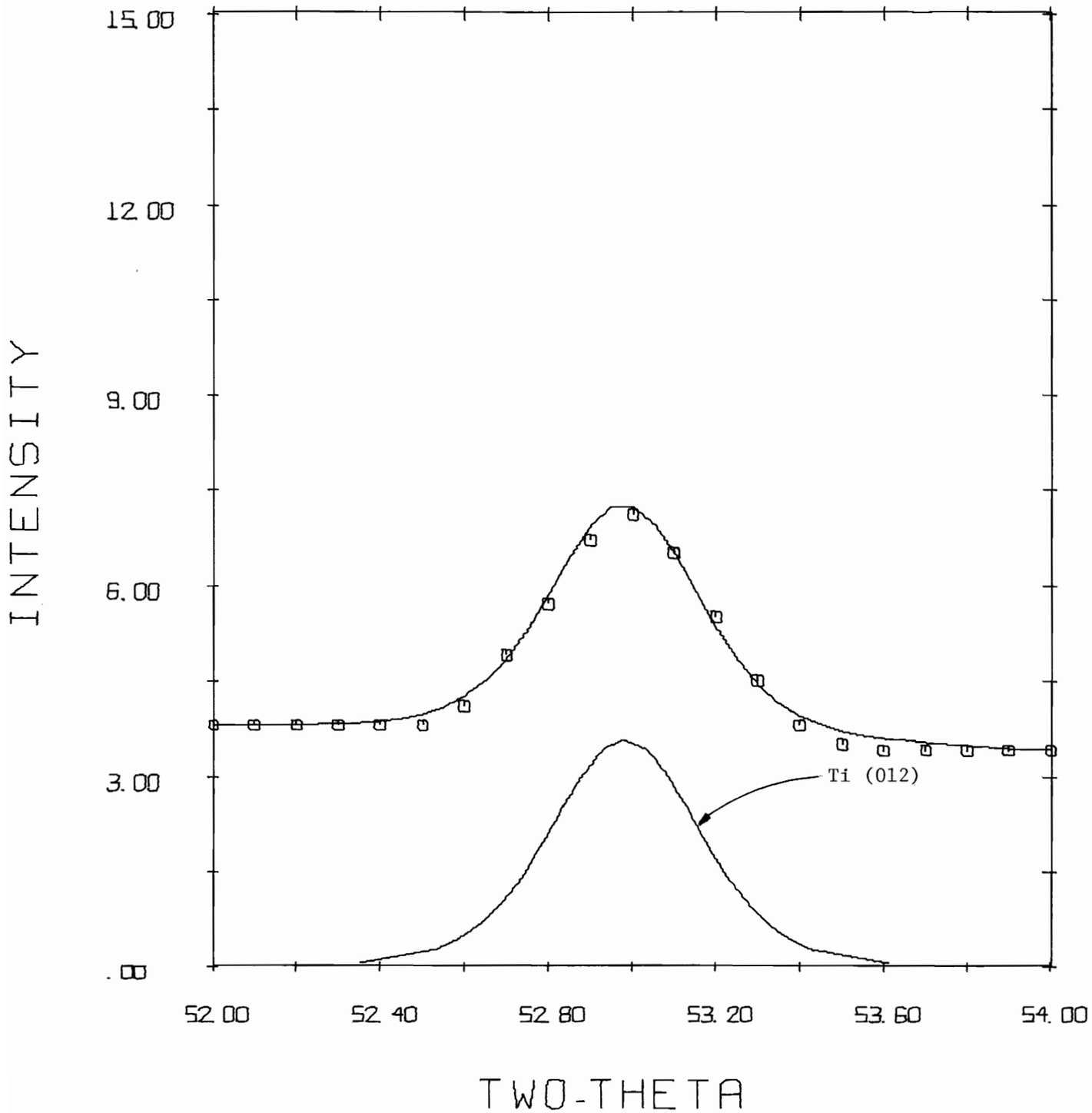

Figure 37. Experimental intensity simulation for as-received, 2.3 μm titanium thin film, 2θ region from 52° to 54°.

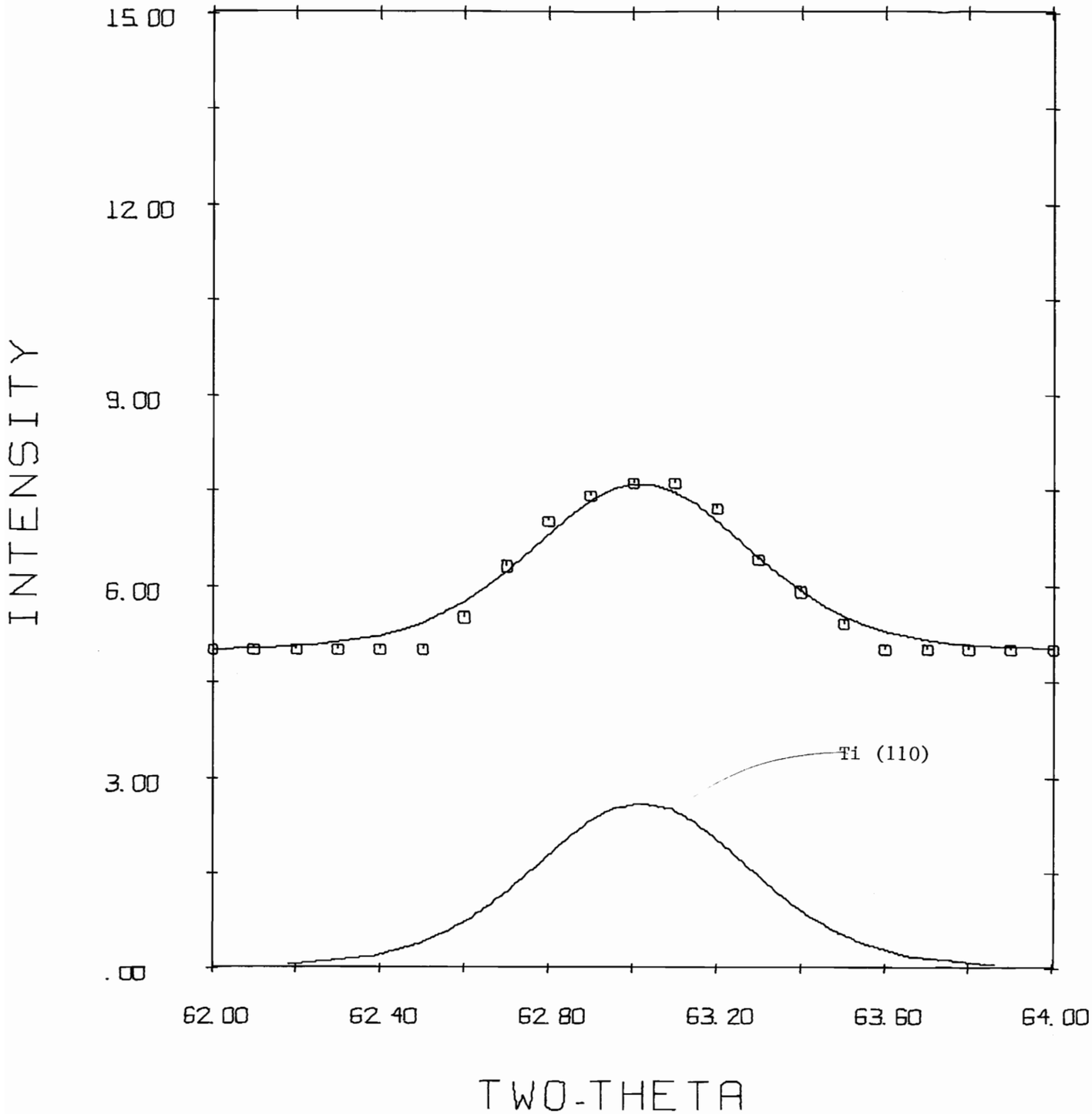

Figure 38. Experimental intensity simulation for as-received, 2.3 μm titanium thin film, 2θ region from 62° to 64°.

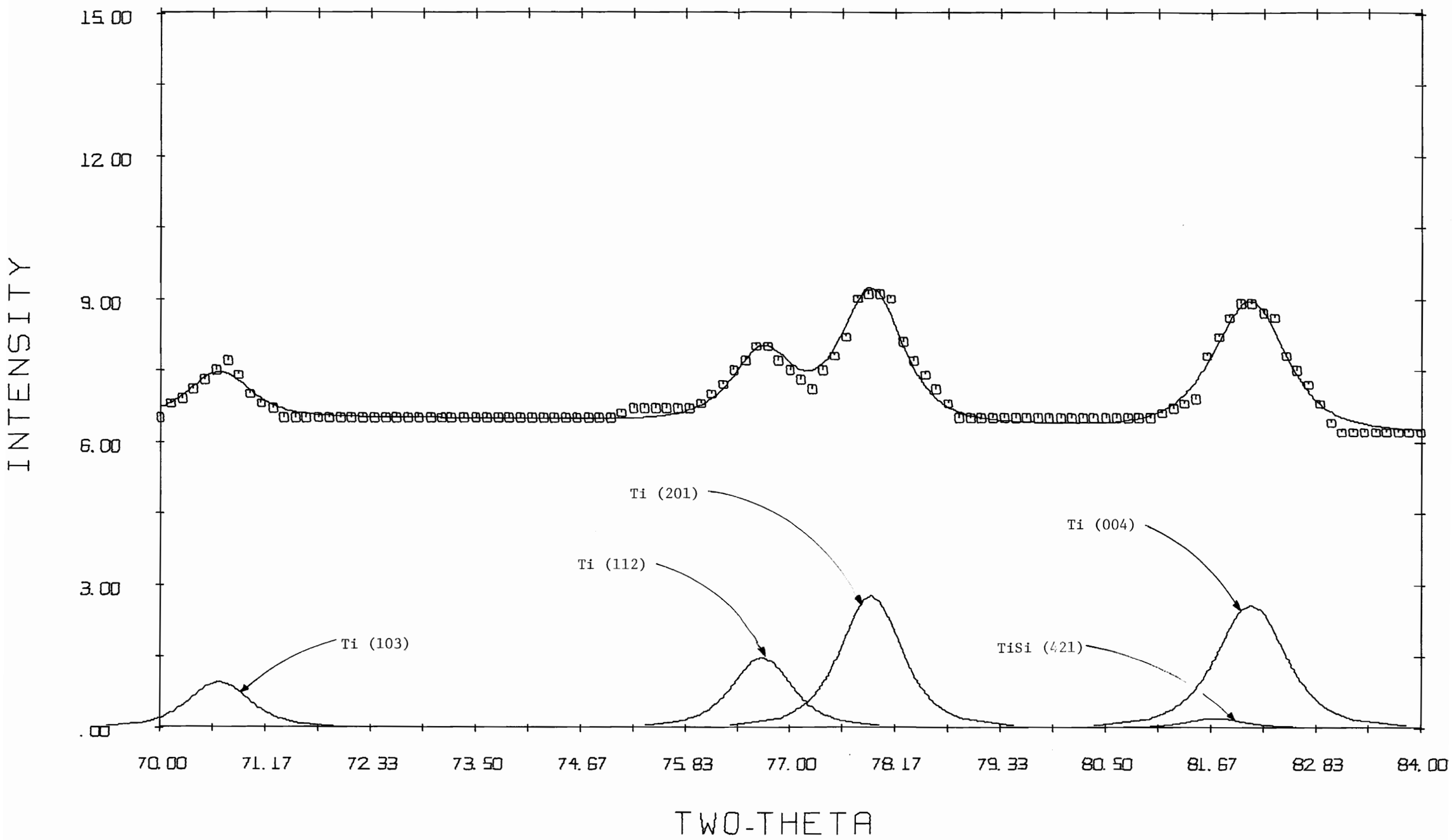

Figure 39. Experimental intensity simulation for as-received, 2.3 μm titanium thin film, 2θ region from 70° to 84°.

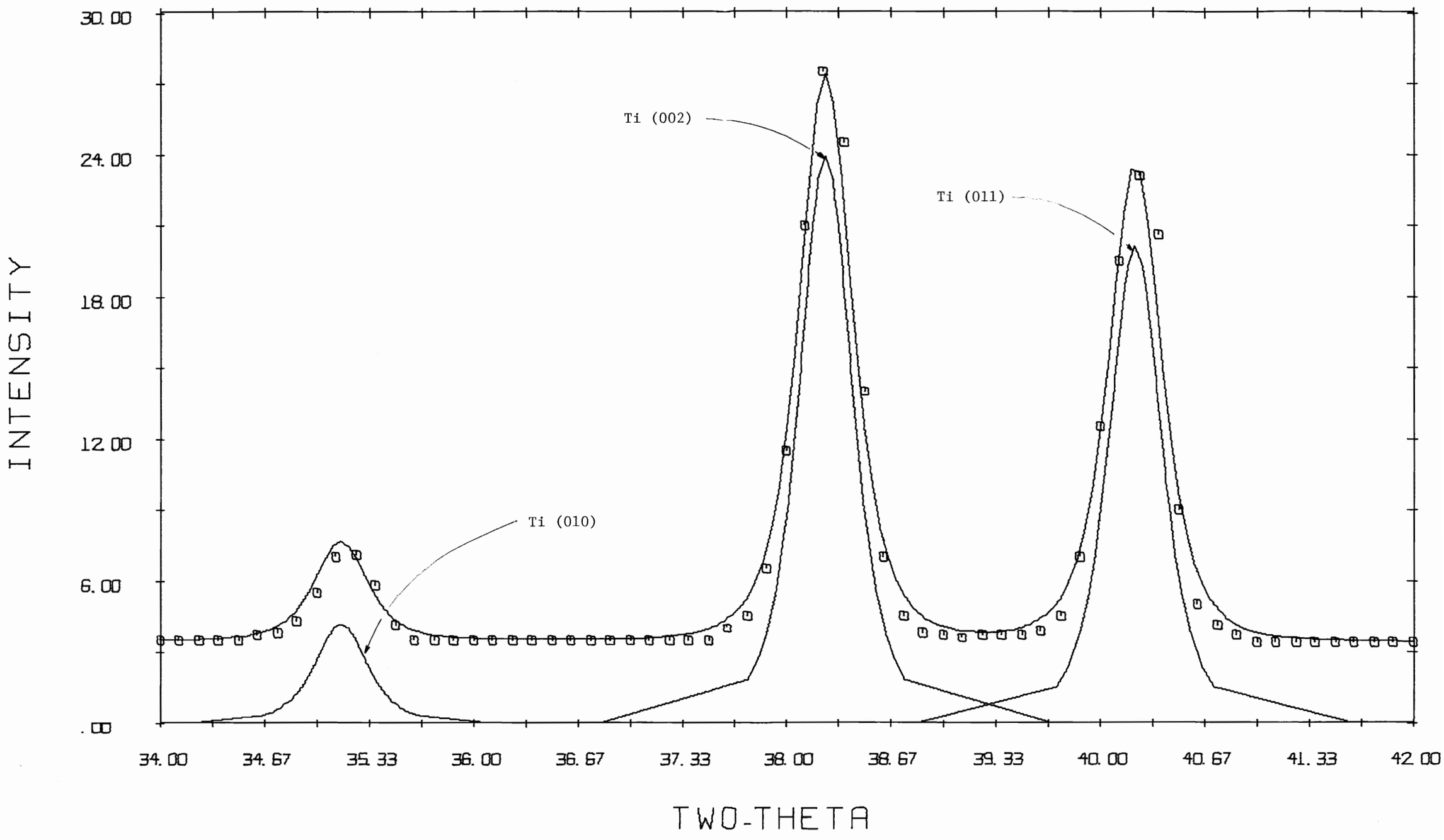

Figure 40. Experimental intensity simulation for 15 minute anneal at 625°C, 2θ region 34° to 42°.

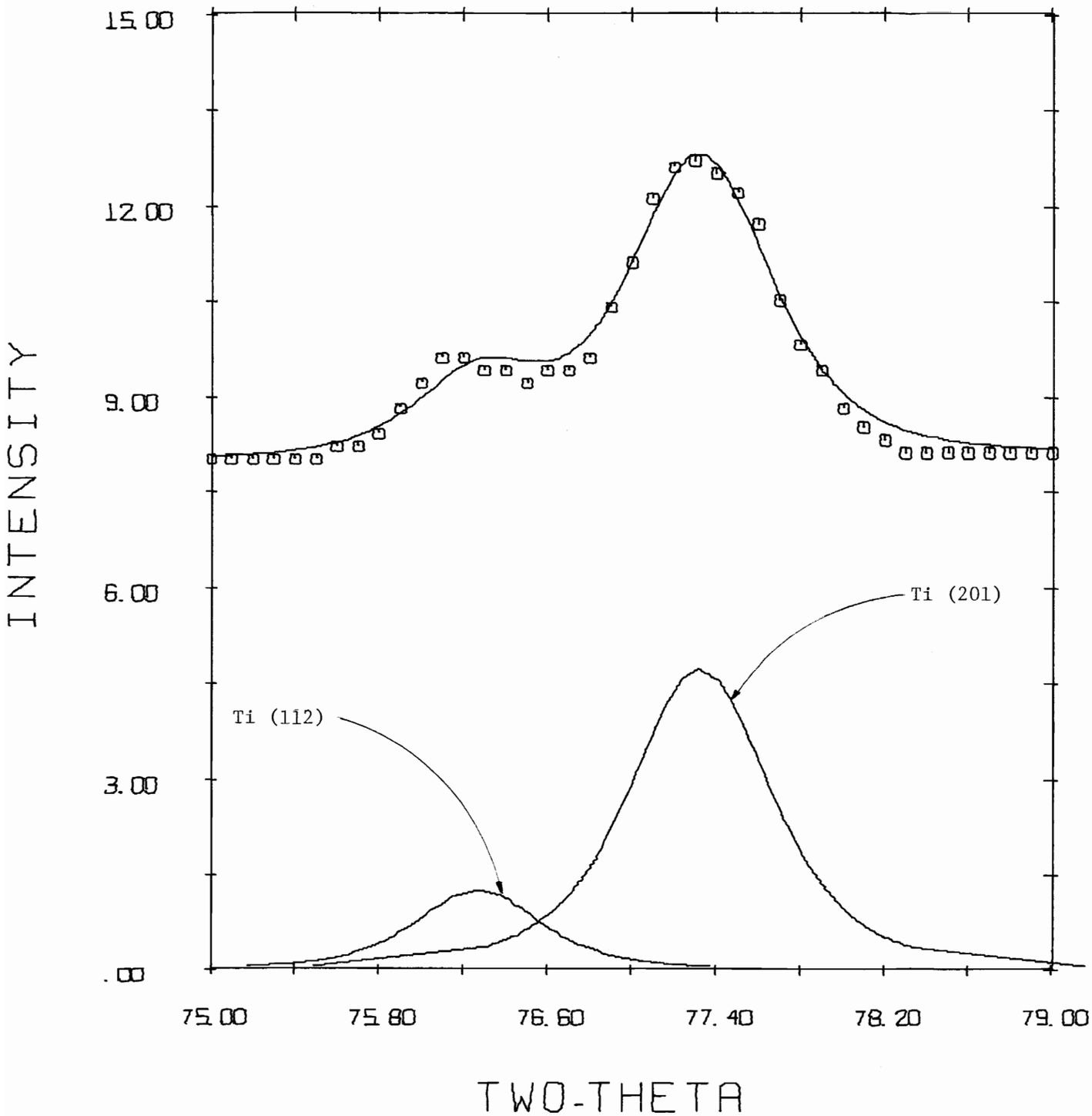

Figure 41. Experimental intensity simulation for 15 minute anneal at 625°C 2θ region 75° to 79°.

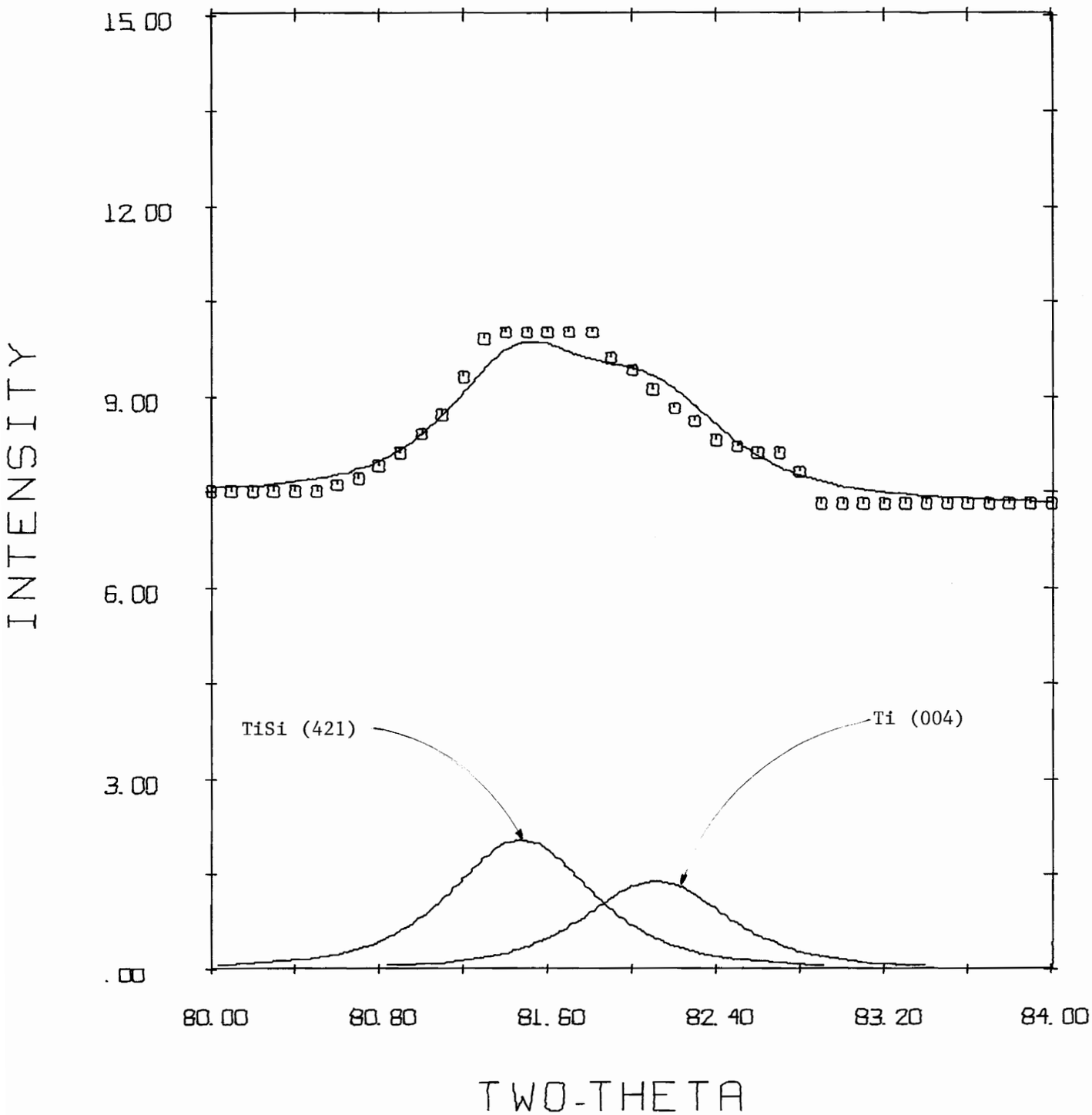

Figure 42. Experimental intensity simulation for 15 minute anneal at 625°C, 2θ region from 80° to 84°.

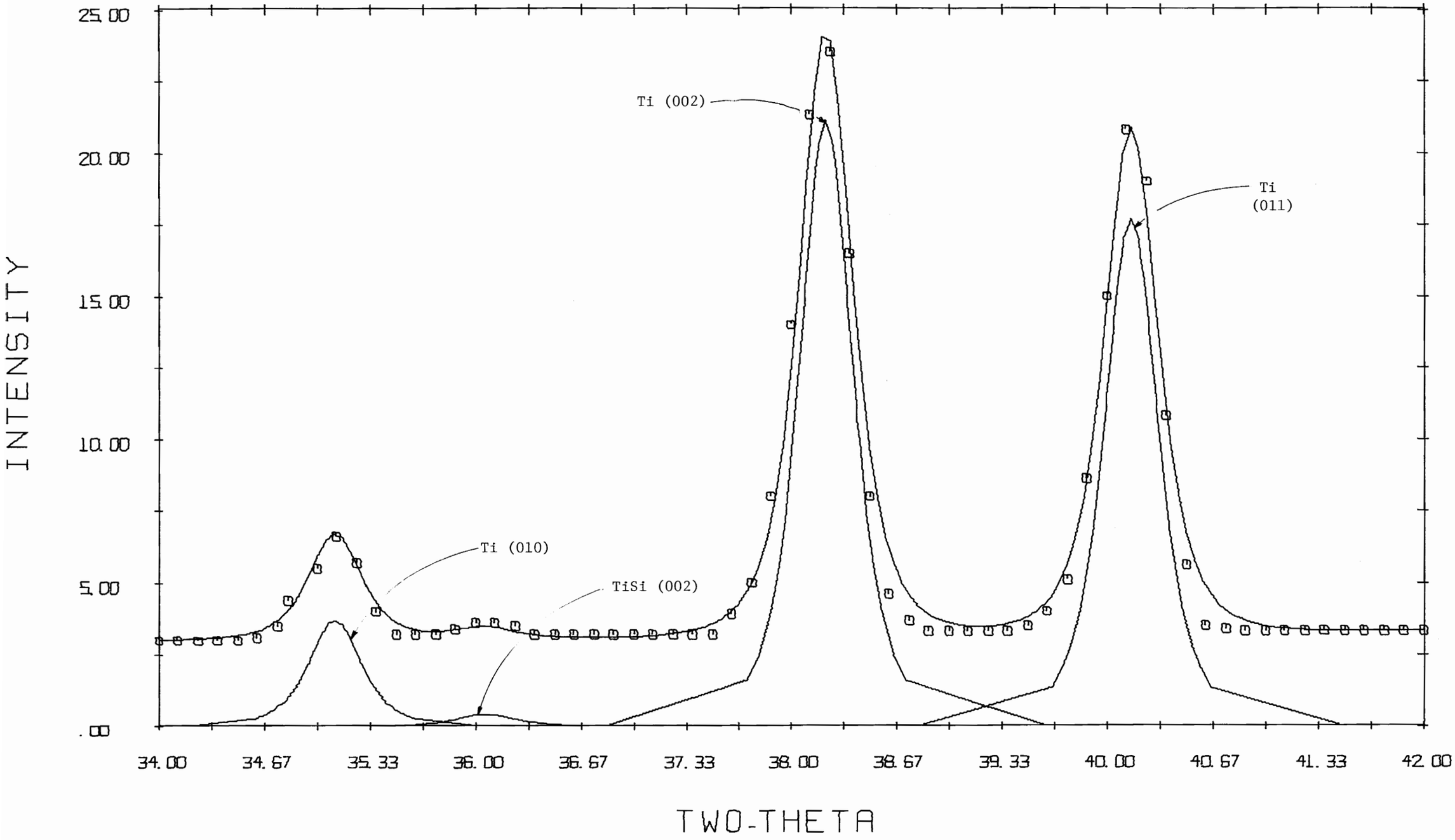

Figure 43. Experimental intensity simulation for 30 minute anneal at 625°C, 2θ region from 34° to 42°.

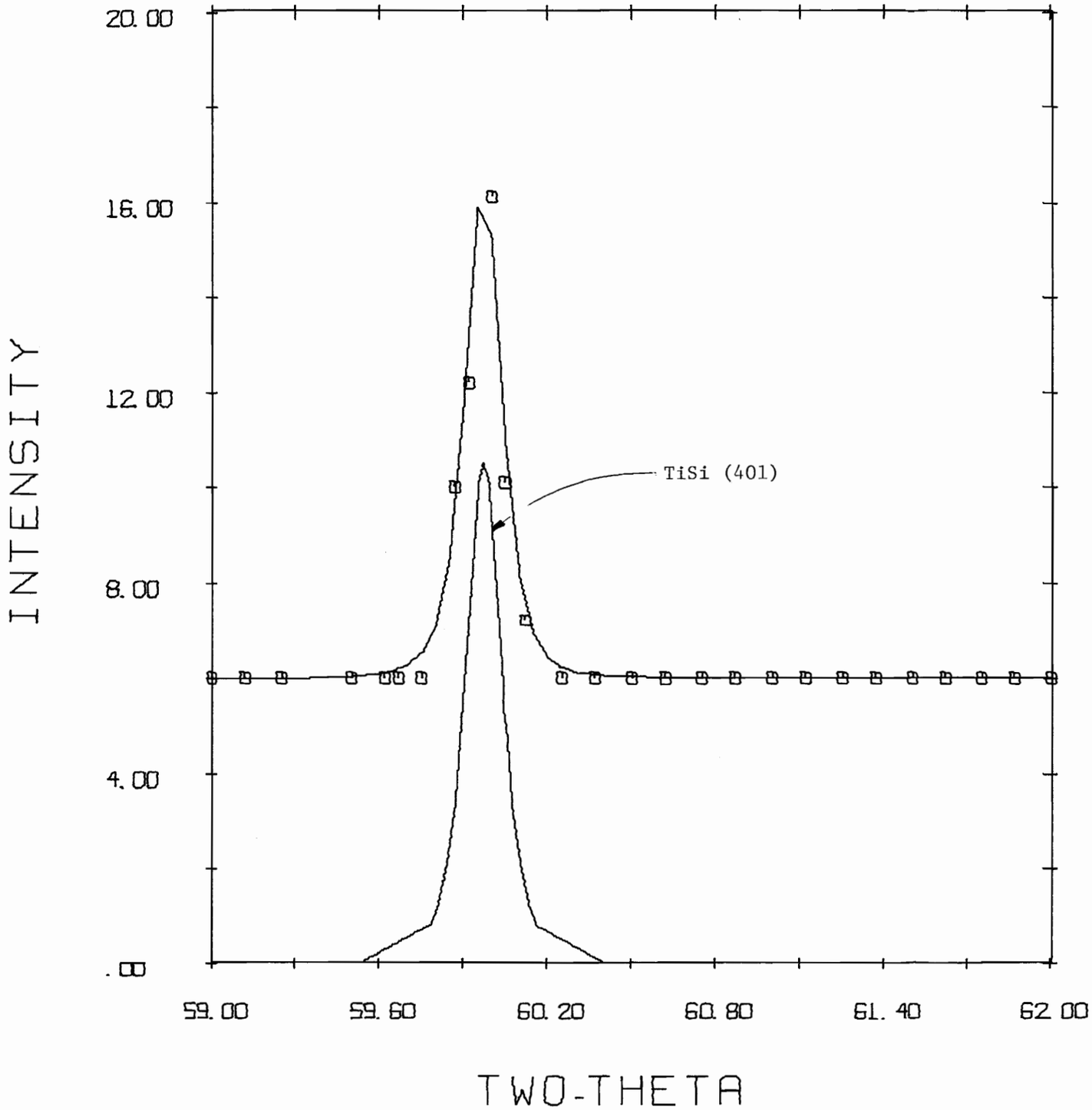

Figure 44. Experimental intensity simulation for 30 minute anneal at 625°C, 2θ region from 59° to 62°.

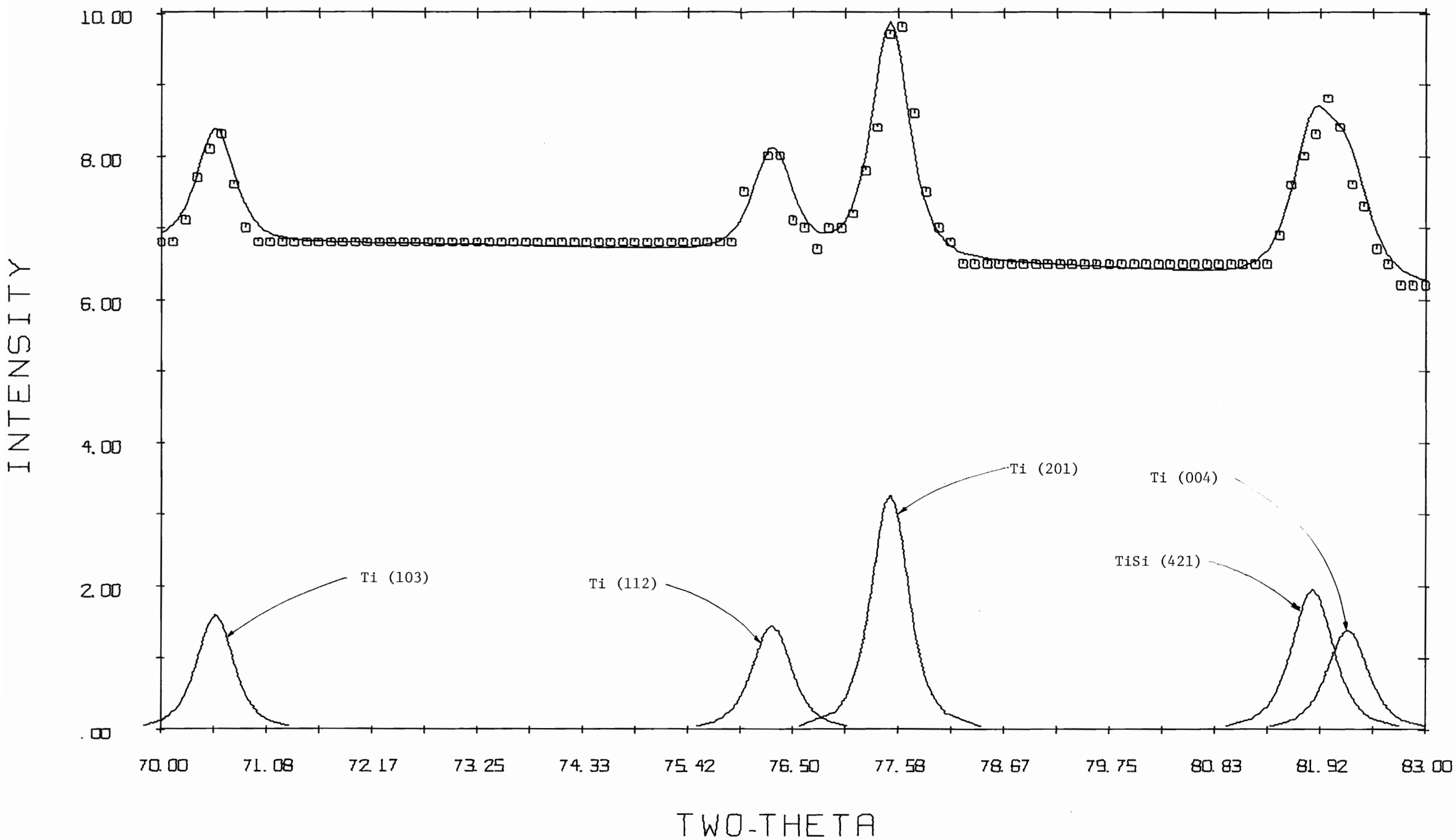

Figure 45. Experimental intensity simulation for 30 minute anneal at 625°C, 2θ region from 70° to 83°.

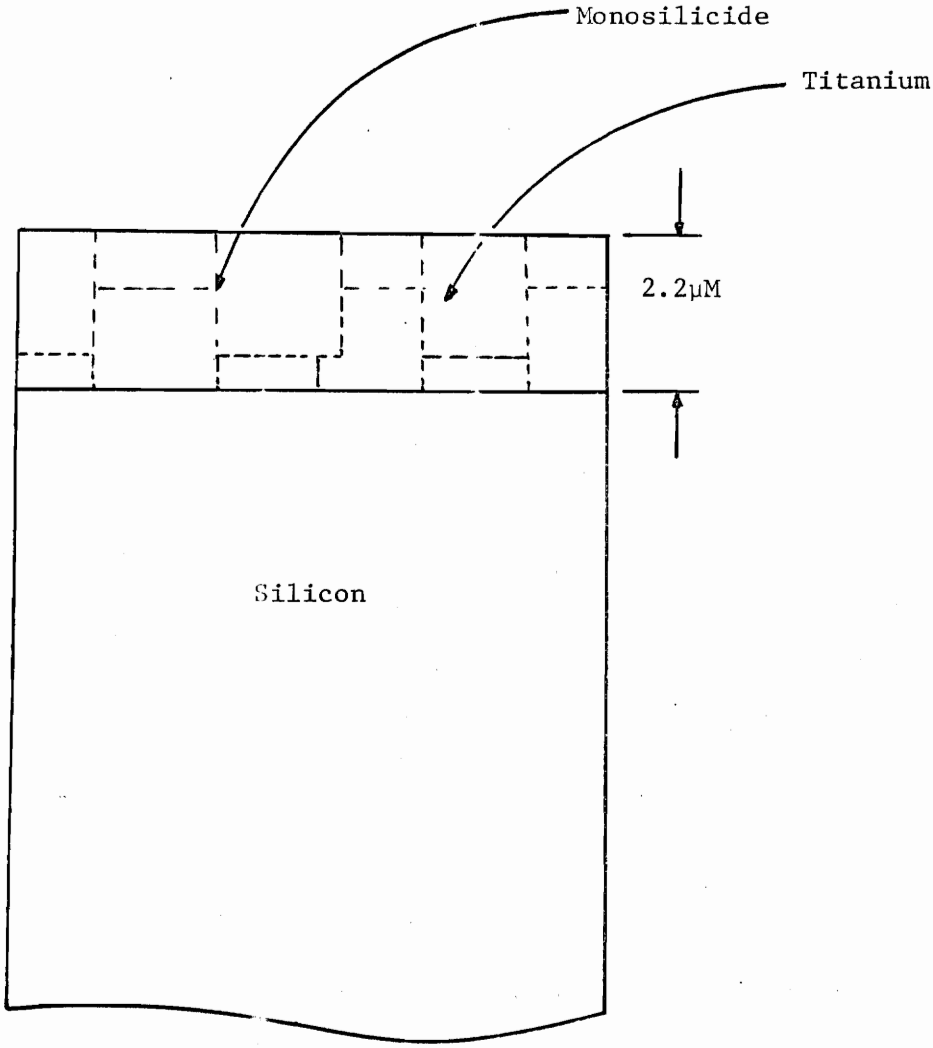

Figure 46. Illustration of cross-section of thin film structure for as-received and 350°C step anneals for 2 hours.

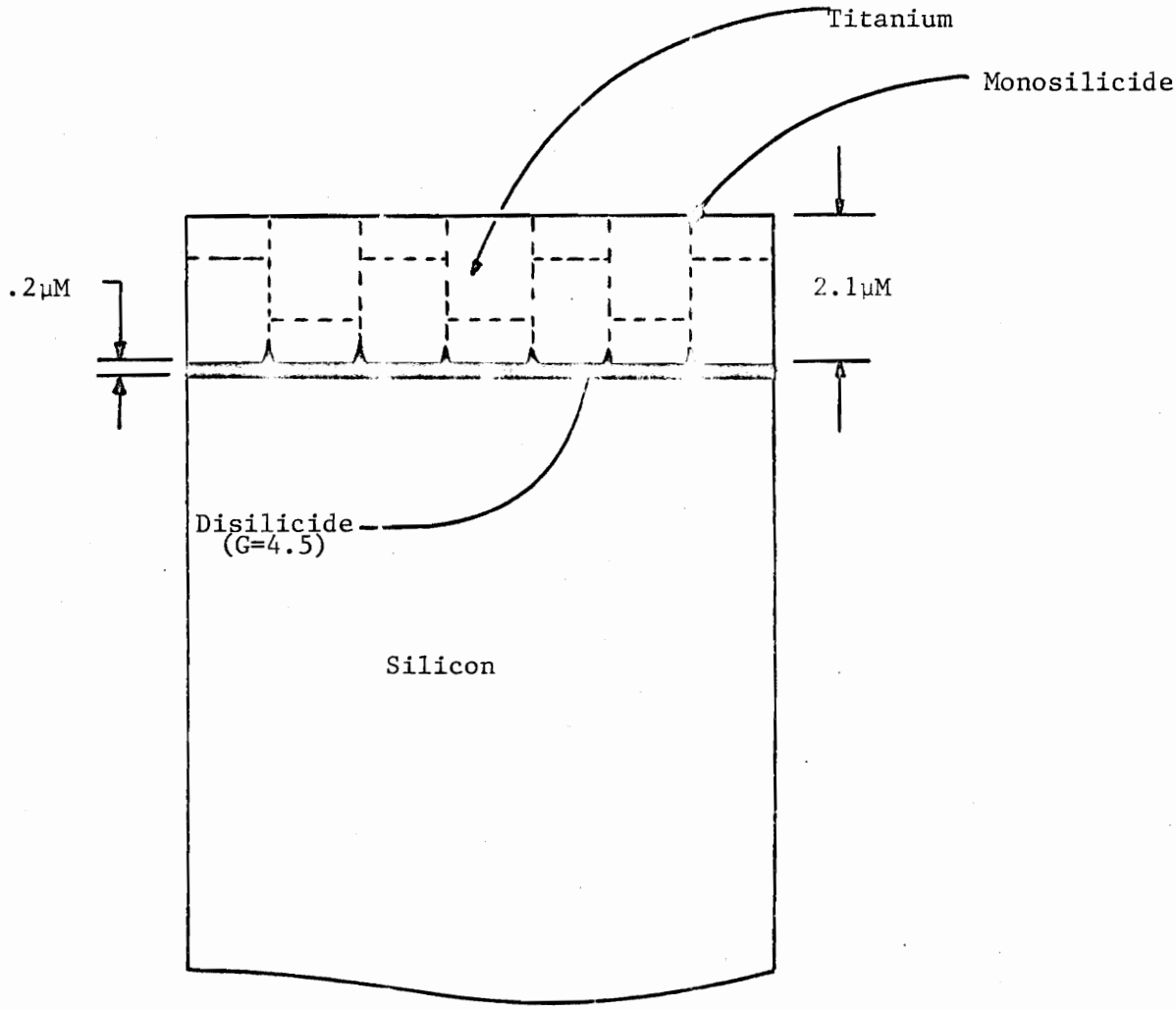

Figure 47. Illustration of cross-section of thin film structure for 450°C step anneal for 2 hours.

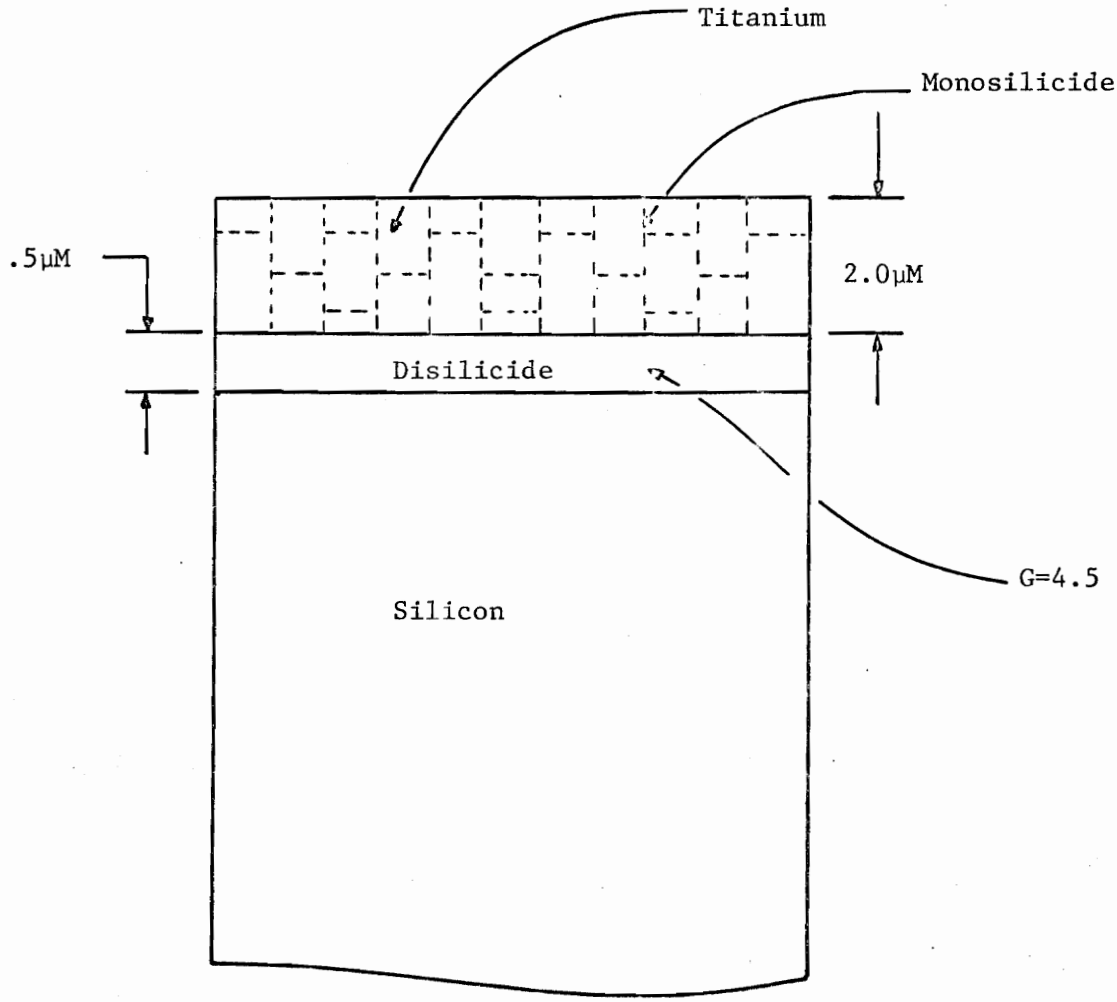

Figure 48. Illustration of cross-section of thin film structure for 500°C anneal for 2 hours.

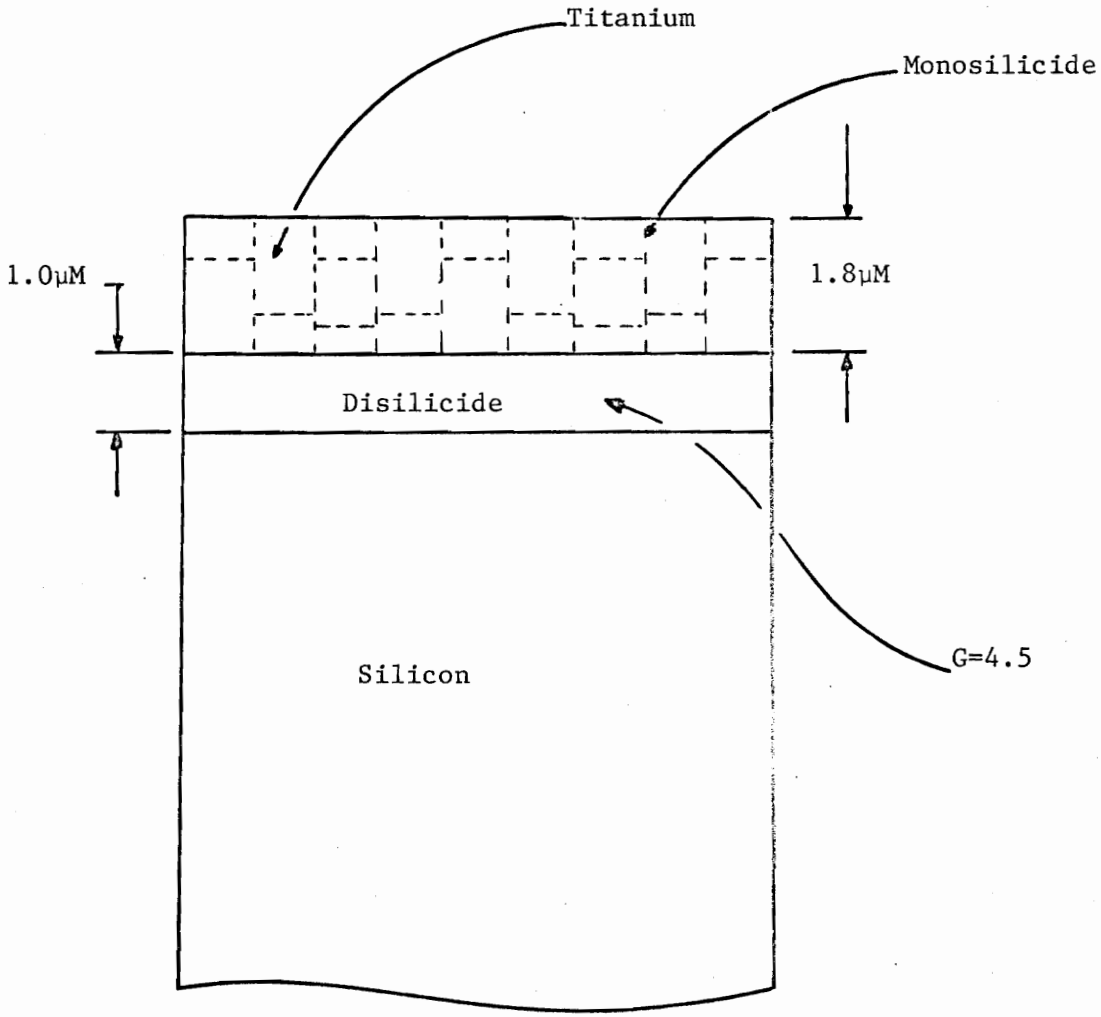

Figure 49. Illustration of cross-section of thin film structure for 550°C step anneal for 2 hours.

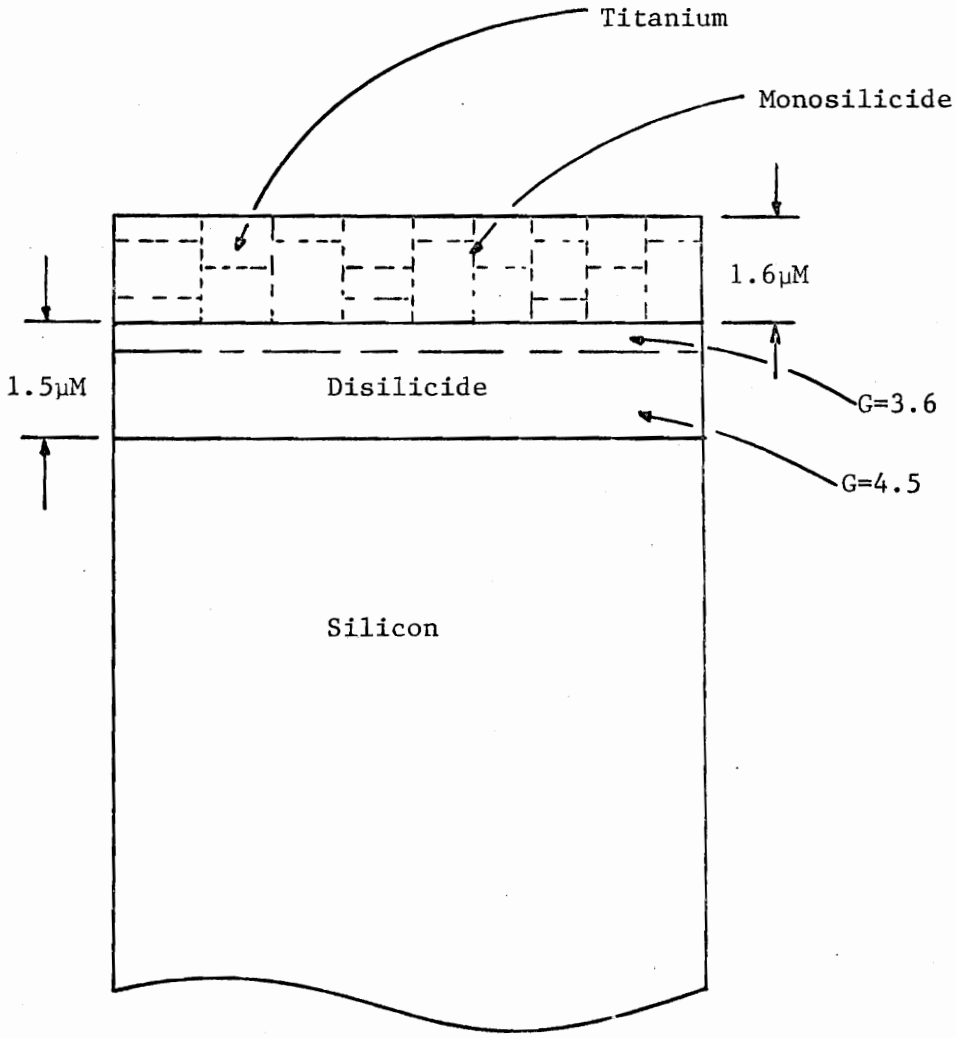

Figure 50. Illustration of cross-section of thin film structure for 575°C step anneal for 2 hours.

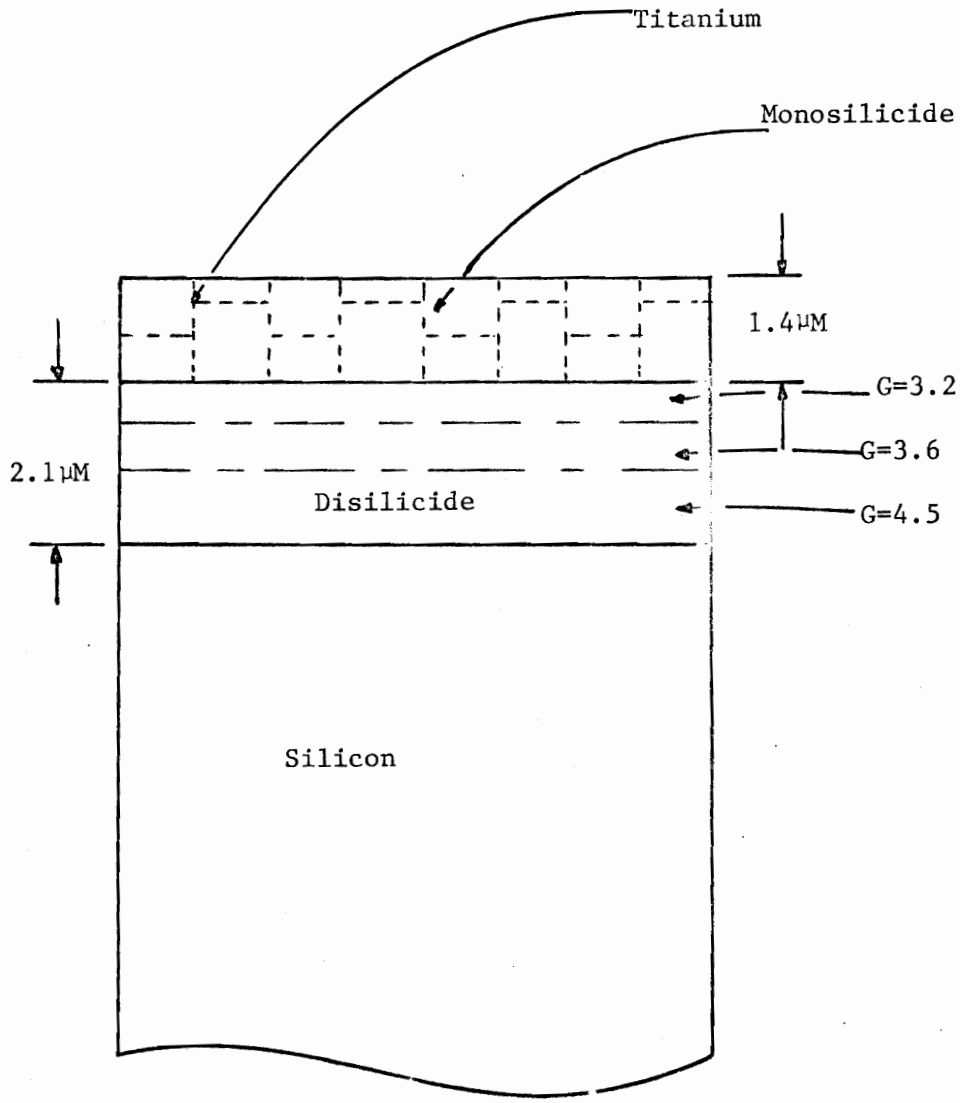

Figure 51. Illustration of cross-section of thin film structure for 600°C step anneal for 2 hours.

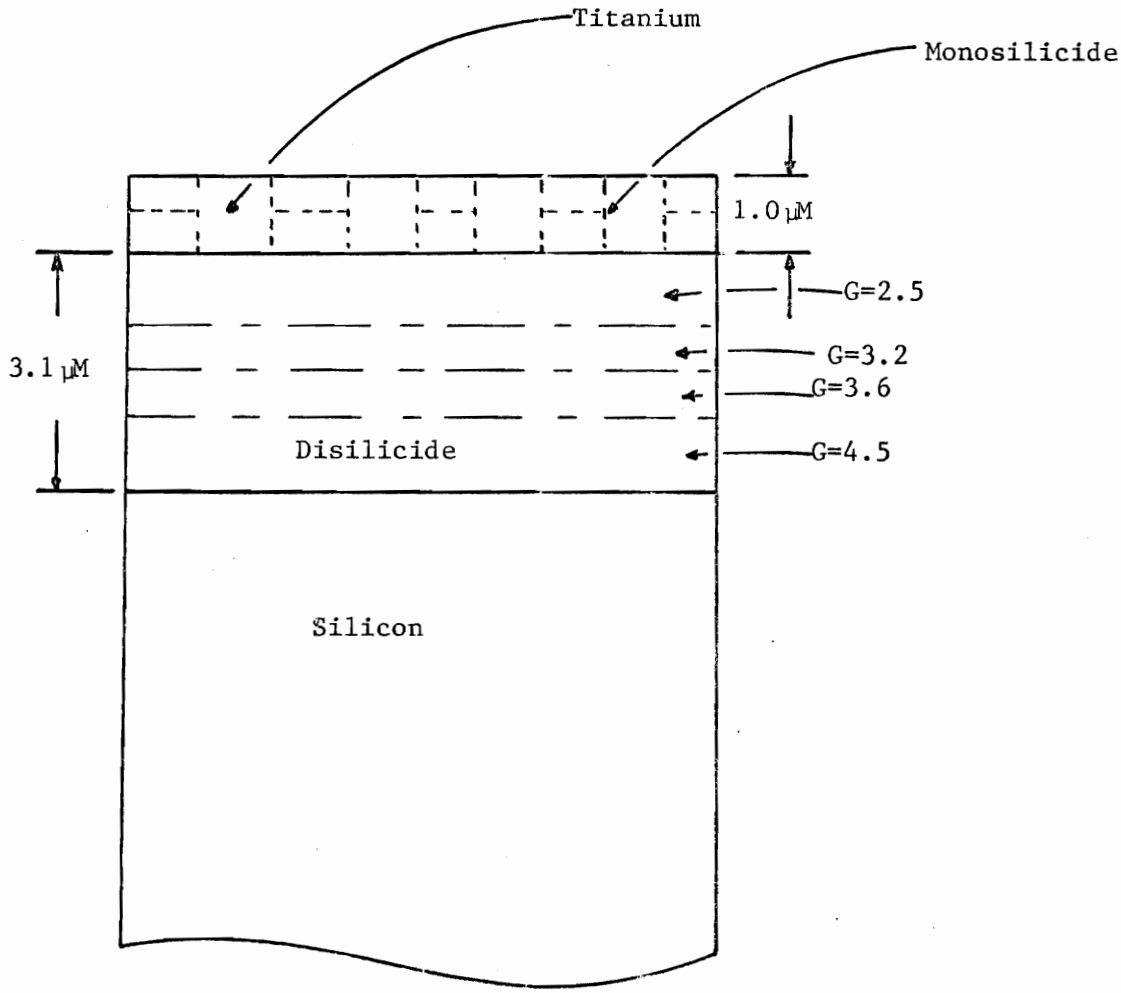

Figure 52. Illustration of cross-section of thin film structure for 625°C step anneal for 2 hours.

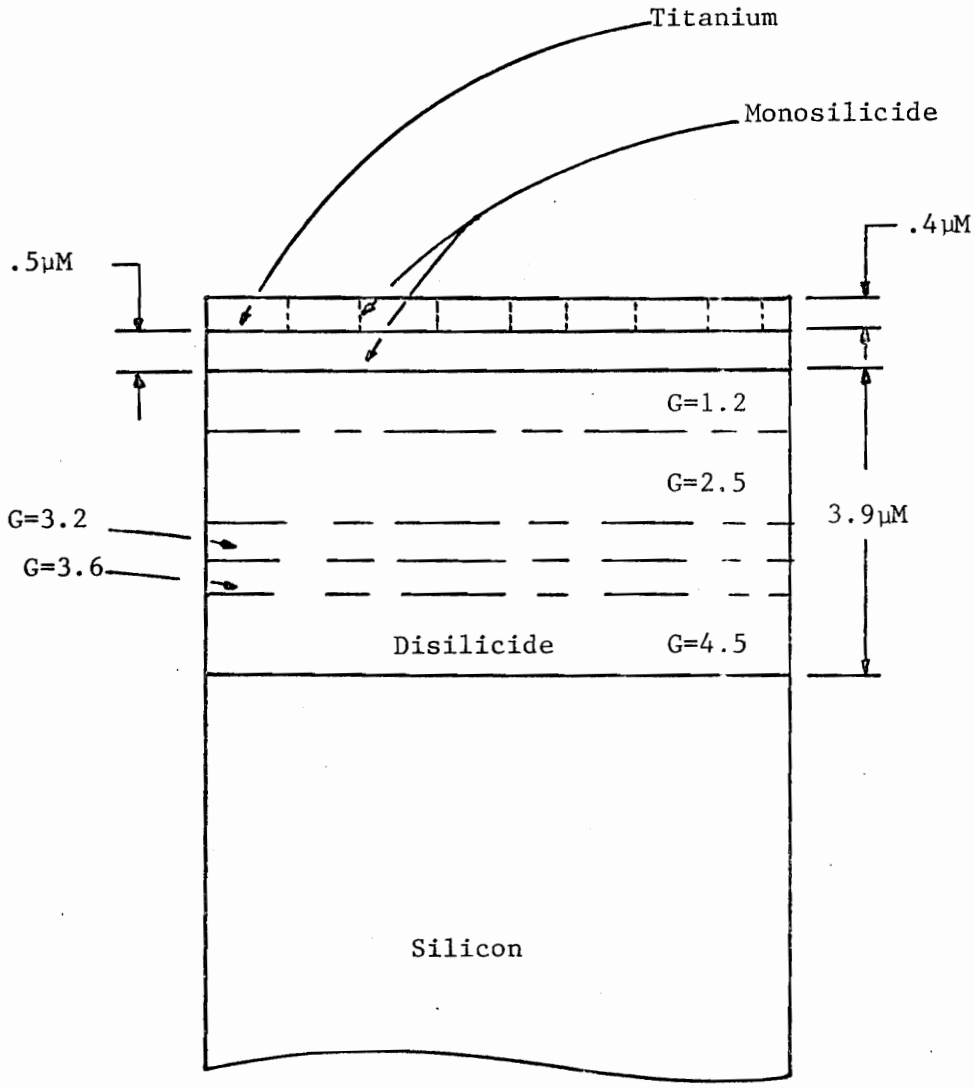

Figure 53. Illustration of cross-section of thin film structure for 650°C step anneal for 2 hours.

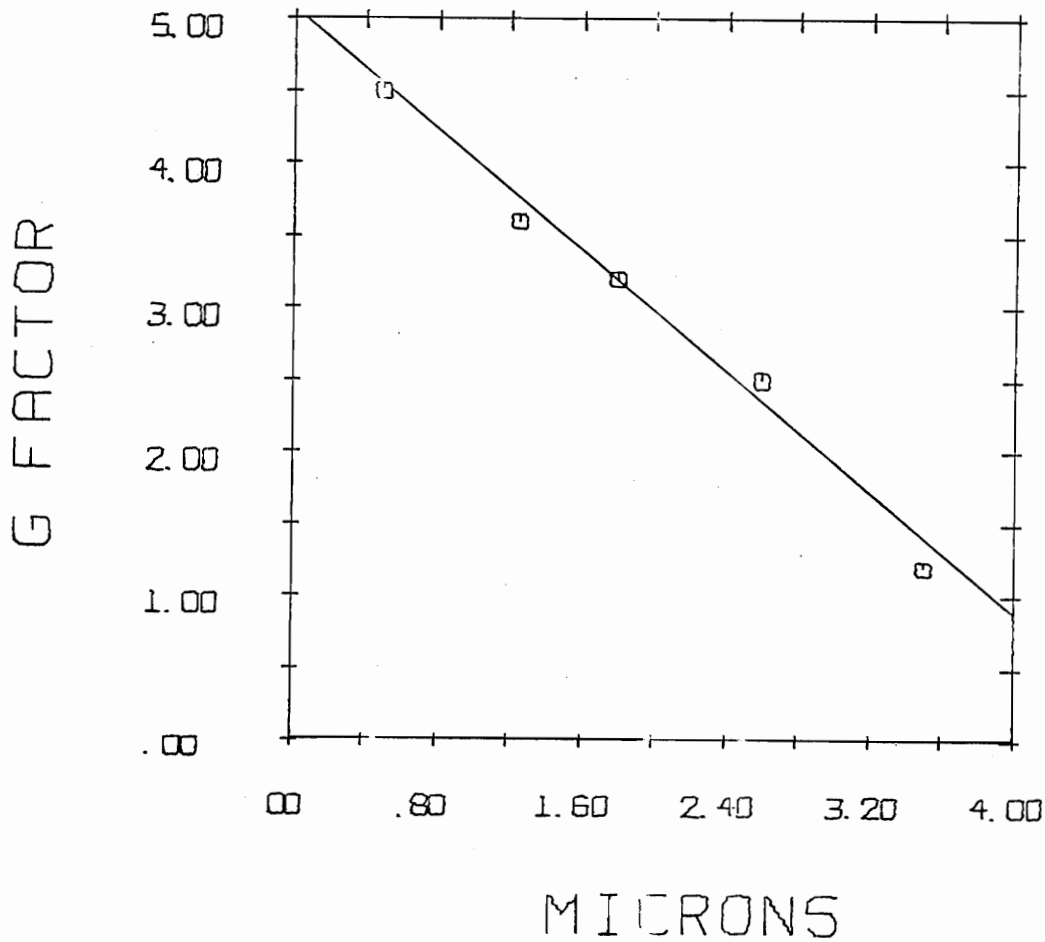

Figure 54. Plot of "G" factor vs. disilicide thickness in final step anneal treatment at 650°C for 2 hours. These points represent an average "G" factor for each thickness.

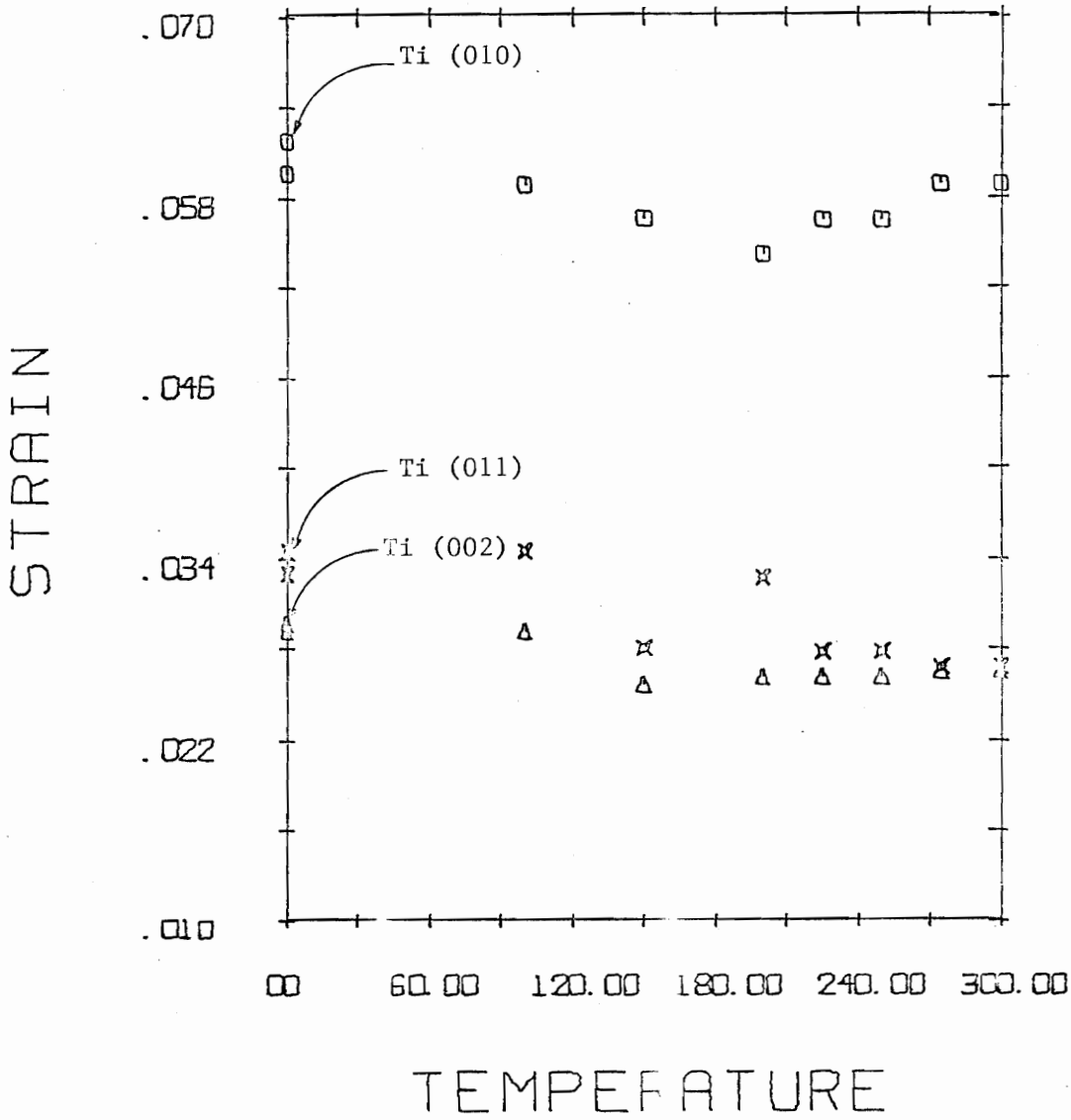

Figure 55. Plot of strain vs. temperature increment above deposition temperature perpendicular to the crystallographic planes in step annealed thin films.

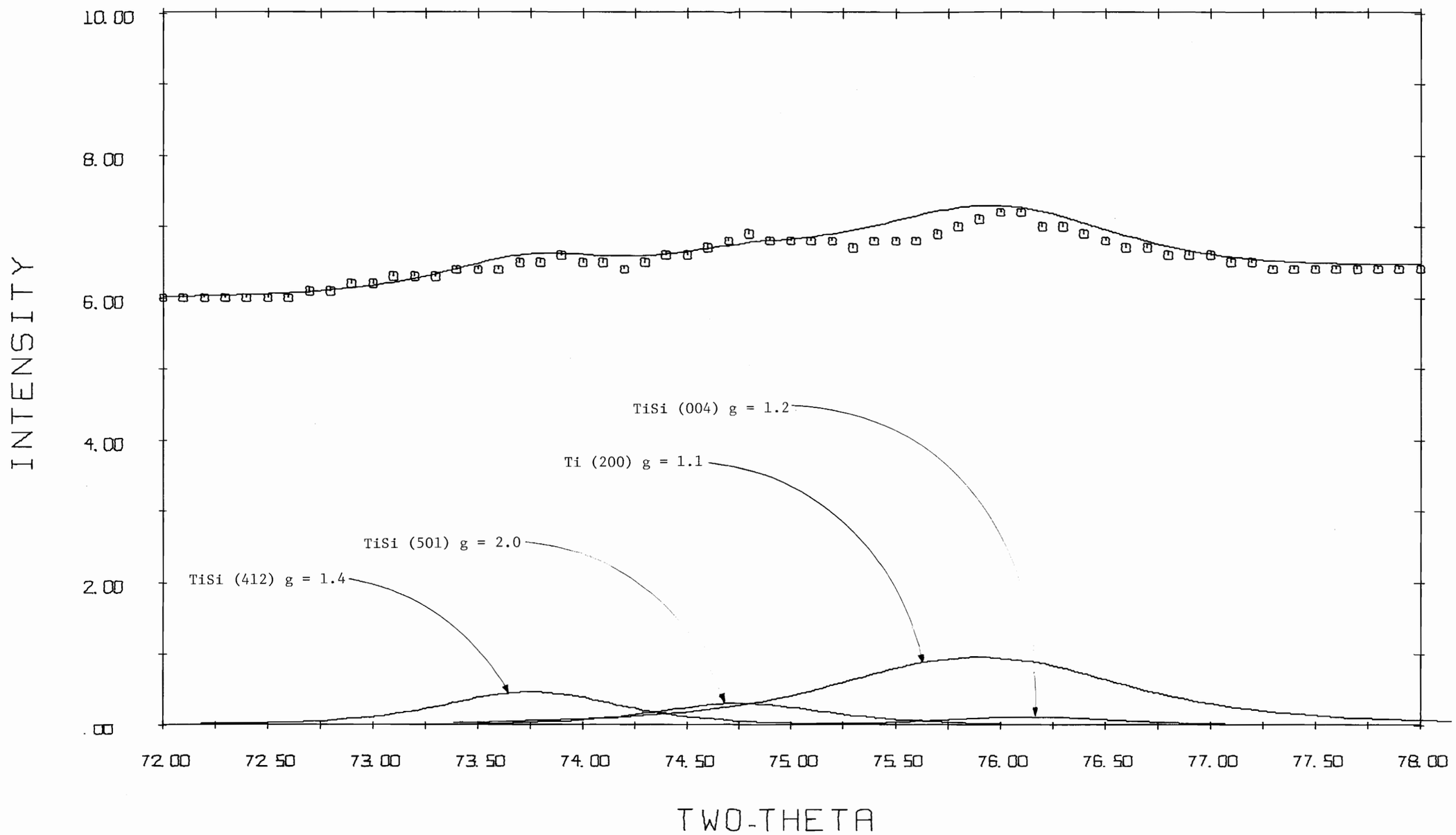

Figure 56. Experimental intensity simulation for step anneal at 350°C for 2 hours, to illustrate the location of monosilicide in this film. Titanium thickness = 1.9 μm.

TABLE I

Completed Reflections of $TiSi_2$ (C54)

HKL	Exp. 2θ	Calc. 2θ*	Laves 2θ*	Exp. d	Calc. d*	Laves d*	Exp. S.R I.I.%	Calc. S.R. I.I.%		Laves S.R. I.I.%
111	23.84	23.812		3.729	3.7336		10.6	11.4		
202	30.06	30.046		2.970	2.9716		9.0	7.5		
113	38.30	38.276		2.348	2.3494		4.8	4.1		
311	39.13	39.107	39.31	2.300	2.3014	2.29	100.0	100.0		100.0
004	42.27	42.242	42.40	2.136	2.1376	2.13	42.8	41.1		70.0
022	43.22	43.201	43.47	2.092	2.0923	2.08	73.2	73.7		90.0
220 400	(43.64)	43.578 43.764		2.072	2.0751 2.0667		5.9	2.3 1.1	3.4	
313	49.76	49.750	50.08	1.831	1.8312	1.82	54.5	48.9		91.5
115	58.35	58.309		1.580	1.5811		0.8	0.8		
131 511	(59.9) (60.2)	59.825 60.121	60.02	1.543 1.536	1.5446 1.5377	1.54	2.4	0.7 0.7	1.4	21.0
224 404	(62.39)	62.307 62.451	62.25	1.489	1.4889 1.4858	1.49	2.3	1.2 0.6	1.8	21.0
422	(63.25)	63.182		1.470	1.4704		0.8	1.2		
315	67.29	67.267	67.30	1.390	1.3907	1.39	18.8	19.3		74.0
133	(68.2)	68.112		1.374	1.3755		0.7	0.4		

TABLE I (Continued)

HKL	Exp. 2	Calc. 2θ*	Laves 2θ*	Exp. d	Calc. d*	Laves d*	Exp. S.R. I.I.%	Calc. S.R. I.I.%		Laves S.R. I.I.%
331	68.70	68.670	68.99	1.365	1.3656	1.36	18.1	18.1		74.0
206	(69.85)	69.742		1.345	1.3472		0.5	0.4		
602	71.97	71.940	72.03	1.310	1.3114	1.31	15.1	15.7		95.0
333	76.50	76.473	76.80	1.244	1.2445	1.24	12.5	13.3		75.0
026	77.92	77.902	78.30	1.225	1.2252	1.22	12.4	12.6		64.0
040	79.90	79.890	80.67	1.1995	1.1997	1.19	13.4	5.9	17.6	96.5
620	80.32	80.280		1.1943	1.1948			11.7		
135	(83.84)	83.505	83.21	1.153	1.1567	1.16	0.4	0.2	0.4	11.0
515		83.764			1.1538			0.2		
531	(85.14)	85.070	85.01	1.138	1.1394	1.14	0.8	0.2	0.4	11.0
711	(85.34)	85.328		1.136	1.1366			0.2		
242	87.69	87.641		1.112	1.1124		0.7	0.4		
317	90.20	90.178		1.087	1.0876		8.6	9.1		
335	91.50	91.478		1.075	1.0755		7.8	8.8		
008		92.222			1.0688			4.3		
533	(92.40)	92.517		1.067	1.0661		4.5	0.2	4.7	
713		92.774			1.0639			0.2		
044	94.88	94.828		1.046	1.0462			8.2		
624	95.23	95.214		1.043	1.0429		22.5	16.4	24.7	
440		95.870			1.0375			0.1		

TABLE I (Continued)

HKL	Exp. 2θ	Calc. 2θ*	Laves 2θ*	Exp. d	Calc. d*	Laves d*	Exp. S.R. I.I.%	Calc. S.R. I.I.%		Laves S.R. I.I.%
606	102.09	102.085		0.9905	0.9905		7.0	7.6		
137	(106.3)	106.047			0.9642		0.4	0.1	0.2	
517		106.314			0.9625			0.1		
228		108.320			0.9502			0.3		
408	(108.4)	108.456			0.9494		0.7	0.1	0.5	
151		108.773			0.9475			0.1		
444	(111.28)	111.221		0.9331	0.9334		0.6	0.3		
119	(112.61)	112.555		0.9258	0.9261		0.6	0.1		
337	114.54	114.540		0.9156	0.9156		7.1	7.3		
153	(117.44)	116.850		0.9013	0.9041		8.4	0.1	7.5	
351		117.434			0.9013			7.4		
911	(118.32)	118.305		0.8971	0.8972		7.7	7.5	7.8	
246		118.570			0.8959			0.3		
642	120.99	120.961		0.8850	0.8852		23.3	15.1	22.7	
319	121.52	121.499		0.8828	0.8828			7.6		
353	126.21	126.197		0.8637	0.8637		6.8	8.0		
913	127.17	127.157		0.8600	0.8601		6.6	8.1		
0210	146.01	146.015		0.8054			10.5	11.4		
355	148.23	148.240		0.8008	0.8008		11.4	12.3		

TABLE I (Continued)

HKL	Exp. 2θ	Calc. 2θ*	Laves 2θ*	Exp. d	Calc. d*	Laves d*	Exp. S.R. I.I.%	Calc. S.R. I.I.%	Laves S.R. I.I.%
915		149.734			0.7979			12.8	
048	(149.7)	149.681		0.7966	0.7980		47.8	12.7	51.8
628	150.45	150.452			0.7966			26.0	
553		150.270			0.7969			0.3	
931	152.42	152.423		0.7931	0.7931		9.3	14.0	

*CuK_{α_1}

TABLE II. Atomic Scattering Factors

Sin θ/λ	Ti	Si	Si_{val}	Si^{+4}
0.0	22.000	14.000	14.000	10.000
0.010	21.954	13.976	13.973	9.998
0.020	21.856	13.904	13.894	9.991
0.030	21.682	13.787	13.766	9.981
0.040	21.451	13.628	13.593	9.966
0.050	21.171	13.434	13.381	9.947
0.060	20.854	13.209	13.138	9.924
0.070	20.511	12.961	12.870	9.896
0.080	20.150	12.695	12.586	9.865
0.090	19.731	12.417	12.293	9.829
0.100	19.410	12.134	11.995	9.790
0.110	19.041	11.849	11.700	9.747
0.120	18.678	11.567	11.410	9.700
0.130	18.322	11.292	11.130	9.649
0.140	[illegible]	[illegible]	10.862	9.595
0.150	17.685	10.769	10.603	9.537
0.160	17.304	10.525	10.368	9.476
0.170	16.930	10.293	10.143	9.411
0.180	16.565	10.070	9.933	9.343
0.190	16.351	9.868	9.737	9.272
0.200	16.044	9.673	9.553	9.199
0.220	15.444	9.319	9.222	9.043
0.240	14.859	9.004	8.931	8.877
0.260	14.572	8.859	8.798	8.790
0.280	14.280	8.722	8.671	8.701
0.290	13.755	8.467	8.435	8.518
0.300	13.198	8.231	8.214	8.327
0.320	12.682	8.011	8.005	8.131

TABLE II (Continued)

Sin θ/λ	Ti	Si	Si_{val}	Si^{+4}
0.340	12.187	7.800	7.803	7.929
0.350	11.949	7.698	7.704	7.827
0.360	11.717	7.597	7.606	7.724
0.380	11.271	7.398	7.410	7.519
0.400	10.852	7.202	7.215	7.306
0.420	10.459	7.008	7.021	7.095
0.440	10.093	6.813	6.826	6.884
0.450	9.920	6.719	6.729	6.779
0.460	9.753	6.622	6.632	6.674
0.480	9.438	6.431	6.437	6.465
0.500	9.148	6.240	6.244	6.259
0.550	8.518	5.769	5.766	5.755
0.600	8.007	5.312	5.303	5.277
0.650	7.588	4.878	4.865	4.830
0.700	7.240	4.470	4.455	4.470
0.800	6.676	3.750	3.734	3.701
0.900	6.200	3.164	3.150	3.124
1.000	5.752	2.702	2.691	2.673
1.100	5.510	2.346	2.338	2.326
1.200	4.872	2.076	2.069	2.063
1.300	4.445	1.872	1.867	1.864
1.400	4.038	1.717	1.713	1.712
1.500	3.660	1.598	1.595	1.595
1.600	3.316	1.505	1.505	1.505
1.700	3.006	1.430	1.430	1.430
1.800	2.734	1.367	1.367	1.367
1.900	2.496	1.313	1.313	1.313
2.000	2.290	1.264	1.264	1.264

TABLE III. Reflections for TiSi

a. TiSi (50% Silicon)

hkl	Exp. 2θ	Calc. 2θ	Previous 2θ	d	Exp. Rel. I.I.	Previous Rel. I.I.
011	30.41	30.397	30.40	2.9381	7.6	20.0
201	32.77	32.751	32.80	2.7321	7.4	20.0
111	33.43	33.415	33.41	2.6793	39.3	80.0
002	35.97	35.953	–	2.4958	5.4	–
210	37.00	36.992	36.88	2.4286	90.1	100.0
102	38.60	38.587	38.52	2.3312	54.3	80.0
211	41.30	41.306	41.20	2.1838	100.0	80.0
301	45.42	45.424	45.30	1.9950	25.3	50.0
112	46.23	46.225	46.20	1.9620	59.6	85.0
020	50.16	50.160	49.99	1.8172	30.0	60.0
311	52.25	52.264	52.19	1.7488	7.8	20.0
401	59.51	59.535	59.38	1.5514	16.1	40.0
221	61.17	61.205	61.12	1.5130	4.5	
013		61.214		1.5128		
312	62.12	62.021	62.12	1.4951	15.7	10.0
410		62.303		1.4890		
113	62.97	63.019	62.82	1.4748	6.0	10.0
122	64.96	65.010	64.87	1.4334	24.9	50.0
411	65.46	65.314		1.4268	5.2	
213	66.23	68.272	68.19	1.3726	5.2	25.0
402	68.79	68.645		1.3661	4.9	
321	69.93	69.970	69.81	1.3434	12.0	40.0
222		70.196		1.3396		
303	71.25	71.285	71.21	1.3218	8.3	20.0
412	(73.85)	74.030	–	1.2767	5.1	–
501	75.10	75.138	75.02	1.2633	1.9	<1.0
004	76.18	76.232	76.22	1.2479	10.3	20.0

TABLE IIIa (Continued)

hkl	Exp. 2θ	Calc. 2θ	Previous 2θ	d	Exp. Rel. I.I.	Previous Rel. I.I.
313	76.58	76.643		1.2422		
421	(81.50)	81.509	81.33	1.1799	12.1	40.0
031		81.730		1.1773		
204		82.724		1.1656		
403	82.65	82.761	82.60	1.1652	3.6	10.0
114	83.26	83.089	83.21	1.1614	2.3	10.0
131		83.339		1.1586		
223	(84.30)	84.222	84.10	1.1487	6.1	5.0
230	85.39	85.404	85.29	1.1358	7.1	20.0
214	(88.00)	87.390	87.78	1.1099		50.0
413		87.927		1.1100		
512	(90.00)	88.637	88.38	1.1025	27.6	25.0
600	-	90.118	89.82	1.0882	-	5.0
132	91.48	91.540	91.[illegible]	1.0750	7.8	20.0
523	92.15	92.206	92.09	1.[illegible]	[illegible]	20.0
610	95.17	95.273	94.97	1.0425		10.0
314		95.375	95.57	1.0375	3.7	5.0
521		95.903		1.0273		
024	96.98	96.970	96.80	1.0267	9.6	20.0
303		97.152		1.0272		
611	97.95	98.020	97.63	1.0204	3.8	5.0
513	102.31	102.377		0.9885	8.8	
224	103.44	103.456		0.9811	6.2	
522	104.24	104.205		0.9761	3.1	
133	(105.30)	105.367		0.9685	1.8	
414	(107.60)	107.290		0.9564	5.5	
233	110.34	110.396		0.9381	3.3	

TABLE IIIa (Continued)

hkl	Exp. 2θ	Calc. 2θ	d	Exp. Rel. I.I.
620	(111.10)	111.187	0.9336	
215	113.03	113.067	0.9233	6.0
603	115.55	115.511	0.9107	5.6
141	(121.00)	120.854	0.8856	2.0
531	123.34	123.366	0.8751	10.9
405	128.92	128.895	0.8538	4.6
712	130.13	130.110	0.8495	6.1
234	(133.00)	132.991	0.8400	11.5
340	133.50	133.465	0.8384	
242	137.65	137.666	0.8260	8.4
604	(140.00)	139.824	0.8202	2.0
722	(142.50)	142.424	0.8136	6.9

TABLE III (Continued)

b. $Ti_{40}Si_{60}$

hkl	Exp. 2θ	Calc. 2θ	Previous 2θ	d	Exp. Rel. I.I.	Previous Rel. I.I.
011	30.36	30.375	30.40	2.9401	7.4	20.0
201	32.70	32.715	32.80	2.7350	10.1	20.0
111	33.40	33.308	33.41	2.6814	52.4	80.0
002	35.95	35.913	–	2.4965	3.1	–
210	36.95	36.951	36.88	2.4306	100.0	100.0
102	38.58	38.544	38.52	2.3337	67.6	80.0
211	41.28	41.268	41.20	2.1858	84.5	80.0
301	45.38	45.374	45.30	1.9970	34.1	50.0
112	46.13	46.180	46.20	1.9641	78.2	85.0
020	50.15	50.130	49.99	1.8182	39.5	60.0
311	52.14	52.212	52.19	1.7504	8.6	20.0
401	59.46	59.467	59.38	1.5530	20.2	40.0
221	61.16	61.157	61.12	1.5141	5.8	10.0
013		61.147		1.5143		
312	61.96	61.955	61.98	1.4965	15.6	20.0
410		62.237		1.4904		
113	62.96	62.949	62.92	1.4752	6.5	10.0
122	64.96	64.965	64.87	1.4343	31.5	50.0
411		65.273		1.4282		
213	68.20	68.195	68.19	1.3740	7.2	25.0
402		68.584		1.3675		
321	69.92	69.905	69.81	1.3444	15.9	40.0
222		70.133		1.3407		
303	71.20	71.198	71.21	1.3232	11.4	20.0
501	75.35	75.047	75.32	1.2646	0.8	<1.0
004	(76.14)	76.135	76.22	1.2492	13.0	20.0

TABLE IIIb (Continued)

hkl	Exp. 2θ	Calc. 2θ	Previous 2θ	d	Exp. Rel. I.I.	Previous Rel. I.I.
313	(76.56)	76.552		1.2434		
511	80.32	80.311	80.18	1.1944	9.5	20.0
421	81.43	81.426	81.33	1.1809	15.5	40.0
031		81.673		1.1779		
403	(82.67)	82.654	82.60	1.1664	7.1	10.0
204		82.615		1.1669		
114	(83.27)	82.935	83.21	1.1626		10.0
131		83.278		1.1593		
223	84.13	84.132	84.10	1.1497	1.6	5.0
230	85.34	85.340	85.29	1.1364	7.5	20.0
413	(87.78)	87.815	87.78	1.1107	27.3	50.0
214	(88.06)	87.777		1.1111		
512	(88.58)	88.526	88.38	1.1036		25.0
600	90.00	90.000	89.82	1.0998	1.2	5.0
132	(91.45)	91.462	91.43	1.0757	20.5	20.0
323	(92.09)	92.101	92.09	1.0699		20.0
[illegible]	[illegible]	[illegible]	94.97	1.0435	8.1	10.0
521		95.792		1.0382		5.0
314		95.745		1.0386		
024	96.85	96.852	96.80	1.0296	11.4	20.0
503		97.016		1.0283		
611	97.87	97.889	97.69	1.0215	3.7	5.0
513	102.23	102.233		0.9895	8.5	
224	103.33	103.322		0.9820	5.3	
522	104.09	104.093		0.9768	1.8	
133	105.26	105.253		0.9692	1.0	
414	(107.50)	107.130		0.9574	5.0	

TABLE IIIb (Continued)

hkl	Exp. 2θ	Calc. 2θ	d	Exp. Rel. I.I.
233	(110.15)	110.271	0.9388	5.3
620	(110.93)	111.036	0.9344	
215	112.89	112.887	0.9243	6.8
503	115.32	115.322	0.9117	5.7
141	(121.03)	120.738	0.8861	2.5
531	123.34	123.341	0.8751	15.8
405	129.23	129.236	0.8526	5.6
712	129.82	129.862	0.8504	7.5
234	132.78	132.775	0.8406	16.6
340	(133.61)	133.[illegible]	0.8390	
242	(136.00)	137.478	0.8265	15.6
604	139.50	139.496	0.8210	7.9
703	142.08	142.074	0.8145	12.2

TABLE III (Continued)

c. Comparison of Previous Relative Line Intensities

hkl	Previous Rel. I.I.	Calc. Rel. I.I.
200	< 1.0	0.5
011	20.0	17.7
201	20.0	22.1
111	80.0	72.3
210	100.0	97.1
102	80.0	86.8
211	80.0	88.9
301	50.0	57.3
112	35.0	100.0
020	60.0	48.4
311	20.0	12.0
121	< 1.0	1.5
302	< 1.0	0.4
400		[illegible]
401	40.0	21.1
[illegible]	10.0	6.2
013		0.3
312	20.0	7.7
410		4.9
113	10.0	12.9
122	50.0	33.7
411		6.1
213	25.0	24.1
402		0.1
321	40.0	29.9
222		0.4

TABLE IIIc (Continued)

hkl	Previous Rel. I.I.	Calc. Rel. I.I.
303	20.0	11.6
501	< 1.0	0.8
004	20.0	12.8
313		2.5
511	20.0	12.4
421	40.0	16.5
031		0.7
403	10.0	9.0
204		0.4
114	10.0	0.6
131		4.2
223	5.0	1.3
230	20.0	7.8
413	50.0	4.1
214		14.1
512	25.0	17.4
600	5.0	4.1
132	20.0	14.6
323	20.0	12.2
610	10.0	6.8
521	5.0	0.8
314		0.7
024	20.0	15.1
503		0.9
611	5.0	2.6

TABLE IV

A. Intensities for 2θ Region 35° to 45°, As Received 2.2 μm Titanium Thin Film

2θ	Int.	2θ	Int.	2θ	Int.	2θ	Int.
34.00	3.2	34.25	3.2	34.50	3.2	34.75	3.3
35.00	3.5	35.25	3.6	35.50	3.7	35.75	3.8
36.00	4.0	36.12	4.0	36.25	4.1	36.37	4.2
[illegible]	[illegible]	36.62	4.4	36.77	4.6	36.87	4.8
37.00	5.1	37.12	5.5	37.25	6.5	37.37	8.1
37.50	9.2	37.62	7.0	37.75	5.3	37.87	4.9
38.00	4.8	38.25	4.8	38.37	4.7	38.50	4.8
38.62	5.1	38.75	5.2	38.87	5.7	39.00	6.1
39.12	6.9	39.25	7.7	39.37	8.5	39.50	9.4
39.62	9.8	39.75	9.5	39.87	8.5	40.00	7.5
40.12	6.9	40.25	6.3	40.37	5.9	40.50	5.7
40.75	5.5	41.00	5.7	41.25	5.6	41.50	5.6
41.75	5.6	41.87	5.6	41.93	5.4	42.00	5.3
42.25	4.3	42.50	4.3	42.75	[illegible]	43.00	3.6
43.25	3.3	43.50	3.2	43.75	3.1	44.00	3.0
44.50	2.9	45.00	2.8				

B. Intensities for 2θ Region 70° to 80°, As Received 2.2 μm Titanium Thin Film

2θ	Int.	2θ	Int.	2θ	Int.	2θ	Int.
70.00	6.0	70.50	6.0	71.00	6.0	71.50	6.0
72.00	6.0	72.13	6.0	72.25	6.0	72.38	6.0
72.50	6.1	72.63	6.1	72.75	6.2	72.88	6.3
73.00	6.3	73.13	6.3	73.25	6.4	73.38	6.5
73.50	6.6	73.63	6.6	73.75	6.7	73.88	6.8
74.00	6.8	74.13	6.8	74.25	6.6	74.38	6.7
74.50	6.6	74.63	6.8	74.75	6.9	74.88	6.9
75.00	6.9	75.13	6.9	75.25	6.9	75.38	6.9
75.50	6.8	75.63	6.8	75.75	6.8	75.88	6.7
76.00	6.9	76.13	7.2	76.25	7.2	76.38	7.2
76.50	7.2	76.63	7.2	76.75	7.1	76.88	6.9
77.00	6.9	77.13	6.8	77.25	6.7	77.38	6.5
77.50	6.4	77.63	6.3	77.75	6.2	77.88	6.2
78.00	6.2	78.25	6.1	78.50	6.0	78.75	6.0
79.00	6.0	79.25	6.0	79.50	6.0	79.75	6.0
80.00	6.0						

TABLE V

A. Intensities for 2θ Region 35° to 45°, Step Anneal for 2 Hours at 350°C

2θ	Int.	2θ	Int.	2θ	Int.	2θ	Int.
35.00	3.8	35.25	3.8	35.50	3.9	35.75	4.0
36.00	4.0	36.15	4.1	36.30	4.3	36.45	4.5
36.60	4.6	36.65	4.7	36.70	4.8	36.75	4.9
36.80	5.0	36.85	5.0	36.95	5.2	37.00	5.4
37.10	5.9	37.15	6.2	37.20	6.6	37.25	7.0
37.30	7.7	37.35	8.3	37.40	8.6	37.45	8.5
37.50	7.6	37.55	6.7	37.60	6.0	37.65	5.5
37.70	5.0	37.75	4.9	37.80	4.8	37.85	4.7
37.90	4.6	37.95	4.6	38.00	4.7	38.10	4.7
38.20	4.7	38.30	4.8	38.40	4.9	38.50	4.9
38.60	5.1	38.70	5.3	38.80	5.7	38.90	6.0
39.00	6.7	39.05	6.8	39.10	7.2	39.15	7.5
39.20	7.9	39.25	8.1	39.30	8.4	39.35	8.8
39.40	9.0	39.45	9.5	39.70	9.5	39.55	9.9
39.60	10.0	39.65	9.9	39.70	9.7	39.75	9.5
39.85	8.8	39.95	8.0	40.00	7.7	40.10	7.3
40.20	6.8	40.30	6.4	40.40	6.1	40.50	5.9
40.60	5.7	40.65	5.7	40.75	5.7	40.85	5.7
40.95	5.7	41.00	5.8	41.10	5.9	41.20	6.1
41.30	6.1	41.40	6.3	41.50	6.4	41.60	6.4
41.65	6.4	41.70	6.3	41.75	6.3	41.80	6.2
41.85	6.2	41.90	6.0	41.95	5.8	42.00	5.6
42.10	5.4	42.20	5.0	42.30	5.0	42.40	4.7
42.50	4.5	42.60	4.3	42.70	4.1	42.80	3.9
42.80	3.9	42.90	3.7	43.00	3.5	43.10	3.4
43.30	3.3	43.50	3.2	43.70	3.1	43.90	3.0
44.00	3.0	44.25	3.0	44.50	3.0	44.75	3.0

B. Intensities for 2θ Region 72° to 78°, Step Anneal for 2 Hours at 350°C

2θ	Int.	2θ	Int.	2θ	Int.	2θ	Int.
72.00	6.0	72.10	6.0	72.20	6.0	72.30	6.0
72.40	6.0	72.50	6.0	72.60	6.0	72.70	6.1
72.80	6.1	72.90	6.2	73.00	6.2	73.10	6.3
73.20	6.3	73.30	6.3	73.40	6.4	73.50	6.4
73.60	6.4	73.70	6.5	73.80	6.5	73.90	6.6
74.00	6.5	74.10	6.5	74.20	6.4	74.30	6.5
74.40	6.6	74.50	6.6	74.60	6.7	74.70	6.8
74.80	6.9	74.90	6.8	75.00	6.8	75.10	6.8
75.20	6.8	75.30	6.7	75.40	6.8	75.50	6.8
75.60	6.8	75.70	6.9	75.80	7.0	75.90	7.1
76.00	7.2	76.10	7.2	76.20	7.0	76.30	7.0
76.40	6.9	76.50	6.8	76.60	6.7	76.70	6.7
76.80	6.6	76.90	6.6	77.00	6.6	77.10	6.5
77.20	6.5	77.30	6.4	77.40	6.4	77.50	6.4
77.60	6.4	77.70	6.4	77.80	6.4	77.90	6.4
78.00	6.4						

TABLE VI

A. Intensities for 2θ Region 35° to 45°, Step Anneal for 2 Hours at 450°C

2θ	Int.	2θ	Int.	2θ	Int.	2θ	Int.
35.00	4.0	35.25	4.0	35.50	4.0	35.75	4.1
35.85	4.2	35.95	4.2	36.00	4.3	36.10	4.4
36.20	4.6	36.30	4.6	36.40	4.8	36.50	4.9
36.60	5.0	36.70	5.1	36.80	5.2	36.90	5.4
36.95	5.6	37.00	5.8	37.05	6.1	37.10	6.3
37.15	6.7	37.20	7.0	37.25	7.6	37.30	8.1
37.35	6.5	37.40	8.6	37.45	7.9	37.50	7.1
37.55	6.3	37.60	5.7	37.65	5.4	37.70	5.2
37.80	5.0	37.90	4.9	38.00	5.0	38.10	5.0
38.20	5.0	38.30	5.2	38.40	5.2	38.50	5.4
38.60	5.6	38.65	5.8	38.70	5.9	38.75	6.2
38.80	6.4	38.85	6.6	38.90	6.7	38.95	7.0
39.00	7.5	39.05	8.0	39.10	8.4	39.15	8.8
39.20	9.4	39.25	9.7	39.30	10.2	39.35	10.7
39.40	10.8	39.45	11.1	39.50	11.2	39.55	11.3
39.60	11.2	39.65	11.0	39.70	10.7	39.75	10.5
39.80	10.1	39.85	9.8	39.90	9.3	39.95	9.0
40.00	8.5	40.10	8.0	40.20	7.3	40.30	6.8
40.40	6.5	40.50	6.3	40.60	6.1	40.70	6.0
40.80	6.0	40.90	6.1	41.00	6.2	41.10	6.3
41.20	6.4	41.25	6.5	41.30	6.5	41.40	6.5
41.50	6.6	41.60	6.6	41.70	6.5	41.75	6.4
41.80	6.4	41.90	6.2	42.00	6.1	42.10	5.8
42.20	5.6	42.30	5.4	42.40	5.1	42.50	4.9
42.60	4.8	42.70	4.6	42.80	4.3	42.90	4.3
43.00	4.2	43.10	4.1	43.20	4.0	43.30	3.8
43.40	3.7	43.50	3.7	43.75	3.5	44.00	3.4

TABLE VI (A) (Continued)

2θ	Int.	2θ	Int.	2θ	Int.	2θ	Int.
44.25	3.3	44.50	3.2	44.75	3.0	45.00	3.0

B. Intensities for 2θ Region 72° to 79°, Step Anneal for 2 Hours at 450°C

2θ	Int.	2θ	Int.	2θ	Int.	2θ	Int.
72.00	6.9	72.10	6.9	72.20	6.9	72.30	7.1
72.40	7.1	72.50	7.1	72.60	7.1	72.70	7.1
72.80	7.2	72.90	7.3	73.00	7.4	73.10	7.4
73.20	7.5	73.30	7.6	73.40	7.6	73.50	7.6
73.60	7.7	73.70	7.8	73.80	7.7	73.90	7.7
74.00	7.6	74.10	7.6	74.20	7.6	74.30	7.6
74.40	7.5	74.50	7.5	74.60	7.5	74.70	7.5
74.80	7.5	74.90	7.6	75.00	7.6	75.10	7.5
75.10	7.5	75.20	7.6	75.30	7.6	75.40	7.7
75.50	7.8	75.60	7.9	75.70	7.9	75.80	8.0
75.90	8.1	76.00	8.1	76.10	8.1	76.20	8.1
76.30	8.0	76.40	8.0	76.50	7.9	76.60	7.8
76.70	7.7	76.80	7.7	76.90	7.7	77.00	7.6
77.10	7.5	77.20	7.3	77.30	7.2	77.40	7.2
77.50	7.1	77.60	7.0	77.70	7.0	77.80	7.0
77.90	7.0	78.00	6.9	78.10	6.8	78.20	6.8
78.30	6.6	78.40	6.6	78.50	6.6	78.60	6.5
78.70	6.5	78.80	6.5	78.90	6.5		

TABLE VII

A. Intensities for 2θ Region 35° to 45°, Step Anneal for 2 Hours at 500°C

2θ	Int.	2θ	Int.	2θ	Int.	2θ	Int.
35.00	2.5	35.25	2.5	35.50	2.5	35.75	2.5
36.00	2.5	36.10	2.6	36.20	2.8	36.30	3.0
36.40	3.1	36.50	3.1	36.60	3.2	36.70	3.4
36.80	3.5	36.90	3.8	37.00	4.2	37.05	4.4
37.10	4.6	37.15	4.9	37.20	5.1	37.25	5.2
37.30	5.1	37.35	4.8	37.40	4.2	37.45	3.9
37.50	3.5	37.55	3.3	37.60	3.1	37.65	3.0
37.75	2.9	37.85	3.0	37.95	2.9	38.00	2.9
38.10	3.1	38.20	3.1	38.30	3.1	38.40	3.3
38.50	3.4	38.55	3.5	38.60	3.8	38.65	3.9
38.70	4.2	38.75	4.5	38.80	4.7	38.85	5.0
38.90	5.0	38.95	5.9	39.00	6.5	39.05	7.2
39.10	7.8	39.15	8.6	39.20	9.0	39.25	9.2
39.30	9.4	39.35	9.6	39.40	9.8	39.45	9.8
39.50	9.5	39.55	8.9	39.60	8.3	39.65	8.0
39.70	7.7	39.75	7.2	39.80	6.9	39.85	6.5
39.90	6.2	39.95	5.9	40.00	5.5	40.05	5.2
40.10	5.0	40.15	4.8	40.20	4.6	40.20	4.4
40.30	4.3	40.40	4.1	40.50	4.0	40.60	3.8
40.70	3.8	40.80	3.9	40.90	3.9	41.00	4.1
41.10	4.3	41.20	4.3	41.30	4.5	41.40	4.6
41.50	4.5	41.60	4.4	41.70	4.3	41.80	4.2
41.90	4.0	42.00	3.9	42.10	3.6	42.20	3.5
42.30	3.3	42.40	3.2	42.50	3.1	42.60	3.0
42.70	3.0	42.80	2.9	42.90	2.8	43.00	2.4
43.10	2.2	43.20	2.0	43.30	1.9	43.40	1.7
43.50	1.6	43.60	1.5	43.70	1.5	43.80	1.5

TABLE VII (A) (Continued)

2θ	Int.	2θ	Int.	2θ	Int.	2θ	Int.
43.90	1.4	44.00	1.4	44.25	1.4	44.50	1.3
44.75	1.3	45.00	1.3				

B. Intensities for 2θ Region 72° to 79°, Step Anneal for 2 Hours at 500°C

2θ	Int.	2θ	Int.	2θ	Int.	2θ	Int.
72.00	6.0	72.10	6.0	72.20	6.1	72.30	6.1
72.40	6.2	72.50	6.4	72.60	6.6	72.70	6.7
72.80	6.8	72.90	7.0	73.00	7.4	73.10	7.6
73.20	7.6	73.30	7.8	73.40	7.7	73.50	7.6
73.60	7.4	73.70	7.4	73.80	7.4	73.90	7.4
74.00	7.4	74.10	7.5	74.20	7.5	74.30	7.5
74.40	7.4	74.50	7.4	74.60	7.4	74.70	7.5
74.80	7.5	74.90	7.6	75.00	7.7	75.10	7.7
75.20	7.8	75.30	7.8	75.40	7.9	75.50	8.0
75.50	8.2	75.70	8.3	75.80	8.5	75.90	8.6
76.00	8.8	76.10	8.8	76.20	9.0	76.30	8.8
76.40	8.6	76.50	8.4	76.60	8.3	76.70	8.0
76.80	7.9	76.90	7.8	77.00	7.4	77.10	7.2
77.20	7.0	77.30	6.9	77.40	6.9	77.50	7.0
77.60	7.0	77.70	6.9	77.80	6.8	77.90	6.8
78.00	6.8	78.10	6.8	78.20	6.7	78.30	6.6
78.40	6.5	78.50	6.5	78.60	6.3	78.70	6.1
78.80	6.0	78.90	6.0	79.00	6.0		

TABLE VIII

A. Intensities for 2θ Region 35° to 46°, Step Anneal for 2 Hours at 550°C

2θ	Int.	2θ	Int.	2θ	Int.	2θ	Int.
35.00	2.0	35.25	2.0	35.50	2.0	35.75	2.1
35.85	2.2	35.95	2.4	36.00	2.5	36.05	2.5
36.10	2.6	36.15	2.7	36.20	2.8	36.25	2.9
36.30	3.0	36.35	3.1	36.40	3.1	36.45	3.1
36.50	3.2	36.55	3.3	36.60	3.3	36.65	3.4
36.70	3.4	36.75	3.5	36.80	3.6	36.90	3.7
36.95	3.8	37.00	4.0	37.05	4.2	37.10	4.4
37.15	4.5	37.20	4.4	37.25	4.2	37.30	3.9
37.35	3.7	37.40	3.6	37.45	3.4	37.50	3.3
37.55	3.2	37.60	3.1	37.65	3.0	37.70	2.9
37.75	2.8	37.85	2.9	37.90	2.8	37.95	2.9
38.00	2.9	38.10	2.9	38.20	3.0	38.30	3.1
38.40	3.3	38.50	3.5	38.55	3.7	38.60	4.0
38.65	4.3	38.70	4.7	38.75	5.0	38.80	5.4
38.85	6.0	38.90	6.8	38.95	7.6	39.00	8.5
39.05	9.8	39.10	10.8	39.15	12.0	39.20	13.0
39.25	13.2	39.30	13.1	39.35	12.4	39.40	11.6
39.45	10.9	39.50	10.1	39.55	9.5	39.60	9.0
39.65	8.6	39.70	8.1	39.75	7.6	39.80	7.1
39.85	6.7	39.90	6.3	39.95	6.0	40.00	5.6
40.05	5.4	40.10	5.1	40.15	4.9	40.20	4.7
40.25	4.5	40.30	4.3	40.35	4.3	40.40	4.1
40.45	4.1	40.50	4.0	40.55	4.0	40.60	4.0
40.65	4.0	40.70	3.9	40.75	3.9	40.80	3.9
40.85	3.8	40.90	3.8	41.00	3.8	41.10	4.0
41.20	4.1	41.30	4.3	41.40	4.4	41.50	4.4
41.60	4.5	41.70	4.5	41.80	4.6	41.90	4.5

TABLE VIII (A) (Continued)

2θ	Int.	2θ	Int.	2θ	Int.	2θ	Int.
42.00	4.4	42.10	4.3	42.20	4.1	42.30	3.8
42.40	3.5	42.50	3.3	42.60	3.0	42.70	2.8
42.80	2.6	42.90	2.4	43.00	2.3	43.10	2.1
43.20	2.0	43.30	2.0	43.40	2.0	43.50	2.0
43.60	1.9	43.70	1.8	43.80	1.7	43.90	1.7
44.00	1.7	44.25	1.6	44.50	1.6	44.75	1.6
45.00	1.6	45.25	1.5	45.50	1.5	45.75	1.5
46.00	1.5						

B. Intensities for 2θ Region 72° to 79°, Step Anneal for 2 Hours at 550°C

2θ	Int.	2θ	Int.	2θ	Int.	2θ	Int.
72.00	8.9	72.10	8.9	72.20	9.0	72.30	9.1
72.40	9.3	72.50	9.5	72.60	9.7	72.70	9.9
72.80	9.9	72.90	10.1	73.00	10.3	73.10	10.5
73.20	10.8	73.30	10.9	73.40	11.0	73.50	11.0
73.60	11.0	73.70	11.1	73.80	11.0	73.90	11.0
74.00	10.9	74.10	10.8	74.20	10.7	74.30	10.7
74.40	10.6	74.50	10.5	74.60	10.5	74.70	10.6
74.80	10.8	74.90	10.9	75.00	11.2	75.10	11.3
75.20	11.4	75.30	11.5	75.40	11.6	75.50	11.8
75.60	12.0	75.70	12.4	75.80	13.0	75.90	13.1
76.00	13.2	76.10	13.0	76.20	12.8	76.30	12.6
76.40	12.4	76.50	12.2	76.60	11.9	76.70	11.6
76.80	11.4	76.90	11.2	77.00	11.0	77.10	10.8
77.20	10.6	77.30	10.4	77.40	10.3	77.50	10.2
77.60	10.0	77.70	9.9	77.80	9.8	77.90	9.8
78.00	9.8	78.20	9.8	78.40	9.8	78.60	9.8
78.80	9.8	79.00	9.8				

TABLE IX

A. Intensities for 2θ Region 34° to 45°, Step Anneal for 2 Hours at 575°C

2θ	Int.	2θ	Int.	2θ	Int.	2θ	Int.
34.00	1.8	34.10	1.9	34.20	2.0	34.30	2.1
34.40	2.2	34.50	2.3	34.60	0.2	34.70	2.3
34.80	2.2	34.90	2.1	35.00	2.2	35.10	2.1
35.20	2.1	35.30	2.1	35.40	2.2	35.50	2.2
35.60	2.2	35.70	2.2	35.80	2.3	35.90	2.4
36.00	2.6	36.05	2.8	36.10	2.9	36.15	3.0
36.20	3.2	36.25	3.3	36.30	3.4	36.40	3.4
36.50	3.6	36.55	3.6	36.60	3.6	36.65	3.7
36.70	3.7	36.75	3.8	36.80	3.8	36.90	3.8
37.00	3.9	37.10	4.0	37.20	4.0	37.25	4.0
37.30	3.9	37.40	3.7	37.50	3.4	37.60	3.2
37.70	3.1	37.80	3.0	37.90	2.9	38.00	2.9
38.10	2.9	38.20	3.0	38.30	3.1	38.40	3.2
38.45	3.4	38.50	3.5	38.60	3.7	38.65	4.0
38.70	4.4	38.75	4.8	38.80	5.3	38.85	5.8
38.90	6.7	38.95	7.4	39.00	8.5	39.05	9.8
39.10	11.0	39.15	12.5	39.20	13.8	39.25	14.4
39.30	14.3	39.35	13.3	39.40	11.9	39.45	10.7
39.50	9.8	39.55	9.0	39.60	8.5	39.65	8.0
39.70	7.5	39.75	7.0	39.80	6.5	39.85	6.0
39.90	5.5	39.95	5.3	40.00	5.0	40.05	4.8
40.10	4.5	40.15	4.3	40.20	4.0	40.25	3.9
40.35	3.7	40.45	3.7	40.50	3.6	40.60	3.6
40.70	3.6	40.80	3.5	40.90	3.5	41.00	3.5
41.10	3.5	41.20	3.5	41.30	3.7	41.40	3.8
41.50	3.9	41.60	4.1	41.70	4.1	41.80	4.1
41.90	4.0	42.00	3.9	42.10	3.9	42.20	3.8

TABLE IX (A) (Continued)

2θ	Int.	2θ	Int.	2θ	Int.	2θ	Int.
42.30	3.7	42.40	3.5	42.50	3.3	42.60	3.0
42.70	2.8	42.80	2.5	42.90	2.4	43.00	2.2
43.10	2.1	43.20	1.9	43.30	1.9	43.40	1.9
43.50	1.8	43.60	1.8	43.70	1.7	43.80	1.7
43.90	1.6	44.00	1.6	44.25	1.5	44.50	1.5
44.75	1.5	45.00	1.5				

B. Intensities for 2θ Region 72° to 79°, Step Anneal for 2 Hours at 575°C

2θ	Int.	2θ	Int.	2θ	Int.	2θ	Int.
72.00	8.9	72.10	8.9	72.20	8.9	72.30	9.0
72.40	9.2	72.50	9.3	72.60	9.5	72.70	9.7
72.80	10.0	72.90	10.5	73.00	10.8	73.10	10.9
73.20	10.9	73.30	10.7	73.40	10.8	73.50	10.8
73.60	10.8	73.70	10.8	73.80	10.9	73.90	10.9
74.00	10.8	74.10	10.7	74.20	10.6	74.30	10.5
74.40	10.5	74.50	10.6	74.60	10.6	74.70	10.7
74.80	10.8	74.90	10.9	75.00	10.9	75.10	11.0
75.20	11.2	75.30	11.4	75.40	11.5	75.50	11.6
75.60	11.8	75.70	12.2	75.80	12.9	75.90	13.5
76.00	13.8	76.10	13.5	76.20	12.8	76.30	12.3
76.40	11.9	76.50	11.7	76.60	11.4	76.70	11.3
76.80	11.2	76.90	11.0	77.00	10.8	77.10	10.5
77.20	10.3	77.30	10.1	77.40	9.9	77.50	9.8
77.60	9.8	77.70	9.8	77.80	9.7	77.90	9.5
78.00	9.4	78.20	9.4	78.40	9.3	78.60	9.3
78.80	9.3	79.00	9.3				

TABLE X

A. Intensities for 2θ Region 34° to 46°, Step Anneal for 2 Hours at 600°C

2θ	Int.	2θ	Int.	2θ	Int.	2θ	Int.
34.00	1.6	34.10	1.6	34.20	1.8	34.30	1.8
34.40	2.0	34.50	2.2	34.60	2.3	34.70	2.3
34.80	2.1	34.90	2.0	35.00	2.0	35.10	2.0
35.20	2.0	35.30	2.0	35.40	2.0	35.50	2.0
35.60	2.0	35.70	2.2	35.80	2.2	35.90	2.3
36.00	2.5	36.05	2.5	36.10	2.8	36.15	2.9
36.20	3.0	36.25	3.0	36.30	3.1	36.35	3.3
36.40	3.4	36.45	3.5	36.50	3.5	36.55	3.6
36.60	3.6	36.65	3.6	36.70	3.7	36.75	3.7
36.80	3.7	36.85	3.7	36.90	3.6	36.95	3.5
37.00	3.5	37.05	3.4	37.10	3.4	37.15	3.4
37.20	3.3	37.25	3.3	37.30	3.3	37.35	3.4
37.40	3.3	37.50	3.1	37.60	3.0	37.70	2.9
37.80	[illegible]	[illegible]	[illegible]	[illegible]	2.6	38.10	2.7
38.20	2.7	38.30	2.8	38.40	3.0	38.50	3.2
38.60	3.5	38.70	4.2	38.75	4.7	38.80	5.2
38.85	5.8	38.90	6.9	38.95	8.0	39.00	9.1
39.05	10.8	39.10	12.3	39.15	13.7	39.20	14.8
39.25	15.3	39.30	14.5	39.35	13.4	39.40	11.9
39.45	10.5	39.50	9.6	39.55	9.0	39.60	8.4
39.65	7.7	39.70	7.0	39.75	6.6	39.80	6.1
39.85	5.7	39.90	5.3	39.95	5.0	40.00	4.6
40.10	4.2	40.20	3.9	40.30	3.7	40.40	3.5
40.50	3.4	40.60	3.3	40.70	3.3	40.80	3.3
40.90	3.2	41.00	3.2	41.10	3.3	41.20	3.4
41.30	3.6	41.40	3.8	41.60	3.9	41.70	4.0
41.80	4.1	41.90	4.2	42.00	4.2	42.10	4.2

TABLE X (A) (Continued)

2θ	Int.	2θ	Int.	2θ	Int.	2θ	Int.
42.20	4.1	42.30	3.8	42.40	3.5	42.50	3.3
42.60	3.3	42.70	2.7	42.80	2.6	42.90	2.3
43.00	2.2	43.10	2.0	43.20	1.9	43.30	1.9
43.40	1.8	43.50	1.7	43.60	1.6	43.70	1.6
43.80	1.6	43.90	1.6	44.00	1.6	44.25	1.5
44.50	1.5	44.75	1.4	45.00	1.4	45.25	1.3
45.50	1.3	45.75	1.3	46.00	1.3		

B. Intensities for 2θ Region 58° to 65°, Step Anneal for 2 Hours at 600°C

2θ	Int.	2θ	Int.	2θ	Int.	2θ	Int.
58.00	11.9	58.20	11.8	58.40	11.7	58.60	11.7
58.80	11.9	59.00	12.1	59.20	12.3	59.40	12.6
59.60	12.9	59.80	13.3	60.00	13.6	60.20	13.8
60.40	14.4	60.60	15.6	60.80	17.0	61.00	20.7
61.20	20.8	61.40	19.5	61.60	18.0	61.80	16.5
62.00	15.2	62.20	14.5	62.40	14.2	62.60	14.1
62.80	13.2	63.00	12.8	63.20	12.6	63.40	12.3
63.60	12.1	63.80	11.9	64.00	11.6	64.20	11.5
64.40	11.4	64.60	11.3	64.80	11.3	65.00	11.3

C. Intensities for 2θ Region 71° to 79°, Step Anneal for 2 Hours at 600°C

2θ	Int.	2θ	Int.	2θ	Int.	2θ	Int.
71.00	9.5	71.10	9.5	71.20	9.5	71.30	9.5
71.40	9.5	71.50	9.5	71.60	9.5	71.70	9.5
71.80	9.8	71.90	9.9	72.00	10.0	72.10	10.0
72.20	9.9	72.30	9.9	72.40	10.1	72.40	10.5
72.60	10.6	72.70	10.8	72.80	10.8	72.90	10.8
73.00	11.1	73.10	11.3	73.20	11.5	73.30	11.6
73.40	11.6	73.50	11.6	73.60	11.6	73.70	11.6
73.80	11.5	73.90	11.5	74.00	11.4	74.10	11.4
74.20	11.4	74.30	11.3	74.40	11.3	74.50	11.3
74.60	11.2	74.70	11.1	74.80	11.1	74.90	11.2
75.00	11.3	75.10	11.4	75.20	11.6	75.30	11.8
75.40	12.0	75.50	12.3	75.60	12.6	75.70	12.8
75.80	13.2	[illegible]	13.6	76.00	14.1	76.10	13.5
76.20	12.6	76.30	12.2	76.40	11.9	76.50	11.8
76.60	11.7	76.70	11.6	76.80	11.4	76.90	11.1
77.00	11.0	77.10	10.8	77.20	10.7	77.30	10.6
77.40	10.5	77.50	10.5	77.60	10.5	77.70	10.5
77.80	10.4	77.90	10.4	78.00	10.3	78.10	10.2
78.20	10.0	78.30	9.9	78.40	9.7	78.50	9.6
78.60	9.5	78.70	9.5	78.80	9.5	78.90	9.5
79.00	9.5						

TABLE XI

A. Intensities for 2θ Region 34° to 46°, Step Anneal for 2 Hours at 625°C

2θ	Int.	2θ	Int.	2θ	Int.	2θ	Int.
34.00	1.9	34.10	1.9	34.20	2.0	34.30	2.1
34.40	2.2	34.50	2.3	34.60	2.2	34.70	2.2
34.80	2.1	34.90	2.1	35.00	2.1	35.10	2.1
35.20	2.1	35.30	2.1	35.40	2.2	35.50	2.2
35.60	2.2	35.70	2.2	35.80	2.2	35.90	2.3
36.00	2.5	36.10	2.7	36.20	2.9	36.30	3.0
36.40	3.2	36.50	3.3	36.60	3.4	36.70	3.3
36.80	3.1	36.90	3.0	37.00	2.9	37.10	2.9
37.20	2.8	37.30	2.8	37.40	2.8	37.50	2.7
37.60	2.7	37.70	2.6	37.80	2.6	37.90	2.6
38.00	2.5	38.10	2.5	38.20	2.7	38.30	2.7
38.40	2.8	38.50	3.1	38.55	3.3	38.60	3.5
38.65	3.7	38.70	4.0	38.75	4.3	38.80	4.8
38.85	5.5	38.90	6.1	38.95	7.0	39.00	8.0
39.05	9.0	39.10	10.4	39.15	11.5	39.20	12.5
39.25	12.5	39.30	11.2	39.35	10.0	39.40	9.0
39.45	8.3	39.50	7.9	39.55	7.2	39.60	6.5
39.65	6.1	39.70	5.8	39.75	5.4	39.80	5.0
39.85	4.8	39.90	4.5	39.95	4.2	40.00	4.0
40.10	3.7	40.20	3.5	40.30	3.3	40.40	3.3
40.50	3.2	40.60	3.1	40.70	3.1	40.80	3.0
40.90	3.1	41.00	3.1	41.10	3.1	41.20	3.1
41.30	3.2	41.30	3.3	41.50	3.4	41.60	3.5
41.70	3.7	41.80	3.9	41.90	4.0	42.00	4.0
42.10	4.0	42.20	3.9	42.30	3.6	42.40	3.3
42.50	3.0	42.60	2.8	42.70	2.5	42.80	2.5
42.90	2.4	43.00	2.2	43.10	2.1	43.20	2.0

TABLE XI (A) (Continued)

2θ	Int.	2θ	Int.	2θ	Int.	2θ	Int.
43.30	2.0	43.40	1.9	43.50	1.8	43.60	1.8
43.70	1.7	43.80	1.7	43.90	1.6	44.00	1.6
44.25	1.5	44.50	1.5	44.75	1.5	45.00	1.5
45.25	1.5	45.50	1.5	45.75	1.5	46.00	1.5

B. Intensities for 2θ Region 59° to 63°, Step Anneal for 2 Hours at 625°C

2θ	Int.	2θ	Int.	2θ	Int.	2θ	Int.
59.00	10.9	59.10	10.9	59.20	10.9	59.30	10.9
59.40	10.9	59.50	11.0	59.60	11.1	59.70	11.1
59.80	11.1	59.90	11.1	60.00	11.3	60.10	11.5
60.20	11.6	60.30	11.6	60.40	11.7	60.50	12.0
60.60	12.4	60.70	12.7	60.80	13.3	60.90	13.7
61.00	13.8	61.10	13.8	61.20	13.4	61.30	13.0
61.40	12.5	61.50	12.3	61.60	12.1	61.70	11.7
61.80	11.3	61.90	11.1	62.00	11.0	62.10	11.0
62.20	11.0	62.30	10.9	62.40	10.7	62.50	10.6
62.60	10.5	62.70	10.5	62.80	10.5	62.90	10.4
63.00	10.4						

C. Intensities for 2θ Region 70° to 88°, Step Anneal for 2 Hours at 625°C

2θ	Int.	2θ	Int.	2θ	Int.	2θ	Int.
70.00	11.2	70.20	11.2	70.40	11.3	70.60	11.3
70.80	11.4	71.00	11.6	71.20	11.7	71.40	11.7
71.60	11.8	71.80	11.8	72.00	11.9	72.20	12.2
72.40	12.7	72.60	13.2	72.80	14.0	73.00	14.7
73.20	15.2	73.40	15.4	73.60	15.4	73.80	15.4
74.00	15.4	74.20	15.2	74.40	15.1	74.60	15.0
74.80	15.1	75.00	15.2	75.20	15.5	75.40	15.8
75.60	17.3	75.80	18.5	76.00	20.0	76.20	19.0
76.40	17.3	76.60	16.5	76.80	15.8	77.00	15.1
77.20	14.5	77.40	14.1	77.60	13.9	77.80	13.5
78.00	13.3	78.20	13.0	78.40	12.8	78.60	12.7
78.80	12.5	79.00	12.4	79.20	12.3	79.40	12.5
79.60	12.6	79.80	12.7	80.00	12.5	80.20	12.3
80.40	12.1	80.60	11.8	80.80	11.7	81.00	11.6
81.20	11.5	81.40	11.5	81.60	11.6	81.80	11.6
82.00	11.5	82.20	11.3	82.40	11.1	82.60	11.0
82.80	11.0	83.00	11.1	83.20	11.2	83.40	11.4
83.60	11.7	83.80	12.1	84.00	12.8	84.20	13.9
84.40	15.6	84.60	15.0	84.80	13.5	85.00	12.8
85.20	12.4	85.40	12.1	85.60	11.9	85.80	11.7
86.00	11.5	86.20	11.4	86.40	11.3	86.60	11.2
86.80	11.1	87.00	11.1	87.20	11.1	87.40	11.1
87.60	11.1	87.80	11.1	88.00	11.1		

TABLE XII

A. Intensities for 2θ Region 32° to 46°, Step Anneal for 2 Hours at 650°C

2θ	Int.	2θ	Int.	2θ	Int.	2θ	Int.
32.00	1.7	32.10	1.7	32.20	1.7	32.30	1.7
32.40	1.7	32.50	1.7	32.60	1.7	32.70	1.8
32.80	1.8	32.90	1.8	33.00	1.8	33.10	1.8
33.20	1.8	33.30	1.8	33.40	1.8	33.50	1.8
33.60	1.8	33.70	1.8	33.80	1.8	33.90	1.8
34.00	1.8	34.10	1.8	34.20	1.9	34.30	1.9
34.40	2.0	34.50	2.1	34.60	2.2	34.70	2.2
34.80	2.2	34.90	2.1	35.00	2.1	35.10	2.0
35.20	2.0	35.30	1.9	35.40	1.9	35.50	1.9
35.60	2.0	35.70	2.1	35.80	2.2	35.90	2.4
36.00	2.5	36.10	2.8	36.20	3.2	36.30	3.5
36.40	3.7	36.50	3.9	36.60	4.0	36.70	4.0
36.80	3.9	36.90	3.8	37.00	3.5	37.10	3.4
37.20	3.3	37.30	3.2	37.40	3.2	37.50	3.1
37.60	3.1	37.70	3.0	37.80	2.9	37.90	2.8
38.00	2.8	38.10	2.7	38.20	2.7	38.30	2.8
38.40	2.8	38.50	3.0	38.55	3.2	38.60	3.4
38.65	3.6	38.70	3.9	38.75	4.2	38.80	4.7
38.85	5.3	38.90	5.8	38.95	6.7	39.00	7.8
39.05	8.9	39.10	10.5	39.15	12.0	39.20	14.0
39.25	15.8	39.30	17.1	39.35	18.5	39.40	16.5
39.45	14.0	39.50	12.4	39.55	11.3	39.60	10.4
39.65	9.2	39.70	8.5	39.75	7.9	39.80	7.4
39.85	6.8	39.90	6.3	39.95	5.9	40.00	5.5
40.10	4.8	40.20	4.3	40.30	4.0	40.40	3.8
40.50	3.7	40.60	3.6	40.70	3.5	40.80	3.4
40.90	3.4	41.00	3.3	41.10	3.3	41.20	3.3

TABLE XII (A) (Continued)

2θ	Int.	2θ	Int.	2θ	Int.	2θ	Int.
41.30	3.3	41.40	3.4	41.50	3.5	41.60	3.7
41.70	4.0	41.80	4.3	41.90	4.5	42.00	4.7
42.10	4.8	42.20	4.9	42.30	4.8	42.40	4.5
42.50	4.2	42.60	3.8	42.70	3.3	42.80	3.0
42.90	2.7	43.00	2.4	43.10	2.4	43.20	2.7
43.30	3.4	43.50	3.0	43.60	2.5	43.70	2.1
43.80	1.9	43.90	1.8	44.00	1.7	44.10	1.6
44.20	1.5	44.30	1.5	44.40	1.5	44.50	1.4
44.60	1.4	44.70	1.4	44.80	1.3	44.90	1.3
45.00	1.3	45.25	1.3	45.50	1.3	45.75	1.3
46.00	1.3						

B. Intensities for 2θ Region 60° to 63°, Step Anneal for 2 Hours at 650°C

2θ	Int.	2θ	Int.	2θ	Int.	2θ	Int.
60.00	11.0	60.10	11.0	60.20	11.0	60.30	11.3
60.40	11.5	60.50	12.0	60.60	12.5	60.70	12.9
60.80	13.6	60.90	14.4	61.00	15.1	61.10	15.7
61.20	15.0	61.30	14.1	61.40	13.5	61.50	12.9
61.60	12.6	61.70	12.2	61.80	11.8	61.90	11.6
62.00	11.4	62.10	11.3	62.20	11.0	62.30	10.9
62.40	10.8	62.50	10.6	62.60	10.6	62.70	10.6
62.80	10.6	62.90	10.6	63.00	10.6		

C. Intensities for 2θ Region 72° to 79°, Step Anneal for 2 Hours at 650°C

2θ	Int.	2θ	Int.	2θ	Int.	2θ	Int.
72.00	9.4	72.10	9.4	72.20	9.5	72.30	9.6
72.40	9.8	72.50	10.1	72.60	10.3	72.70	10.5
72.80	10.8	72.90	11.0	73.00	11.2	73.10	11.6
73.20	11.9	73.30	12.1	73.40	12.1	73.50	12.3
73.60	12.4	73.70	12.5	73.80	12.4	73.90	12.3
74.00	12.0	74.10	11.9	74.20	11.9	74.30	11.9
74.40	11.9	74.50	11.9	74.60	11.9	74.70	11.9
74.80	11.9	74.90	11.9	75.00	11.9	75.10	11.9
75.20	12.0	75.30	12.1	75.40	12.3	75.50	12.5
75.60	13.2	75.70	14.2	75.80	15.1	75.90	16.0
76.00	17.0	76.10	16.8	76.20	15.9	76.30	14.9
76.40	14.4	76.50	14.0	76.60	13.6	76.70	13.3
76.80	12.7	76.90	12.3	77.00	12.0	77.10	11.6
77.20	11.3	77.30	11.2	77.40	11.1	77.50	11.0
77.60	11.0	77.70	10.9	77.80	10.7	77.90	10.6
78.00	10.4	78.10	10.3	78.20	10.2	78.30	10.1
78.40	10.0	78.50	10.0	78.60	10.0	78.70	10.0
78.80	10.0	78.90	9.8	79.00	9.8		

D. Intensities for 2θ Region 82° to 87°, Step Anneal for 2 Hours at 650°C

2θ	Int.	2θ	Int.	2θ	Int.	2θ	Int.
82.00	9.1	82.10	9.1	82.20	9.1	82.30	9.1
82.40	9.1	82.50	9.1	82.60	9.1	82.70	9.1
82.80	9.1	82.90	9.1	83.00	9.1	83.10	9.1
83.20	9.1	83.30	9.2	83.40	9.4	83.50	9.7
83.60	9.9	83.70	10.0	83.80	10.0	83.90	10.1
84.00	10.3	84.10	10.6	84.20	10.8	84.30	11.3
84.40	12.3	84.50	12.7	84.60	12.6	84.70	12.0
84.80	11.3	84.90	10.9	85.00	10.7	85.10	10.5
85.20	10.3	85.30	10.0	85.40	9.8	85.50	9.7
85.60	9.5	85.70	9.5	85.80	9.4	85.90	9.3
86.00	9.3	86.10	9.2	86.20	9.1	86.30	9.0
86.40	9.0	86.50	9.0	86.60	9.0	86.70	9.0
86.80	9.0	86.90	9.0	87.00	9.0		

TABLE XIII. Intensities for 2θ Region 34° to 42°, 52° to 54°, 62° to 64°, 75° to 84°, as Received 2.3 μm Ti Thin Film.

2θ	Intensity	2θ	Intensity	2θ	Intensity	2θ	Intensity
34.00	1.2	34.10	1.2	34.20	1.2	34.30	1.2
34.40	1.3	34.50	1.4	34.60	1.4	34.70	1.4
34.80	1.8	34.85	2.1	34.90	2.4	34.95	2.7
35.00	3.1	35.05	3.4	35.10	3.7	35.15	3.8
35.20	3.7	35.25	3.3	35.30	2.8	35.35	2.5
35.40	2.1	35.45	1.9	35.50	1.6	35.55	1.5
35.60	1.4	35.70	1.3	35.80	1.3	35.90	1.2
36.00	1.2	36.10	1.2	36.20	1.2	36.30	1.2
36.40	1.2	36.50	1.2	36.60	1.2	36.70	1.2
36.80	1.2	36.90	1.2	37.00	1.2	37.10	1.2
37.20	1.2	37.30	1.2	37.40	1.3	37.50	1.5
37.60	1.8	37.70	2.3	37.80	3.5	37.85	4.3
37.90	5.4	37.95	5.7	38.00	8.4	38.05	9.8
38.10	11.2	38.15	12.1	38.20	12.0	38.25	11.6
38.30	10.8	38.35	9.5	38.40	8.5	38.45	7.3
38.50	6.4	38.55	5.4	38.60	4.5	38.65	3.8
38.70	3.3	38.75	2.6	38.80	2.4	38.85	2.1
38.90	1.9	38.95	1.7	39.00	1.6	39.10	1.4
39.20	1.4	39.30	1.5	39.40	1.6	39.50	1.7
39.60	2.0	39.70	2.7	39.75	3.2	39.80	3.8
39.85	4.6	39.90	5.7	39.95	7.0	40.00	8.3
40.05	9.8	40.10	11.0	40.15	11.8	40.20	11.8
40.25	11.0	40.30	9.5	40.35	8.0	40.40	6.2
40.45	5.0	40.50	4.0	40.55	3.7	40.60	2.6
40.65	2.2	40.70	1.9	40.75	1.7	40.80	1.5
40.85	1.4	40.90	1.3	41.00	1.2	41.10	1.2

TABLE XIII (Continued)

2θ	Intensity	2θ	Intensity	2θ	Intensity	2θ	Intensity
41.20	1.2	41.30	1.2	41.40	1.2	41.50	1.2
41.60	1.2	41.70	1.2	41.80	1.2	41.90	1.2
42.00	1.2						
52.00	3.8	52.10	3.8	52.20	3.8	52.30	3.8
52.40	3.8	52.50	3.8	52.60	4.1	52.70	4.9
52.80	5.7	52.90	6.7	53.00	7.1	53.10	6.5
53.20	5.5	53.30	4.5	53.40	3.8	53.50	3.5
53.60	3.4	53.70	3.4	53.80	3.4	53.90	3.4
54.00	3.4						
62.00	5.0	62.10	5.0	62.20	5.0	62.30	5.0
62.40	5.0	62.50	5.0	62.60	5.5	62.70	6.3
62.80	7.0	62.90	7.4	63.00	7.6	63.10	7.6
63.20	7.2	63.30	6.4	63.40	5.9	63.50	5.4
63.60	5.0	63.70	5.0	63.80	5.0	63.90	5.0
64.00	5.0						

TABLE XIII (Continued)

2θ	Intensity	2θ	Intensity	2θ	Intensity	2θ	Intensity
75.00	8.0	75.10	8.0	75.20	8.0	75.30	8.0
75.40	8.0	75.50	8.0	75.60	8.2	75.70	8.2
75.80	8.4	75.90	8.8	76.00	9.2	76.10	9.6
76.20	9.6	76.30	9.4	76.40	9.4	76.50	9.2
76.60	9.4	76.70	9.4	76.80	9.6	76.90	10.4
77.00	11.1	77.10	12.1	77.20	12.6	77.30	12.7
77.40	12.5	77.50	12.2	77.60	11.7	77.70	10.5
77.80	9.8	77.90	9.4	78.00	8.8	78.10	8.5
78.20	8.3	78.30	8.1	78.40	8.1	78.50	8.1
78.60	8.1	78.70	8.1	78.80	8.1	78.90	8.1
79.00	8.1	79.10	7.9	79.20	7.6	79.30	7.5
79.40	7.5	79.50	7.5	79.60	7.5	79.70	7.5
79.80	7.5	79.90	7.5	80.00	7.5	80.10	7.5
80.20	7.5	80.30	7.5	80.40	7.5	80.50	7.5
80.60	7.6	80.70	7.7	80.80	7.9	80.90	8.1
81.00	8.4	81.10	8.7	81.20	9.3	81.30	9.9
81.40	10.0	81.50	10.0	81.60	10.0	81.70	10.0
81.80	10.1	81.90	9.8	82.00	9.4	82.10	9.1
82.20	8.8	82.30	8.6	82.40	8.3	82.50	8.2
82.60	8.1	82.70	8.1	82.80	7.8	82.90	7.5
83.00	7.5	83.10	7.5	83.20	7.5	83.30	7.5
83.40	7.5	83.50	7.5	83.60	7.5	83.70	7.5
83.80	7.5	83.90	7.5	84.00	7.5		

TABLE XIV. Intensity for 2θ Region 34° to 42°, 70° to 83°, 15 Minute Anneal at 625°C.

2θ	Intensity	2θ	Intensity	2θ	Intensity	2θ	Intensity
34.00	3.5	34.12	3.5	34.25	3.5	34.37	3.5
34.50	3.5	34.62	3.7	34.75	3.8	34.87	4.3
35.00	5.5	35.12	7.0	35.25	7.1	35.37	5.8
35.50	4.1	35.62	3.5	35.75	3.5	35.87	3.5
36.00	3.5	36.12	3.5	36.25	3.5	36.37	3.5
36.50	3.5	36.62	3.5	36.75	3.5	36.87	3.5
37.00	3.5	37.12	3.5	37.25	3.5	37.37	3.5
37.50	3.5	37.62	4.0	37.75	4.5	37.87	6.5
38.00	11.5	38.12	21.0	38.24	27.5	38.37	24.5
38.50	14.0	38.62	7.0	38.75	4.5	38.87	3.8
39.00	3.7	39.12	3.6	39.25	3.7	39.37	3.7
39.50	3.7	39.62	3.9	39.75	4.5	39.87	7.0
40.00	12.5	40.12	19.5	40.25	23.1	40.37	20.6
40.50	9.0	40.62	5.0	40.75	4.1	40.87	3.7
41.00	3.4	41.12	3.4	41.25	3.4	41.37	3.4
41.50	3.4	41.62	3.4	41.75	3.4	41.87	3.4
42.00	3.4						
70.00	6.5	70.12	6.7	70.25	7.1	70.37	7.7
70.50	8.1	70.62	8.3	70.75	7.6	70.87	7.0
71.00	6.8	71.12	6.8	71.25	6.8	71.37	6.8
71.50	6.8	71.62	6.8	71.75	6.8	71.87	6.8
72.00	6.8	72.12	6.8	72.25	6.8	72.37	6.8

TABLE XIV (Continued)

2θ	Intensity	2θ	Intensity	2θ	Intensity	2θ	Intensity
72.50	6.8	72.62	6.8	72.75	6.8	72.87	6.8
73.00	6.8	73.12	6.8	73.25	6.8	73.37	6.8
73.50	6.8	73.62	6.8	73.75	6.8	73.87	6.8
74.00	6.8	74.12	6.8	74.25	6.8	74.37	6.8
74.50	6.8	74.62	6.8	74.75	6.8	74.87	6.8
75.00	6.8	75.12	6.8	75.25	6.8	75.37	6.8
75.50	6.6	75.62	6.6	75.75	6.6	75.87	6.6
76.00	7.3	76.25	7.6	76.37	8.0	76.50	7.1
76.62	7.0	76.75	6.7	76.87	7.0	77.00	7.0
77.12	7.2	77.25	7.8	77.37	8.4	77.50	9.7
77.62	9.8	77.75	8.6	77.87	7.5	78.00	7.0
78.12	6.8	78.25	6.5	78.37	6.5	78.50	6.5
78.62	6.5	78.75	6.5	78.87	6.5	79.00	6.5
79.12	6.5	79.25	6.5	79.37	6.5	79.50	6.5
79.62	6.5	79.75	6.5	79.87	6.5	80.00	6.5
80.12	6.5	80.25	6.5	80.37	6.5	80.50	6.5
80.62	6.5	80.75	6.5	80.87	6.5	81.00	6.5
81.12	6.5	81.25	6.5	81.37	6.5	81.50	6.9
81.62	7.6	81.75	8.0	81.87	8.3	82.00	8.8
82.12	8.4	82.25	7.6	82.37	7.3	82.50	6.7
82.62	6.5	82.75	6.2	82.87	6.2	83.00	6.2

TABLE XV. Intensities for 2θ Region 34° to 42°, 59° to 62°, 70° to 84°, 30 Minute Anneal at 625°C.

2θ	Intensity	2θ	Intensity	2θ	Intensity	2θ	Intensity
34.00	3.0	34.12	3.0	34.25	3.0	34.37	3.0
34.50	3.0	34.62	3.1	34.75	3.5	34.82	4.4
35.00	5.5	35.12	6.6	35.25	5.7	35.37	4.0
35.50	3.2	35.62	3.2	35.75	3.2	35.87	3.4
36.00	3.6	36.12	3.6	36.25	3.5	36.37	3.2
36.50	3.2	36.62	3.2	36.75	3.2	36.87	3.2
37.00	3.2	37.12	3.2	37.25	3.2	37.37	3.2
37.50	3.2	37.62	3.9	37.75	5.0	37.87	8.0
38.00	14.0	38.12	21.3	38.25	23.5	38.37	16.5
38.50	8.0	38.62	4.6	38.75	3.7	38.87	3.3
39.00	3.3	39.12	3.3	39.25	3.3	39.37	3.3
39.50	3.5	39.62	4.0	39.75	5.1	39.87	8.6
40.00	15.0	40.12	20.8	40.25	19.0	40.37	10.8
40.50	3.6	40.62	3.5	40.75	3.4	40.87	3.3
41.00	3.3	41.12	3.3	41.25	3.3	41.37	3.3
41.50	3.3	41.62	3.3	41.75	3.3	41.87	3.3
42.00	3.3						
59.00	6.0	59.12	6.0	59.25	6.0	59.67	6.0
59.50	6.0	59.62	6.0	59.75	6.0	59.87	10.0
59.92	12.2	60.00	16.1	60.05	10.1	60.12	7.2
60.25	6.0	60.37	6.0	60.50	6.0	60.62	6.0
60.75	6.0	60.87	6.0	61.00	6.0	61.12	6.0

TABLE XV (Continued)

2θ	Intensity	2θ	Intensity	2θ	Intensity	2θ	Intensity
61.25	6.0	61.37	6.0	61.50	6.0	61.62	6.0
61.75	6.0	61.87	6.0	62.00	6.0		
70.00	6.5	70.12	6.5	70.25	6.5	70.37	7.1
70.50	7.3	70.62	7.5	70.75	7.7	70.87	7.4
71.00	7.0	71.12	6.8	71.25	6.7	71.37	6.5
71.50	6.5	71.62	6.5	71.75	6.5	71.87	6.5
72.00	6.5	72.12	6.5	72.25	6.5	72.37	6.5
72.50	6.5	72.62	6.5	72.75	6.5	72.87	6.5
73.00	6.5	73.12	6.5	73.23	6.5	73.37	6.5
73.50	6.5	73.62	6.5	73.75	6.5	73.87	6.5
74.00	6.5	74.12	6.5	74.25	6.5	74.37	6.5
74.50	6.5	74.62	6.5	74.75	6.5	74.87	6.5
75.00	6.5	75.12	6.6	75.25	6.7	75.37	6.7
75.50	6.7	75.62	6.7	75.75	6.7	75.87	6.7
76.00	6.8	76.12	7.0	76.25	7.2	76.37	7.5
76.50	7.7	76.62	8.0	76.75	8.0	76.87	7.7
77.00	7.5	77.12	7.3	77.25	7.1	77.37	7.5
77.50	7.8	77.62	8.2	77.75	9.0	77.87	9.1
78.00	9.1	78.12	9.0	78.25	8.1	78.37	7.7
78.50	7.4	78.62	7.1	78.75	6.8	78.87	6.5
79.00	6.5	79.12	6.5	79.25	6.5	79.37	6.5
79.50	6.5	79.62	6.5	79.75	6.5	79.87	6.5

TABLE XV (Continued)

2θ	Intensity	2θ	Intensity	2θ	Intensity	2θ	Intensity
80.00	6.5	80.12	6.5	80.25	6.5	80.37	6.5
80.50	6.5	80.62	6.5	80.75	6.5	80.87	6.5
81.00	6.5	81.12	6.6	81.25	6.7	81.37	6.8
81.50	6.9	81.62	7.8	81.75	8.2	81.87	8.6
82.00	8.9	82.12	8.9	82.25	8.7	82.37	8.6
82.50	7.3	82.62	7.5	82.75	7.2	82.87	6.8
83.00	6.4	83.12	6.2	83.25	6.2	83.37	6.2
83.50	6.2	83.62	6.2	83.75	6.2	83.87	6.2
84.00	6.2						

TABLE XVIa. 2θ Positions for Experimental Intensity Simulations (Figures 12 through 33)

αTi Lines

hkl	$2\theta_{as\ rec.}$	$2\theta_{350}$	$2\theta_{450}$	$2\theta_{500}$	$2\theta_{550}$	$2\theta_{575}$	$2\theta_{600}$	$2\theta_{625}$	$2\theta_{650}$
010	37.47	37.38	37.35	37.26	37.16	37.25	37.25	37.35	37.35
002	39.62	39.60	39.60	39.45	39.47	39.47	39.47	39.49	39.49
011	41.53	41.65	41.65	41.36	41.57	41.35	41.35	41.30	41.30
103	74.20	–	–	–	–	73.10	73.15	73.30	73.45
200	75.80	75.80	75.80	75.80	75.90	75.90	75.80	–	–
112	76.55	–	–	–	–	76.70	76.90	77.00	77.20
004	–	–	–	–	–	–	–	–	84.00

TiSi Lines

111	–	–	–	–	–	–	–	–	33.53
002	–	–	–	–	–	–	–	–	36.05
210	36.98	36.98	36.98	36.88	36.65	36.58	36.58	36.52	36.69
102	38.59	38.59	38.59	38.59	38.52	38.52	38.52	38.40	38.90
211	41.31	41.31	41.31	41.31	41.30	41.43	41.52	41.65	41.80
312	–	–	–	–	–	–	61.25	61.10	61.10
410	–	–	–	–	–	–	61.70	61.70	61.60
412	–	73.75	73.75	73.55	73.65	73.80	73.80	74.20	74.20
501	–	74.85	74.85	74.75	74.75	74.75	74.75	74.70	74.85
004	76.22	76.20	76.20	76.10	–	–	–	–	76.65
421	–	–	–	–	–	–	–	81.30	–
223	–	–	–	–	–	–	–	84.20	84.55
230	–	–	–	–	–	–	–	85.40	85.20

TABLE XVIa (Continued)

$TiSi_2$ Lines

hkl	$2\theta_{as\ rec.}$	$2\theta_{350}$	$2\theta_{450}$	$2\theta_{500}$	$2\theta_{550}$	$2\theta_{575}$	$2\theta_{600}$	$2\theta_{625}$	$2\theta_{650}$
113	–	–	–	–	–	–	–	–	38.20
311	–	–	39.13	39.13	39.17	39.20	39.20	39.19	39.19
004	–	–	42.24	42.24	42.20	42.26	42.26	42.19	42.29
022	–	–	43.22	43.22	43.20	43.22	43.22	43.00	43.49
131	–	–	–	–	–	–	59.80	–	–
511	–	–	–	–	–	–	59.80	–	–
602	–	–	–	–	–	–	72.05	72.00	–
333	–	–	76.47	76.47	76.80	76.40	76.20	76.10	76.03
026	–	–	77.90	77.90	78.00	78.00	77.90	–	–
040	–	–	–	–	–	–	–	–	–

TABLE XVIb. Halfwidth for Experimental Intensity Simulations (Figures 12 through 33).

αTi Lines hkl	half width as rec.	half width 350	half width 450	half width 500	half width 550	half width 575	half width 600	half width 625	half width 650
010	0.40	0.33	0.33	0.46	0.46	0.60	0.80	1.15	1.15
002	0.95	1.06	1.00	0.82	0.85	0.85	0.90	0.95	0.95
011	1.35	1.36	1.50	1.85	1.85	2.00	2.00	2.10	2.10
103	2.10	–	–	–	–	1.50	1.50	1.10	1.40
200	1.00	1.05	1.00	1.10	1.10	1.20	1.20	–	–
112	1.70	–	–	–	–	1.60	1.60	1.50	1.50
004	–	–	–	–	–	–	–	–	1.50
TiSi Lines									
111	–	–	–	–	–	–	–	–	0.85
002	–	–	–	–	–	–	–	–	0.85
210	1.40	1.40	1.40	1.20	1.00	0.95	0.85	0.85	0.85
102	1.40	1.40	1.40	1.20	1.00	0.95	0.85	0.85	0.85
211	1.40	1.40	1.40	1.20	1.00	0.95	0.87	0.87	0.87
312	–	–	–	–	–	–	1.05	1.05	1.00
410	–	–	–	–	–	–	1.05	1.05	1.00
412	–	1.45	1.45	1.50	1.10	1.20	1.00	1.00	1.30
501	–	1.45	1.45	1.50	1.10	1.20	1.00	1.00	1.30
004	1.50	1.50	1.50	1.50	1.20	1.20	–	–	1.00
421	–	–	–	–	–	–	–	1.20	–
223	–	–	–	–	–	–	–	1.30	1.00
230	–	–	–	–	–	–	–	1.30	1.30

TABLE XVIb (Continued)

$TiSi_2$ Lines

hkl	half width as rec.	half width 350	half width 450	half width 500	half width 550	half width 575	half width 600	half width 625	half width 650
113	–	–	–	–	–	–	–	–	0.50
311	–	–	1.00	1.00	0.47	0.47	0.42	0.45	0.43
004	–	–	1.00	1.00	0.50	0.73	0.73	0.75	0.75
022	–	–	1.00	1.00	0.60	0.70	0.70	0.75	0.75
131	–	–	–	–	–	–	1.00	–	–
511	–	–	–	–	–	–	1.00	–	–
602	–	–	–	–	–	–	0.80	0.80	–
333	–	–	1.20	1.20	1.00	1.20	1.00	1.00	0.68
026	–	–	1.20	1.20	1.00	1.20	0.85	–	–
040	–	–	–	–	–	–	–	1.00	–

TABLE XVIc. G Factors for Experimental Intensity Simulations (Figures 12 through 33)

αTi Lines

hkl	$G_{as\ rec.}$	G_{350}	G_{450}	G_{500}	G_{550}	G_{575}	G_{600}	G_{625}	G_{650}
010	0.63	0.38	0.34	0.37	0.37	0.37	0.37	0.37	0.37
002	2.06	2.94	2.90	2.92	2.92	2.92	2.92	2.92	2.92
011	0.31	0.27	0.26	0.31	0.31	0.31	0.31	0.31	0.31
103	1.15	-	-	-	-	1.00	1.00	1.00	1.00
200	0.62	0.40	0.40	0.40	0.40	0.38	0.38	0.38	-
112	1.23	-	-	-	-	1.11	1.12	1.12	-
004	-	-	-	-	-	-	-	-	2.95

TiSi Lines

111	-	-	-	-	-	-	-	-	1.00
002	-	-	-	-	-	-	-	-	0.60
210	1.00	1.00	1.00	1.00	1.00	1.00	1.00	1.00	2.00
102	1.00	1.00	1.00	1.00	1.00	1.00	1.00	1.00	1.00
211	1.00	1.00	1.00	1.00	1.00	1.00	1.00	1.00	0.80
312	-	-	-	-	-	-	1.00	1.00	0.70
410	-	-	-	-	-	-	1.00	1.00	0.60
412	-	1.00	1.00	1.00	1.00	1.00	1.00	1.00	-
501	-	1.00	1.00	1.00	1.00	1.00	1.00	1.00	-
004	1.00	1.00	1.00	1.00	-	-	-	-	0.30
421	-	-	-	-	-	-	-	1.00	-
223	-	-	-	-	-	-	-	1.00	1.00
230	-	-	-	-	-	-	-	1.00	1.00

TABLE XVIc (Continued)

$TiSi_2$ Lines

hkl	$G_{as\ rec.}$	G_{350}	G_{450}	G_{500}	G_{550}	G_{575}	G_{600}	G_{625}	G_{600}
113	–	–	–	–	–	–	–	–	1.00
311	–	–	4.50	4.50	4.50	3.60	3.20	2.50	1.20
004	–	–	1.50	2.00	2.45	0.85	0.85	0.70	0.30
022	–	–	1.00	0.50	0.05	0.05	0.05	0.15	0.65
131	–	–	–	–	–	–	0.05	–	–
511	–	–	–	–	–	–	0.05	–	–
602	–	–	–	–	–	–	0.50	0.85	–
333	–	–	–	–	–	–	0.50	0.55	0.75
026	–	–	–	–	–	–	0.15	0.15	–
040	–	–	–	–	–	–	–	1.00	–

TABLE XVIIa. 2θ Positions for Experimental Intensity Simulations (Figures 36 through 45)

αTi Lines

hkl	$2\theta_{cards}$	$2\theta_{as\ rec.}$	$2\theta_{15\ min.}$	$2\theta_{30\ min.}$
010	35.06	35.15	35.15	35.11
002	38.40	38.22	38.25	38.25
011	40.15	40.15	40.22	40.15
012	53.01	53.01	–	–
110	62.96	63.02	–	–
103	70.66	70.66	–	–
200	74.26	–	–	–
112	76.29	76.49	76.30	76.29
201	77.32	77.70	77.42	77.50
004	82.28	82.21	82.21	82.20
202	86.71	–	–	–
014	92.61	–	–	–
203	102.23	–	–	–
211	109.05	–	–	–
114	114.13	–	–	–
212	119.27	–	–	–
015	122.25	–	–	–

TiSi Lines

hkl	$2\theta_{as\ rec.}$	$2\theta_{15\ min.}$	$2\theta_{30\ min.}$
002	–	–	36.05
401	–	–	59.95
421	81.70	81.70	81.74

TABLE XVIIb. Halfwidths for Experimental Intensity Simulations (Figures 36 through 45)

αTi Lines

hkl	as rec.	15 min.	30 min.
010	0.48	0.40	0.40
002	0.50	0.40	0.40
011	0.48	0.40	0.40
012	0.49	-	-
110	0.51	-	-
103	0.80	-	0.45
112	0.80	0.60	0.48
201	0.80	0.75	0.45
004	0.90	0.80	0.50

TiSi Lines

002	-	-	0.45
401	-	-	0.20
421	0.50	0.60	0.50

TABLE XVIIc. "G" Factors for Experimental Intensity Simulations (Figures 36 through 45)

αTi Lines

hkl	as rec.	15 min.	30 min.
010	0.38	0.36	0.36
002	2.07	2.10	2.10
011	0.52	0.53	0.53
012	0.85	-	0.53
110	1.13	-	-
103	0.25	-	0.20
112	0.73	0.57	0.51
201	1.10	1.34	1.20
004	2.07	2.10	2.10

TiSi Lines

002	-	-	2.50
401	-	-	4.40
421	5.00	4.00	3.10

TABLE XVIII. Thin Film Specimen 2.5 Micron of Titanium Cut Within 3.5° of the 111 Planes Annealed at Various Temperatures for 2 Hours, Measured at Room Temperature

Identification	2θ Cards	2θ As Rec.	2θ 350	2θ 450	2θ 500	2θ 550
α Ti (300	129.80	-	-	129.7*	129.7*	129.6*
TiSi (610)	94.97	-	-	-	94.94	94.97
α Ti (202)	86.71	86.5*	86.5*	86.6*	86.6*	-
α Ti (004)	82.28	-	-	-	82.2*	81.9*
α Ti (201)	77.32	77.24	77.25	77.29	77.25	77.30
α Ti (112)	76.29	76.16	76.05	76.16	76.11	76.12
α Ti (200)	74.26	74.11	74.01	74.04	74.05	74.10
α Ti (110)	62.96	-	-	62.88	-	62.78
α Ti (011)	40.15	39.99	40.01	40.01	40.01	40.03
α Ti (002)	38.40	38.23	38.17	38.16	38.16	38.11
TiSi (210)	36.88	-	-	-	-	36.87
α Ti (010)	35.06	34.92	34.97	34.97	34.97	35.00

Identification	Rel. Inten. Cards	Rel. Inten. As Rec.	Rel. Inten. 350	Rel. Inten. 450	Rel. Inten. 500	Rel. Inten. 550
α Ti (300)	4	-	-	16	16	11
TiSi (610)	10	-	-	-	10	15
α Ti (202)	2	1	1	4	1	1
α Ti (004)	2	-	-	-	4	5
α Ti (201)	14	8	16	19	18	16
α Ti (112)	17	2	7	10	8	8
α Ti (200)	2	1	7	9	8	9
α Ti (110)	18	-	-	2	1	1
α Ti (011)	100	88	27	30	32	29
α Ti (002)	26	100	100	100	92	93
TiSi (201)	20	-	-	-	-	20
α Ti (010)	30	21	91	92	100	100

*Determination of peak position better than one decimal place was not possible.

TABLE XVIII (Continued)

Identification	ε As Rec.	ε 350	ε 450	ε 500	ε 550
α Ti (300)	-	-	*	*	*
TiSi (610)	-	-	-	0.0	0.0
α Ti (202)	*	*	*	*	-
α Ti (004)	-	-	-	*	*
α Ti (201)	0.002	0.002	0.002	0.002	0.002
α Ti (112)	0.002	0.004	0.002	0.003	0.003
α Ti (200)	0.003	0.003	0.003	0.003	0.003
α Ti (110)	-	-	0.002	-	0.002
α Ti (011)	0.004	0.005	0.005	0.005	0.005
α Ti (002)	0.006	0.007	0.007	0.007	0.009
TiSi (210)	-	-	-	-	0.00
α Ti (010)	0.004	0.003	0.003	0.003	0.002

*Determination of peak position better than one decimal place was not possible.

REFERENCES

1. Balluffi, R. W. and Blakely, J. M., "Special Aspects of Diffusion in Thin Films", Thin Solid Films, 25, (1975), pp. 363-392.

2. Bower, R. W. and Mayer, J. W., Appl. Phys. Lett., 20, (1972) p. 359.

3. Mayer, J. W. and Tu, K. N., J. Vac. Sci. Technol., 11, (1974), p. 86.

4. Picraux, S. T., "Mass Transport Between Two Metal Layers as Studied by Ion Scattering", 6th International Vacuum Congress, Kyoto, Japan (1974).

5. Tu, K. N., Electrochemical Society, Extended Abstracts, 1, Vol. 116, (1975), p. 267.

6. Chu, W. K., Krautle, H., Mayer, J. W., Muller, H., and Nicolet, M. A., Appl. Phys. Lett., 25, Vol. 8 (1974), p. 454.

7. Chopra, K. L., Thin Film Phenomenon, McGraw-Hill, New York, (1969), p. 266.

8. Campbell, D. S., in L. I. Maissel and R. Glang (eds.), Handbook of Thin Film Technology, McGraw-Hill, New York, (1970), p. 12-13.

9. Gangulee, A., Acta. Met., 22, (1974), p. 177.

10. Dearnaley, G. and Hartley, N. E. W., Phys. Lett., 46a, (1974) p. 345.

11. Cotter, P. G., Kohn, J. A., and Potter, R. A., J. Amer. Ceram. Soc., 39, (1959), p. 11-12.

12. Laves, V. F. and Wallbaum, H. J., Z. Krist., 101 (1939), p. 78-92.

13. Kato, H. and Nakamura, Y., Thin Solid Films, 34, (1976), p. 135-138.

14. Schob, O., Nowotny, H., and Benesovsky, F., Planseeber. Pulvermet., 10, (1962), p. 65-71.

15. Svechnikov, V. N., A. Kad. Nauk, SSSR, 193, No. 2, (1970) p. 393.

16. Burkl et al. Monatsh. Chem., 92, (1961), pp. 781-88.

17. Nat. Bureau of Std. Circular, 539, 8, 64, (1958).

18. S. S. Lau, W. K. Chu and J. W. Mayer, "Evaluation of Glancing Angle X-Ray Diffraction and MeV ^{4}He Backscattering Analyses of Silicide Formation", (submitted to Thin Solid Films, March, 1974).

19. Hutchins, G. A., Shepala, A., Thin Solid Films (to be published).

20. C. R. Houska, J. Appl. Phys. 41, 69 (1970).

21. C. R. Houska, High Temperature - High Press, 4, 417 (1972).

22. Houska, C. R., Thin Solid Films, 25 (1975) pp. 451-464.

23. James, R. W., The Optical Principles of the Diffraction of X-Rays, Vol. II, The Crystalline State, Cornell University Press, Ithaca, New York (1965).

24. Guinier, A., X-Ray Diffraction in Crystals, Imperfect Crystals and Amorphous Bodies, W. H. Freeman and Company, San Francisco (1963).

25. Harris, G. B., Phil. Mag., Ser 7, Vol. 43, No. 336, Jan. 1952, pp. 113-123.

26. Elderton, W. D., and Johnson, N. L., "Systems of Frequency Curves", Cambridge Press, New York (1969) pp. 77-78.

27. Hall, M. M., Veeraraghavan, V. G., Herman, Rubin, and Winchell, P. G., J. Appl. Cryst., 10, (1977) pp. 66-68.

28. "Thermophysical Properties of Matter", IFI/Plenum Data Company, Division of Plenum Publishing Gorporation, New York, New York (1975).

29. Schultz, L. G., J. Appl. Phys., 20, 1030 (1949).

30. Ventron Corporation, Alfa Products, Danvers, MA.

31. Dietrich, F., Smith, T., and Houska, C. R., J. Appl. Crystallography, to be published.

32. Siemens America, Incorporated, New York, New York.

33. Diffin, W. J., Parthe, E. and Norton, J. T., Acta. Cryst. 17 (1964) p. 450-451.

34. "International Tables for X-Ray Crystallography", Kynoch Press, Birmingham, England, Vol. IV (1959) p. 74,76.

35. "OS/8 Handbook", Digital Equipment Corporation, (1974) Section 1, p. 93-97.

36. Ageev, N. and Samsonov, V., J. Neorg. Chim. 4, (1950) p. 950.

37. Hans-Ulrich Pheifer, Schubert, K., Zs. Metallkunde, 57 (1966) p. 884.

38. "International Tables for X-Ray Crystallography", Kynoch Press, Birmingham, England, Vol. III (1959).

39. "Handbook of the Phyicochemical Properties of the Elements", edited by Samsonon, G. V., IFI/Plenum, New York, New York (1968) p. 388.

40. Anderson, E. A., Jillson, D. C., and Dunbar, S. R., Trans. AIME, 197 (1953) p. 191.

APPENDIX I

Automated Texture Diffractometer

Computer controls allow the automated texture diffractometer[29] to operate continuously without the presence of an operator. The data collection technique is continuous, measuring diffracted intensity over an increment of angular region rather than conventional step scanning. The computer incorporates relative angular positions rather than absolute values in execution of any movement. The purpose of this appendix is to describe the operation of the following data collection programs:

1. CH.RL - operated with a chart recorder in the usual collection of x-ray data.
2. "Search" - quickly collects data to identify angular regions of interest.
3. RSCAN.RL - will provide integrated intensity, mean and variance with scanning speed from 1° to $1/100^{o}$ per minute.

<u>Bringing the System UP</u>[+]

The data collection system consists of two Sykes 7100 disks and a PDP 8/e minicomputer which are interfaced into a timer-scalar and stepping motors on the Siemens diffractometer. The following prepares the system for operation:

[+]Refer to PDP 8/e small computer handbook pg. 3-1 to 3-5.

1. Insert the system programs disk which is placed with slot to the back in the upper Sykes unit, push in, and lower cover to the vertical position.
2. Insert the data disk which is placed in the lower Sykes unit as above.
3. Turn the key switch on the PDP 8/e (left side) to the power position (center) (see Figure 58).
4. Select the appropriate terminal, either teletype or teleray by switches directly above the PDP unit (see Figure 57).
5. Activate terminal
   a. Teleray - turn switch on left to desired brightness, position middle two switches down and all others to the middle on box above terminal.
   b. Teletype - turn switch on right to "Line".

In the event of a line power interupt to the computer, a boot strap load (see next section) will be necessary if the following results in no response from the computer. Initiating the system (first five keys up, 0 through 4, refer Figure 58) is accomplished by:

1. Place HALT button in "UP" position.
2. Pressing ADDRESS LOAD, CLEAR, CONTINUE, on the right of PDP 3/e.

which results in a dot display on the active terminal.

Boot Strap Load

If a 7600 start has failed, the following load will bring the system up without damaging any system programs. This must be loaded on the switch register of the PDP 8/e in the following order:

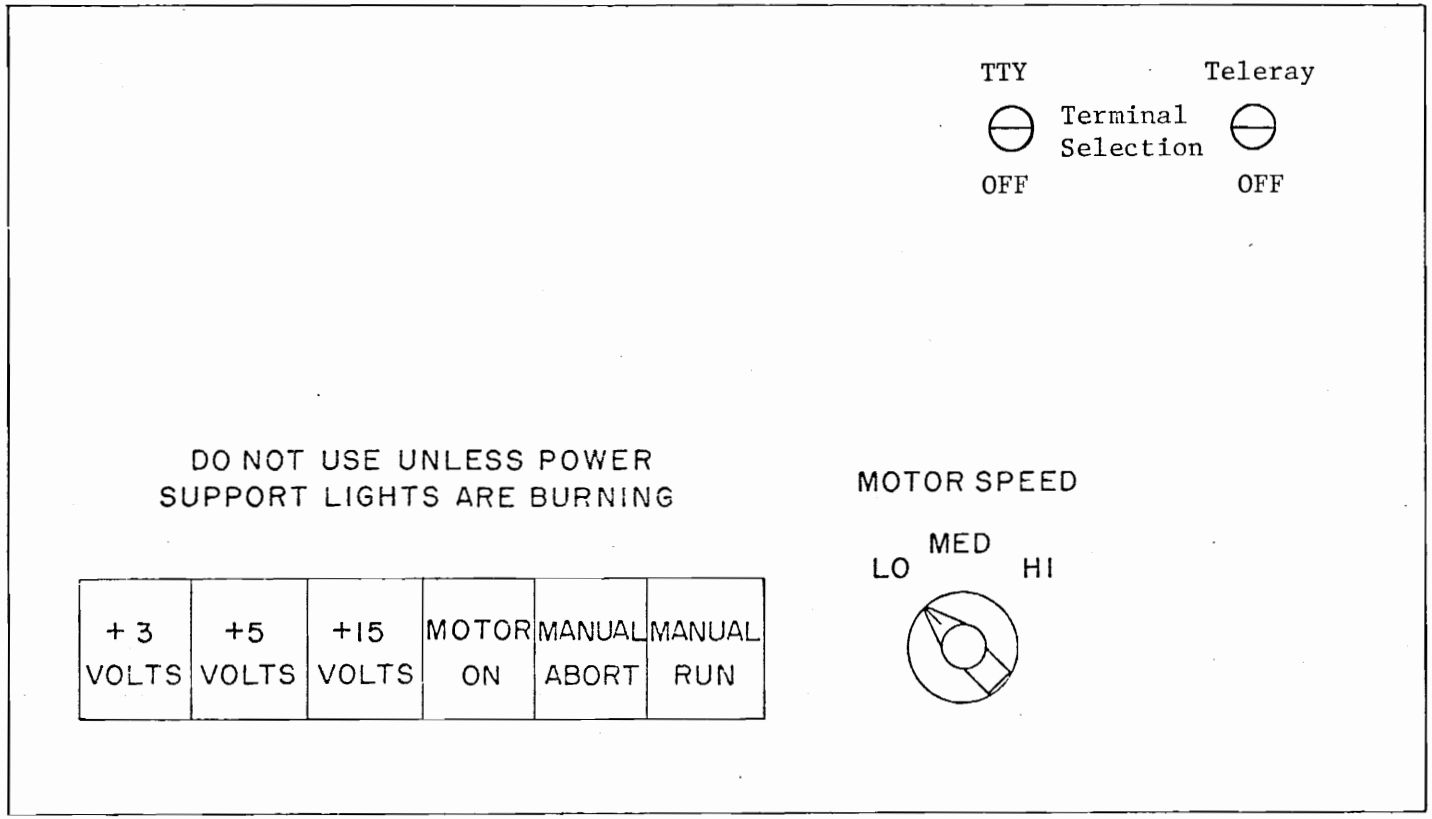

Figure 57. Terminal selection panel on the PDP 8/e rack.

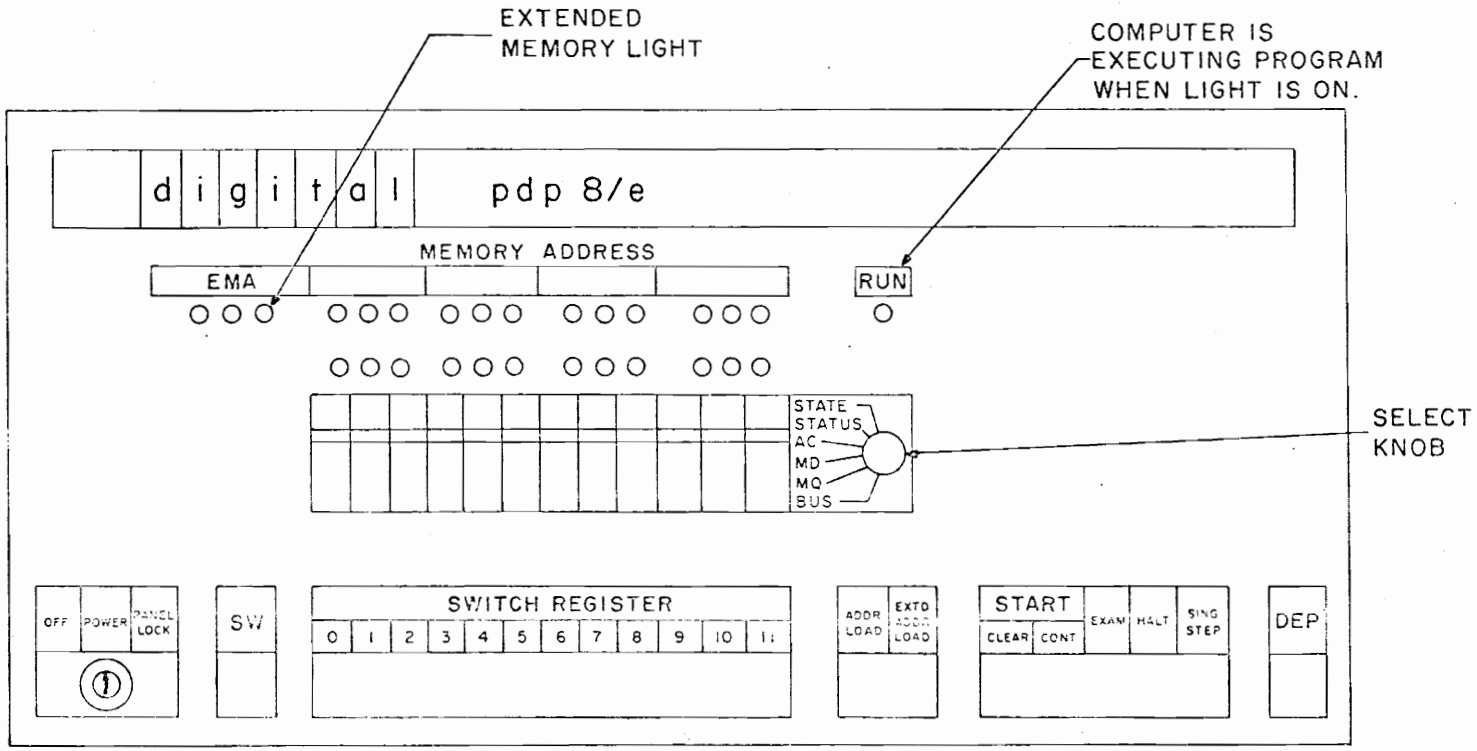

Figure 58 . PDP 8/e computer.

1. Pull switch "4" up, press "ADDR LOAD", key down (all others are down).
2. Enter the following numbers by pulling up the appropriate keys and pulling up the "DEP" key after every set is entered:

1127	2,4,7,9,10,11
6731	0,1,3,4,5,7,8,11
6731	0,1,3,4,5,7,8,11
7600	0,1,2,3,4
6732	0,1,3,4,5,7,8,10
5204	0,2,9
6734	0,1,3,4,5,7,8,9
7106	0,1,2,5,9,10
7006	0,1,2,9,10
3232	1,2,4,7,8,10
6734	0,1,3,4,5,7,8,9
7012	0,1,2,5,10
7012	0,1,2,5,10
0226	4,7,9,10
1232	2,4,7,8,10
3631	1,2,3,4,7,8,11
2231	1,4,7,8,11
2230	1,4,7,8
5204	0,2,4,9
1203	2,4,10,11
6731	0,1,3,4,5,7,8,11
5014	0,2,8,9
0017	8,9,10,11
0401	4,11
7400	0,1,2,3
0000	None

At this point, go back and check the locations and corresponding entries. This procedure is listed below:

1. Pull switch "4" up (all others down). Press "ADDR LOAD", key down.

2. Push "EXAM" key down (to sequentially examine each location).

3. The lower lights on the front of the PDP 8/e will indicate the numbers which were entered.

4. The upper set of lights will indicate the location.

Location	Light Numbers	Previous Entry	Light Numbers
400	3	1227	2,4,7,9,10,11
401	3,11	6731	0,1,3,4,5,7,8,11
402	3,10,11	6731	0,1,3,4,5,7,8,11
403	3,10,11	7600	0,1,2,3,4
404	3,9	6732	0,1,3,4,5,7,8,10
405	3,9,11	5204	0,2,9
406	3,9,10	6734	0,1,3,4,5,7,8,9
407	3,9,10,11	7106	0,1,2,5,9,10
410	3,8	7006	0,1,2,9,10
411	3,8,11	3232	1,2,4,7,8,10
412	3,8,10	6734	0,1,3,4,5,7,8,9
413	3,8,10,11	7012	0,1,2,5,10
414	3,8,9	7012	0,1,2,5,10
415	3,8,9,11	0226	4,7,9,10
416	3,8,9,10	1232	2,4,7,8,10
417	3,8,9,10,11	3631	1,2,3,4,7,8,11
420	3,7	2231	1,4,7,8,11
421	3,7,11	2230	1,4,7,8
422	3,7,10	5204	0,2,4,9
423	3,7,10,11	1203	2,4,10,11
424	3,7,9	6731	0,1,3,4,5,7,8,11
425	3,7,9,11	5014	0,2,8,9
426	3,7,9,10	0017	8,9,10,11
427	3,7,9,10,11	0401	4,11
430	3,7,8	7400	0,1,2,3
431	3,7,8,11	0000	None

When load is checked:

1. Enter 400 (Key 3 UP)

2. Press down "ADDR LOAD", "CLEAR", and "CONT".

Listing and Typing Files

A list of the file names contained on the upper disk are printed by typing "DIR" on the active terminal. The information in each file

is typed by entering "TYPE _ File Name File Type". Substituting "FLP:" after each command, Dir or Type, will accomplish the same as that above except the information will be generated form the lower disk.

Changing to Another Terminal

Either one of the two terminals (teletype or teleray+) can be used with the PDP 8/e, at the discretion of the operator. During the operation of the system, it may become necessary to change from one terminal to another (i.e., to receive a hard copy - teletype) which is the simple procedure listed below:

Type the following on operating terminal after dot appears:

R_TLS (press return)

1. When computer halts, (PDP 8/e, "RUN" light goes off) change terminal switches (see Fig. 57) for desired terminal.
2. Press continue.
3. Computer should print a dot on now active terminal.

PDP 8/e Programs

A. Position Program - POS.RL

This program enables the operator to conveniently position the diffractometer at any 2θ, χ, Φ, or ω setting.

Type on operating terminal after viewing dot:

R_POS (press return)

The response from the computer will be a series of questions which, when answered correctly, can position the instrument to any

+Teleray is preferred because of its speed.

set point. The smallest movement in this program is 0.0025 degrees which is one step of a motor. An example:

```
 THE PROGRAM WILL NOW SLEW A MOTOR, INPUT MOTOR SELECT NUMBER:
 1=2-THETA,2=OMEGA,3=CHI,4-FI
1
 IN WHICH DIRECTION DO YOU WISH TO GO:0=UP,1=DOWN. (UP-HIGHER ANGLE
 DOWN-LOWER ANGLE)
1
 HOW MANY DEGREES DO YOU WISH TO MOVE? (F9.4)
100.0
 DO YOU WANT TO SLEW AGAIN?: 1=YES,0=NO.
0
 THE PROGRAM WILL NOT TAKE OUT BAKLASH
 1=2-THETA,2=OMEGA,3=CHI,4-FI
1
 IN WHICH DIRECTION DO YOU WISH TO GO: 0=UP,1=DOWN.
0
 HOW MANY DEGREES DO YOU WISH TO MOVE? (F9.4)
1.
 DO YOU WANT TO TAKE OUT BAKLASH AGAIN:1=YES,0=NO
0
```

In this example, two theta was positioned 99° below its original value prior to execution of data collection. It should be emphasized that no data is collected with POS.RL.

B. Data Collection Programs

1. As in any of the following programs, POS.RL is available as a separate program as given in "A" to the operator for positioning the diffractometer. The program CH.RL is used with the usual chart recorder operation while scanning either 2θ, χ, Φ, or ω. The program is self-explanatory and is operated by typing the following on the active terminal after viewing a dot:

R_CH

The response from the computer will be a series of questions which

must be answered to initiate the scan. If a scanning speed of 1/32°/min is desired the following should be typed on the active terminal instead of that above:

R_CH32

2. A combination of a loading, running, and scaling program, "Search" will quickly collect data over as many as nine different regions. Scanning speeds of 5 or 1.25 degrees per min. along with interrupt times of .1, .2, .3, and .4 min. yield a variable range of detail which is then plotted by the teletype in the form of an intensity bar graph. The optimum choice of speed and interrupt time depends upon the c/m and is determined by experience. After viewing a dot type:

R_G1

The computer will now ask the appropriate question on the teleray screen so that the scanning program will be loaded. The load including the data will be stored in a file called "KMAND2.DA". An example of a load is given for a Chi scan:

```
 THIS PROGRAM SCANS SPECIFIC REGIONS FOR AVERAGE COUNTS,
 AND OUTPUTS THEM IN GRAPHIC FORM
FOR IDENTIFICATION, FILL IN THE INFORMATION BELOW THE * S
SPECIMEN      MONTH DAY YEAR
**********    **    **  **
SAMPLE
TARGET    VOLTAGE (KV)    CURRENT (MA)    MONOCHROMATOR
**        **              **              **
CU        50              20              C
ENT. SLIT (DEG)    REC. SLIT (DEG)
***                ***
1.0                1.0
SCANNING SPEED (DEG/MIN)
****
1.0
ON THE NEXT THREE LINES GIVE OTHER INFORMATION (20 CHARS./LINE)
```

```
 DO YOU WISH TO SLEW A MOTOR?:1=YES,0=NO
0
 DO YOU WISH TO TAKE OUT THE BACKLASH?:1=YES,0=NO
0
 IT IS NOW TIME TO COLLECT DATA ON THE CURVE
 1=2-THETA,2=OMEGA,3=CHI,4=FI
3
 INPUT SCAN SPEED:1=5,2=1.25 (DEG/MIN)
1
 INPUT INTERRUPT RATE: 1=0.1, 2=0.2, 3=0.4 (MIN)
1
 DO YOU WANT TO SPIN CHI: 1=YES,0=NO
0
 HOW MANY PEAKS ARE TO BE SCANNED?
1
 IN RESPONSE TO EACH QUESTION, INPUT LO, THEN HI ANGLE FOR
 EACH PEAK IN F9.4 FORMET.
 ?
 LO        HI
00.00        90.00
    0.0000        90.0000
 INPUT PRESENT POSITION, FORMAT F9.4
0.00
```

To start data collection:

```
R_G2
```

The run light on the front of the PDP 8/e will go out. The program will start execution when the "continue" button is pressed down.

The program "GRAPH" will output the intensity bar graph on the teletype and is run by typing the following;

```
R_GRAPH
```

The input needed for the graph program is the data file name and a file name in which the graph is to be stored. If a second copy of the output from the scan program is desired, type on the teleray/teletype the following after viewing a dot:

```
R_READ
```

The input data file used for "READ" is "GRAPH1.DA".

3. Twenty different motor operations, each executing scans over as many as nine different regions, can be accomplished by the following pair of programs. Included in the output from RSCAN will be the Integrated Intensity, Mean, and Variance without a correction for background, see program "IMV" for the correction. Background points are determined by the operator prior to the execution of IMV. To load this program:

Type on operating terminal:

R_LSCAN

The response from the computer will be a series of questions which will operate the "RSCAN" program, for example:

```
 THIS PROGRAM SCANS SPECIFIC REGIONS FOR AVERAGE COUNTS,
 INTEGRATED INTENSITY, MEAN, AND AVERAGE VALUES.
 DO YOU WISH TO SLEW A MOTOR?: 1=YES, 0=NO
0
 DO YOU WISH TO TAKE OUT THE BACKLASH?: 1=YES, 0=NO
0
 IT IS NOW TIME TO COLLECT DATA ON THE CURVE*
 1=2-THETA,2=2-OMEGA,3=CHI,4=PHI
3
 INPUT SCAN SPEED: 1=1/5,2=1/10,3=1/20,4=1/50,5=1/100,8=1 (DEG/MIN)
8
 DO YOU WANT TO SPIN CHI: 1=YES,0=NO
0
 HOW MANY PEAKS ARE TO BE SCANNED?
1
 IN RESPONSE TO EACH QUESTION, INPUT LO, THEN HI ANGLE FOR
 EACH PEAK IN F9.4 FORMAT.
LO        HI
00.00      90.00
    0.0000     90.0000
 INPUT PRESENT POSITION, FORMAT F9.4
0.00
```

*the motor desired to operate

```
FOR IDENTIFICATION, FILL IN THE INFORMATION BELOW THE * S
SPECIMEN      MONTH  DAY  YEAR
**********    **     **   **
SAMPLE
TARGET    VOLTAGE (KV)    CURRENT (MA)    MONOCHROMATOR
**        **              **              **
CU         50             20               C
ENT. SLIT (DEG)    REC. SLIT (DEG)
***                ***
1.0                 1.0
SCANNING SPEED (DEGREE/MIN)
****
1.0
ON THE NEXT THREE LINES GIVE OTHER INFORMATION (20 CHARS./LINE)



END OF IDENTIFICATION FIELD
ANOTHER SET OF DATA?: 1=YES, 0=NO
0
```

If an additional operation is to be made, a "1" should be typed instead of the "0" in the last statement, which circles the program back to the beginning. This load will collect data in the same manner as the example Chi scan from the previous section. The data collection is activated by typing on the operating terminal:

R_RSCAN

(Symbols between dotted lines will be typed <u>by the computer</u>).

1. Run light will go out on PDP 8/e
2. Press "Continue"

<u>NOTE</u>: Termination of a program at any point can be accomplished by pressing <u>down</u> the halt switch on the front of PDP 8/e.

After the data collection is completed, the computer will return a dot to the active terminal. A background correction can be made on

the integrated intensity, mean and variance through the use of "IMV" which again is a self-explanatory program. Type on the active terminal

R_IMV

An input and output file along with the background points determined by the operator are the only information required in this program.

Data Analysis

The IBM 370 has many distinctive advantages in analyzing the data obtained from the automated diffractometer. A plot of experimental data along with much faster printing rates are easily accessed over the phone line. Connection to the IBM 370 is made by:

Part 1

1. Position button box on top of teleray as follows (left to right)
   A. 1st up position
   B. 2nd middle position
   C. 3rd down position
   D. 4th middle position
2. Turn "VADIC" on (located in rear)
3. Dial "9" for an outside line
4. Dial 951-7020, a tone will be given when switching is complete
5. Lift "up" on white button on top, left of phone
6. IBM 370 will print on terminal "370 on line"
7. Type "log User I.D. _____ Password _____

8. Press "Return"

9. When computer stops printing, press "Return" again.

At this point the log-on has been completed. The data transfer to the IBM 370 from the PDP 8/e requires:

Part 2

1. Place the data transfer disk in upper Sykes unit.

2. Re-positioning the switch box on top of teleray to the operating position for PDP (middle two down, all others in middle position)

3. Type on active terminal R IBM which requires an input and output file name. This input will be used for "GAPHIT" (see below in plotting).

4. Type on terminal:

   | · | R TO 370

5. The computer will print "Enter name of file to be transferred"

6. Enter the file name and press return

7. Re-position switches on box at top of teleray as given in Part 1, statement 1.

8. Press "Continue" on PDP 8/e

9. Computer's run light will go out after data transfer is complete.

This procedure will copy all data in the given file to the IBM 370 permanently. Graphing of data is accomplished by:

A. Typing on terminal (switches in same position as for transfer)

   "GRAPHIT file name file type A

NOTE: File name is name of file, file type is kind of information (i.e. Data).

and the printing of a file:

B. Type on terminal (switches in same position as for transfer)

TYPOUT file name file type A

Editing Files

Information for editing a file on either the PDP 8/e or IBM 370 can be found in the OS/8 Handbook[35] or the VPI CMS User's Guide, respectively. Some useful commands are listed below:

1. PDP 8/e Editor

Command	Format	Meaning
R	#R	Read file
L	#L	List file
	#NL	List line N of file
	#M,NL	List lines M through N
C	#NC	Change line
	#M,NC	Delete and insert following lines
D	#ND	Delete line
	#M,ND	Delete lines M through N
S	#S	Search for character entered
E	#E	Close the output file

2. IBM 370 Editor

Command	Meaning
TYP	List line
TYP N	List N Lines
N	List next line
DO	Down to next line
UP	Up to line
C/QQ/ZZ	Change characters QQ to ZZ
FILE	Close output file

APPENDIX II

```
C       PROGRAM  INTENSITY
C
C
C       THIS PROGRAM CALCULATES INTEGRATED INTENSITY FOR A BINARY COMPOUND
C       FROM THE ATOMIC POSITIONS OF THE INDIVIDUAL ATOMS AND THE ATOMIC
C       SCATTERING FACTORS. THE STRUCTURE IS ORTHORHOMBIC BUT CAN BE
C       MODIFIED TO ANY KIND. THE MULTIPLICITY MUST BE CHANGED IN THIS
C       CASE.
C
C
        COMPLEX *8 CMPLX,FT,F1(80),F2(80),CFJ(2,80)
        DIMENSION U(2,20),V(2,20),W(2,20),F(80),FF(80),FFF(80),H(80),K(80)
       1,X(80),Y(80),Z(80),SF(80),NQ(80),SL(80),L(80),ASF(80),A1(2,80),IFA
       2C(80),LP(80),CFT(2,80),CFF(80),CF(2,80),FG(80),LLP(80),FFG(80)
        REAL NQ,LP,LLP
        INTEGER H,K,L,X,Y,Z,SF1,SF2,QP
C
C       THESE ARE THE FORMATS FOR THE PROGRAM
C
      1 FORMAT(3I2)
      3 FORMAT(3I1,3I1,3I1,3I1,3I1,3I1,3I1,3I1,3I1,3I1,3I1,3I1,3I1,3I1,3I1
       1,3I1,3I1,3I1,3I1,3I1,3I1,3I1,3I1,3I1,8X,/  3I1,3I1,3I1,3I1,3I1,3I1
       2,3I1,3I1,3I1,3I1,3I1,3I1,3I1,3I1,3I1,3I1,  3I1,3I1,3I1,3I1,3I1,3I1
       3,3I1,3I1,8X,/  3I1,3I1,3I1,3I1,3I1,3I1,3I2,3I1,3I1,3I1,3I1,3I1,3I1
       4,3I1,3I1,3I1,3I1,3I1,3I1,3I1,3I1,3I1,3I1)
      4 FORMAT (F8.5,F8.5,F8.5)
     18 FORMAT (10X,3I1,11X,2F8.5,10X,2F8.5)
     44 FORMAT (F8.5,2X,F8.5)
    165 FORMAT(5X,'HKL',7X,'2THETA',6X,'SIN/LAMBDA',6X,'F1',11X,'F2',11X,'
       1F**2',10X,'P',  8X,'LP',22X,'S.R.I.I.',4X,'D')
    166 FORMAT(3X,3I2,4X,F9.5,5X,F8.5,5X,F8.5,5X,F8.5,5X,F9.2,5X,I4,5X,F8.
       15,5X,E9.2,7X,F5.2,2X,F6.4)
```

```
  171 FORMAT(30X,' THE TABLE FOR TISI2 IS AS FOLLOWS:'///)
  222 FORMAT(3F8.5)
 1199 FORMAT(3X,F8.5,5X,F8.5,5X,F8.5)
      PI=6.283185307
  888 FORMAT (2X,////////////////////////////////////)
C
C NUM   /TOTAL NUMBER OF HKL TO BE READ (MAXIMUM 72)
C N     /TOTAL NUMBER OF ATOMS PER UNIT CELL
C JNJ   /NUMBER OF ATOMS OF THE FIRST KIND
C HKL   /PLANE DESIGNATIONS TO BE CALCULATED, AN ARRAY
C
      READ (5,1)NUM,N,JNJ
    2 READ (5,3) (H(I),K(I),L(I),I=1,71)
      QP=N-JNJ
      DO 5 J=1,JNJ
C
C UVW    /THE POSITIONS OF THE ATOMS IN THE UNIT CELL, AN ARRAY
C
      READ(5,4) U(1,J),V(1,J),W(1,J)
    5 WRITE (6,1199)U(1,J),V(1,J),W(1,J)
      DO 60 JK=1,QP
      READ (5,4) U(2,JK),V(2,JK),W(2,JK)
   60 WRITE (6,1199)U(2,JK),V(2,JK),W(2,JK)
      DO 6 IJ=1,NUM
      DO 8 JII=1,2
      IF (JII.EQ.1)NN=JNJ
      IF (JII.EQ.2)NN=QP
      SF3=0.0
      SF4=0.0
      DO 7 JI=1,NN
      SF3=SF3+COS((U(JII,JI)*H(IJ)+V(JII,JI)*K(IJ)+W(JII,JI)*L(IJ))*PI)
      SF4=SF4+SIN((U(JII,JI)*H(IJ)+V(JII,JI)*K(IJ)+W(JII,JI)*L(IJ))*PI)
```

```
    7 CONTINUE
      RE1=SF3
      RE2=SF4
      IF (JII.EQ.1) GO TO 20
      F2(IJ)=CMPLX(RE1,RE2)
      GO TO 8
   20 CONTINUE
      F1(IJ)=CMPLX(RE1,RE2)
    8 CONTINUE
      WRITE(6,18)H(IJ),K(IJ),L(IJ),F1(IJ),F2(IJ)
    6 CONTINUE
      IK=0
      DO 100 NI=1,NUM
      A=REAL(F1(NI))
      B=AIMAG(F1(NI))
      C=REAL(F2(NI))
      D=AIMAG(F2(NI))
      IF (A.EQ.0.AND.B.EQ.0)GO TO 77
      GO TO 79
   77 CONTINUE
      IF (C.EQ.0.AND.D.EQ.0)GO TO 100
   79 CONTINUE
      IK=IK+1
      X(IK)=H(NI)
      Y(IK)=K(NI)
      Z(IK)=L(NI)
      F1(IK)=F1(NI)
      F2(IK)=F2(NI)
  100 CONTINUE
C
C AAA   /THE A PARAMETER OF THE UNIT CELL
C BBB   /THE B PARAMETER OF THE UNIT CELL
```

```
C CCC    /THE C PARAMETER OF THE UNIT CELL
C
      READ (5,222)AAA,BBB,CCC
      DO 110 JN=1,IK
      F(JN)=((1.54051**2.0)/4.0)*(((X(JN)**2.0)/(AAA**2.0))+((Y(JN)**2.0
     1)/(BBB**2.0))+((Z(JN)**2.0)/(CCC**2.0)))
      FF(JN)=SQRT(F(JN))
      FG(JN)=(1.54051/2.0)/FF(JN)
      FFF(JN)=ARSIN(FF(JN))*57.2958
      FFG(JN)=2.*FFF(JN)
      SL(JN)=FF(JN)/1.54051
  110 CONTINUE
  333 CONTINUE
      IK=JN-1
      INP=0
  112 CONTINUE
      DO 111 IN=1,56
C
C     THE ATOMIC SCATTERING FACTORS ARE READ
C NQ    /SIN(THETA)/LAMBDA
C ASF   /ATOMIC SCATTERING FACTOR FOR TABLE FOR X-RAY CRYSTALLOGRAPHY
C     A TOTAL OF 56 VALUES FROM 0.0 TO 2.0 SIN(THETA)/LAMBDA FOR EACH
C     ELEMENT. THE PROGRAM READS THE VALUES FOR THE FIRST ELEMENT FIRST.
C
  111 READ (5,44) NQ(IN),ASF(IN)
      INP=INP+1
      DO 113 IIN=1,IK
      INT=1
      DO 115 INI=1,55
      INT=INT+1
      IF (SL(IIN).GT.NQ(INI).AND.SL(IIN).LT.NQ(INT)) GO TO 116
      GO TO 115
```

```
  116 CONTINUE
      AT(INP,IIN)=ASF(INI)+((ASF(INT)-ASF(INI))/(NQ(INT)-NQ(INI))*(SL(II
     1N)-NQ(INI)))
  115 CONTINUE
  113 CONTINUE
      IF (INP.EQ.1) GO TO 112
      DO 1100 NIJ=1,IK
C
C     THE MULTIPLICITY IS EXPRESSED IN THE FORM OF "IF" STATEMENTS
C     FOR THE ORTHORHOMBIC STRUCTURE.
C
C ***********************************************************************
      IFAC(NIJ)=4
      IF(X(NIJ).NE.0.AND.Y(NIJ).NE.0.AND.Z(NIJ).NE.0)IFAC(NIJ)=8
      IF(X(NIJ).EQ.0.AND.Y(NIJ).EQ.0.OR.X(NIJ).EQ.0.AND.Z(NIJ).EQ.0.OR.Z
     1(NIJ).EQ.0.AND.Y(NIJ).EQ.0)IFAC(NIJ)=2
C ***********************************************************************
C
C     THE LORENTZ POLARIZATION FACTOR CORRECTED FOR A GRAPHITE
C     MONOCHROMATOR.
C
      LLP(NIJ)=(1+(COS(26.6  /57.2958)**2)*(COS(  FFG(NIJ)/57.2958)**2))
     1/(1+(COS(FFG(NIJ)/57.2958)**2))
      LP(NIJ)=(1+COS(  FFG(NIJ)/57.2958)**2)/(F(NIJ)*COS(FFF(NIJ)/57.295
     18))*(LLP(NIJ))
C ***********************************************************************
 1100 CONTINUE
      DO 141 JJI=1,IK
      CFJ(1,JJI)=(AT(1,JJI)*F1(JJI))+(AT(2,JJI)*F2(JJI))
      CFJ(2,JJI)=CONJG(CFJ(1,JJI))
      CFF(JJI)=CFJ(1,JJI)*CFJ(2,JJI)
  141 CONTINUE
```

```
      DO 161 NIN=1,IK
      CFT(1,NIN)=CFF(NIN)*LP(NIN)*IFAC(NIN)
  161 CONTINUE
      CRT=0.0
      DO 162 NMN=1,IK
  162 IF (CFT(1,NMN).GT.CRT) CRT=CFT(1,NMN)
      DO 163 JMN=1,IK
  163 CFT(2,JMN)=(CFT(1,JMN)/CRT)*10.
      WRITE (6,838)
      WRITE (6,171)
      WRITE (6,165)
      DO 164 NMJ=1,IK
  164 WRITE (6,166)X(NMJ),Y(NMJ),Z(NMJ),FFG(NMJ),SL(NMJ),AT(1,NMJ),AT(2,
     1NMJ),CFF(NMJ),IFAC(NMJ),LP(NMJ),CFT(1,NMJ),CFT(2,NMJ),FC(NMJ)
      STOP
      END
```

VITA

The author was born on November 27, 1953 in York, Pennsylvania. He received his elementary and secondary school education in York, along with two years at York College of Pennsylvania majoring in engineering.

In December of 1975 he finished the requirements for a Bachelor of Science in Metallurgical Engineering from Virginia Polytechnic Institute and State University. He worked on his master's degree from the Fall of 1975 as a graduate research assistant for Dr. Charles R. Houska. In July of 1977 he joined Bethlehem Steel Corporation's Steelton Plant in the Steel Operations Department.

The author is a member of the American Society for Metals, Alpha Sigma Mu, and Sigma Xi.

He married the former Robin Lou Kramer on June 28, 1975.

Frank E. Dietrich

An X-Ray Study of the Behavior of
Titanium Films on Silicon Substrates

by

Frank E. Dietrich

(ABSTRACT)

The thin film reaction between silicon and titanium did differ from the ordinary diffusion process in bulk samples at elevated temperatures. The lower free energy monosilicide formed prior to the disilicide in bulk standards and was also the dominant reaction product at lower temperatures in films. Titanium thin films, 2.3 microns thick, sustained considerable mechanical deformation during cooling from elevated temperatures. Line broadening, greater than that obtained from cold worked filings of titanium at room temperature, necessitated the use of computer simulation techniques to analyze the diffracted intensity from the reacted structure.

The structure and space group of titanium disilicide was confirmed along with a determination of both structure factor forms and accurate lattice parameters. A range of compositions for the monosilicide of titanium was observed along with the identification of Ti_5Si_4[37] as a high temperature compound. The identification of the inaccuracies and omissions present in the ASTM powder diffraction card files should resolve the confusion in the literature on the reaction between titanium films and silicon.

The temperatures for formation of silicides in thin films was found to be substantially lower than previously reported[2], indicative of the oxide free interface of the silicon substrates. The identification of the reactant silicides, deposited at the grain boundaries and as planar film at interfaces, establishes this study as the first attempt to develop a quantitative model for silicide formation in this transition metal system.